Ecological and Oceanographic Overview of the Napu'saqnuk / St. Mary's River Estuary, Nova Scotia, an Ecologically Significant Area Candidate under Canada's Fisheries Act

Meredith S. Fraser, Aimee Gromack, Melisa C. Wong, Holly Blackmore, Ben Collison, Emmanuel Devred, Brent A. Law, Hunter Stevens, Madison Stewart, Angelica Whiteway, Kristen L. Wilson, Yongsheng Wu, Vanessa Zions

Science Branch and
Aquatic Ecosystems Branch
Maritimes Region, Fisheries and Oceans Canada
Bedford Institute of Oceanography
1 Challenger Drive
Dartmouth, NS B2Y 4A2

2024

Canadian Technical Report of
Fisheries and Aquatic Sciences 3649

Fisheries and Oceans Canada | Pêches et Océans Canada

Canada

Canadian Technical Report of Fisheries and Aquatic Sciences

Technical reports contain scientific and technical information that contributes to existing knowledge but which is not normally appropriate for primary literature. Technical reports are directed primarily toward a worldwide audience and have an international distribution. No restriction is placed on subject matter and the series reflects the broad interests and policies of Fisheries and Oceans Canada, namely, fisheries and aquatic sciences.

Technical reports may be cited as full publications. The correct citation appears above the abstract of each report. Each report is abstracted in the data base *Aquatic Sciences and Fisheries Abstracts*.

Technical reports are produced regionally but are numbered nationally. Requests for individual reports will be filled by the issuing establishment listed on the front cover and title page.

Numbers 1-456 in this series were issued as Technical Reports of the Fisheries Research Board of Canada. Numbers 457-714 were issued as Department of the Environment, Fisheries and Marine Service, Research and Development Directorate Technical Reports. Numbers 715-924 were issued as Department of Fisheries and Environment, Fisheries and Marine Service Technical Reports. The current series name was changed with report number 925.

Rapport technique canadien des sciences halieutiques et aquatiques

Les rapports techniques contiennent des renseignements scientifiques et techniques qui constituent une contribution aux connaissances actuelles, mais qui ne sont pas normalement appropriés pour la publication dans un journal scientifique. Les rapports techniques sont destinés essentiellement à un public international et ils sont distribués à cet échelon. II n'y a aucune restriction quant au sujet; de fait, la série reflète la vaste gamme des intérêts et des politiques de Pêches et Océans Canada, c'est-à-dire les sciences halieutiques et aquatiques.

Les rapports techniques peuvent être cités comme des publications à part entière. Le titre exact figure au-dessus du résumé de chaque rapport. Les rapports techniques sont résumés dans la base de données *Résumés des sciences aquatiques et halieutiques.*

Les rapports techniques sont produits à l'échelon régional, mais numérotés à l'échelon national. Les demandes de rapports seront satisfaites par l'établissement auteur dont le nom figure sur la couverture et la page du titre.

Les numéros 1 à 456 de cette série ont été publiés à titre de Rapports techniques de l'Office des recherches sur les pêcheries du Canada. Les numéros 457 à 714 sont parus à titre de Rapports techniques de la Direction générale de la recherche et du développement, Service des pêches et de la mer, ministère de l'Environnement. Les numéros 715 à 924 ont été publiés à titre de Rapports techniques du Service des pêches et de la mer, ministère des Pêches et de l'Environnement. Le nom actuel de la série a été établi lors de la parution du numéro 925.

Canadian Technical Report of Fisheries and Aquatic Sciences 3649

2024

Ecological and Oceanographic Overview of the Napu'saqnuk / St. Mary's River Estuary, Nova Scotia, an Ecologically Significant Area Candidate under Canada's *Fisheries Act*

Meredith S. Fraser[1], Aimee Gromack[2], Melisa C. Wong[1], Holly Blackmore[2], Ben Collison[2], Emmanuel Devred[1], Brent A. Law[1], Hunter Stevens[3], Madison Stewart[3], Angelica Whiteway[3], Kristen L. Wilson[1], Yongsheng Wu[1], Vanessa Zions[1]

[1] Science Branch and
[2] Aquatic Ecosystems Branch
Maritimes Region
Fisheries and Oceans Canada
Bedford Institute of Oceanography
1 Challenger Drive
Dartmouth, NS, B2Y 4A2

[3] Canadian Parks and Wilderness Society
Nova Scotia Chapter
51086 Rockingham Ridge
Halifax, NS B3M 4R8

Cat. No. Fs97-6/3649E-PDF ISBN 978-0-660-74568-8 ISSN 1488-5379

https://doi.org/10.60825/j47r-2215

Correct citation for this publication:

Fraser, M.S., Gromack, A., Wong, M.C., Blackmore H., Collison, B., Devred, E., Law, B.A., Stevens, H., Stewart, M., Whiteway, A., Wilson, K.L., Wu, Y., and Zions, V., 2024. Ecological and Oceanographic Overview of the Napu'saqnuk / St. Mary's River Estuary, Nova Scotia, an Ecologically Significant Area Candidate under Canada's *Fisheries Act*. Can. Tech. Rep. Fish. Aquat. Sci. 3649: xiii + 107 p. https://doi.org/10.60825/j47r-2215

Contents

List of Figures

List of Tables

List of Contributors

The following contributors provided data and wrote or edited the respective sections in the document.

Introduction and Literature Summary of the St. Mary's River Estuary Ecology

Holly Blackmore, Ben Collison and Aimee Gromack, Fisheries and Oceans Canada

Physical Oceanography

Yongsheng Wu, Fisheries and Oceans Canada

Sediment Dynamics

Brent Law and Vanessa Zions, Fisheries and Oceans Canada

Macrophyte Communities

Meredith Fraser and Melisa Wong, Fisheries and Oceans Canada

Satellite Mapping

Kristen Wilson and Emmanuel Devred, Fisheries and Oceans Canada

Faunal Communities

Madison Stewart, Angelica Whiteway and Hunter Stevens, Canadian Parks and Wilderness Society – Nova Scotia Chapter (CPAWS-NS)

List of Abbreviations

ADCP	Acoustic Doppler Current Profiler
AGBM	Aboveground biomass
AGBG	Aboveground:Belowground (ratio)
AZMP	Atlantic Zone Monitoring Program
BGBM	Belowground biomass
CDOM	coloured dissolved organic matter
COSEWIC	Committee on the Status of Endangered Wildlife in Canada
CPAWS-NS	Canadian Parks and Wilderness Society – Nova Scotia Chapter
CTD	conductivity-temperature-depth (instrument)
DFO	Fisheries and Oceans Canada
DM	Dry Mass
eDNA	Environmental DNA
ESA	Ecologically Significant Area
FVCOM	Finite Volume Community Model
LAI	Leaf area index
MPA	Marine Protected Area
NTU	Nephelometric turbidity unit
OECMs	Other Effective Area-based Conservation Measures
PCA	Principal component analysis
PSU	Practical salinity unit
REEF	Reef Environmental Education Foundation
SAV	Submerged aquatic vegetation
SPM	Suspended particulate matter
SSC	Suspended sediment concentration
Tu	Turbidity

Abstract

Fraser, M.S., Gromack, A., Wong, M.C., Blackmore H., Collison, B., Devred, E., Law, B.A., Stevens, H., Stewart, M., Whiteway, A., Wilson, K.L., Wu, Y., and Zions, V., 2024. Ecological and Oceanographic Overview of the Napu'saqnuk / St. Mary's River Estuary, Nova Scotia, an Ecologically Significant Area Candidate under Canada's *Fisheries Act*. Can. Tech. Rep. Fish. Aquat. Sci. 3649: xiii + 107 p. https://doi.org/10.60825/j47r-2215

This overview of Napu'saqnuk / St. Mary's River estuary summarizes what is known about its key physical and biological components. Napu'saqnuk is an Ecologically Significant Area (ESA) candidate under Canada's *Fisheries Act.* The estuary exhibits a strong estuarine gradient in salinity, water temperature, and bottom sediments. This gradient supports diverse habitats including bare rock and sand/mud sediments, macroalgae, and seagrasses (eelgrass, widgeongrass). The distribution and species composition of macrophyte communities vary along the estuary and support fishes including the American Eel, Rainbow Smelt, Gaspereau, and Atlantic Salmon. Napu'saqnuk is a regionally unique and highly natural ecosystem within the Eastern Shore of Nova Scotia, with few barriers to fish passage, low human impacts, and no current industrial development. Although some knowledge gaps were identified, including lack of long-term *in situ* biological and physical data, this report provides a preliminary summary of the estuary's physical and biological status. This description demonstrates that it meets the ESA ecological criteria of being highly productive, sensitive, and unique. This work can support the planning and development phase for this ESA candidate, and also the development of relevant conservation and protection objectives.

Résumé

Fraser, M.S., Gromack, A., Wong, M.C., Blackmore H., Collison, B., Devred, E., Law, B.A., Stevens, H., Stewart, M., Whiteway, A., Wilson, K.L., Wu, Y., and Zions, V., 2024. Ecological and Oceanographic Overview of the Napu'saqnuk / St. Mary's River Estuary, Nova Scotia, an Ecologically Significant Area Candidate under Canada's *Fisheries Act*. Can. Tech. Rep. Fish. Aquat. Sci. 3649: xiii + 107 p. https://doi.org/10.60825/j47r-2215

Cet aperçu de l'estuaire de la Napu'saqnuk (rivière St. Mary's) résume ce que l'on sait des principales composantes physiques et biologiques. La Napu'saqnuk est une candidate comme zone d'importance écologique (ZIE) en vertu de la *Loi sur les pêches* du Canada. L'estuaire présente un gradient considérable de salinité, de température de l'eau et de types de sédiments de fond. Ce gradient soutient une diversité d'habitats constitués de roches nues et de sédiments de sable et de boue, macroalgues, et d'herbiers marins (zostères, persil d'eau). La répartition et la composition des communautés de macrophytes varient le long de l'estuaire et abritent de nombreux poissons, dont l'anguille d'Amérique, l'éperlan arc-en-ciel, le gaspareau et le saumon atlantique. Napu'saqnuk est un écosystème régional unique et très naturel sur la côte est de la Nouvelle-Écosse, avec peu d'obstacles au passage des poissons, peu d'effets anthropiques et aucun développement industriel en cours. Bien que certaines lacunes dans les connaissances aient été soulevées, notamment l'absence de données physiques et biologiques *in situ* à long terme, ce rapport fournit un résumé de l'état physique et biologique de l'estuaire. Cette description montre qu'il répond aux critères écologiques d'une ZIE, soit être très productif, sensible et unique. On peut se servir de ces travaux pour orienter la phase de planification et de développement de ce candidat ZIE, y compris l'élaboration d'objectifs de conservation et de protection.

1 Introduction

Napu'saqnuk, which translates to 'At the place of stringing beads' (Transcriptions of Father Pacifique Guide to MicMac Place Names, 1934 as cited in Ta'n Weju-sqalia-tiek Mi'kmaw Place Names Digital Atlas), also known as the St. Mary's River and estuary, is an Ecologically Significant Area (ESA) candidate for designation under Canada's *Fisheries Act*. ESAs are designated to support conservation and protection of fish and fish habitat, providing regulations to minimize threats to conservation objectives specific to that area. ESA regulations are focussed on regulating projects and not fishing. The ESA provisions were originally added to the *Fisheries Act* in 2013 and then amended in 2019 as a result of public consultation to make them clearer, stronger, and easier to implement. Although there are no ESAs currently in Canada, the 2019 *Fisheries Act* changes initiated dedicated efforts by Fisheries and Oceans Canada (DFO) to develop a national ESA framework and explore ESA implementation.

A case study on the Napu'saqnuk watershed was initiated by DFO to help understand the new ESA provisions and inform the development of the National Framework for Identifying, Establishing and Managing ESAs (DFO 2023a) herein the ESA Framework. The area was recently approved as an ESA candidate. External engagement on the candidate is underway and information continues to be collected to support regulatory development.

The St. Mary's River estuary is considered a strong ESA candidate, as it has several features that meet the ESA ecological criteria for sensitive, highly productive, and rare or unique areas identified in the ESA Framework (DFO 2023a). Furthermore, the St. Mary's River estuary aligns with several priority considerations that include the freshwater and estuarine habitats that support key species such as the Southern Upland Atlantic Salmon population. Napu'saqnuk is a highly important river for this species and is one of DFO's two index rivers for population monitoring. The area is highly natural, with few barriers to fish passage, a low human population (2,161 in 2021), minimal shoreline alteration, and no current industrial development.

The St. Mary's river and estuary are located on the eastern shore of NS, between Wine Harbour to the east and Liscomb to the west (Figure 1). The study area for the ESA candidate includes all the connected water within the watershed spanning the estuary to the headwaters, and includes wetlands, sand flats, subtidal marine waters, riparian shorelines focused on Crown land, and river habitats (Figure 2). As such, an ESA designation could protect up to 160 km^2 of water and a diverse array of aquatic habitat. The estuary itself comprises 11 km^2 of that total and would additionally contribute to Canada's international protection targets and the national Marine Conservation Target. The Napu'saqnuk estuary is included in DFO's Maritimes Region Draft Conservation Network (DFO 2024).

In addition to Atlantic salmon, other anadromous species of regional importance transit through the estuary to the river system including American Eel, Gaspereau, and sea-run Brook Trout (Davis 1976, Mitchell 2012). These species and other marine species use eelgrass (*Zostera marina*) and other macrophytes which are found throughout the estuary (DFO 2019, DFO 2021). Protection of these vegetated habitats, as well as other estuarine features and processes would support fishes and their invertebrate prey. Furthermore, protection of macrophytes supports climate change resiliency, provides nature-based solutions to climate change impacts such as coastal erosion, and allows for carbon sequestration (Barbier et al. 2011, Bouchama et al. 2019, Fourqurean et al. 2012, Vercaemer et al. 2022).

DFO collaborating with the Mi'kmaq, and hopes to include Mi'kmaq knowledge in the regulatory development process. Discussions are ongoing with Mi'kmaq partners on the best practice to share and incorporate Indigenous knowledge, along with western science to inform

the ESA implementation process, with the intent to adopt Etuaptmumk (two-eyed seeing, Reid et al. 2020). This knowledge and information will inform a risk assessment required to develop regulations for works, undertakings, and activities that could impact fish habitat.

This report consolidates physical and biological information gathered in 2023 to support the evaluation of the St. Mary's River and estuary as an ESA candidate. The focus is on the marine influenced portion of the area, specifically the St. Mary's River estuary, which extends from the head of tide at Sherbrooke to the open coastal area outside of Sonora (Figure 1). This report consists of a literature summary of the biological and ecological information relevant to the area (Section 2), as well as sections that describe the area's physical oceanography (Section 3), sediment dynamics (Section 4), macrophyte ecology (Section 5), macrophyte distribution examined through satellite mapping (Section 6), and faunal diversity (Section 7). The report concludes by outlining remaining knowledge gaps (Section 8) and summarizes aspects (Section 9) that support the evaluation of the Napu'saqnuk / St. Mary's River estuary as an ESA candidate and the development of future potential conservation and protection objectives. A separate report that describes the freshwater ecosystem is in progress.

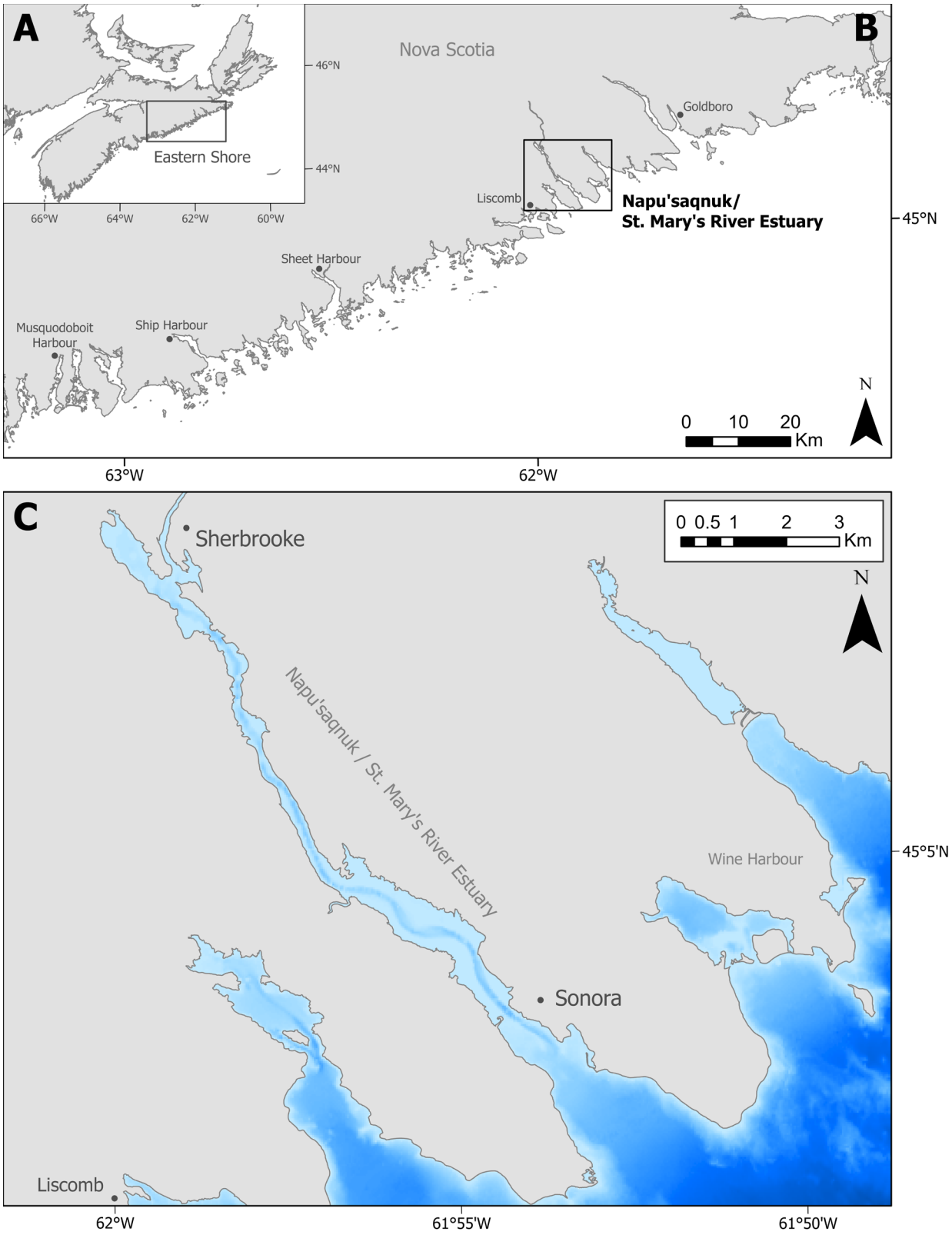

Figure 1. Location of (A) Nova Scotia, Eastern Shore region indicated by gray box. (B) Napu'saqnuk / St. Mary's River estuary location (outlined in black box) within the Eastern Shore region. (C) Overview of the Napu'saqnuk / St. Mary's River Estuary.

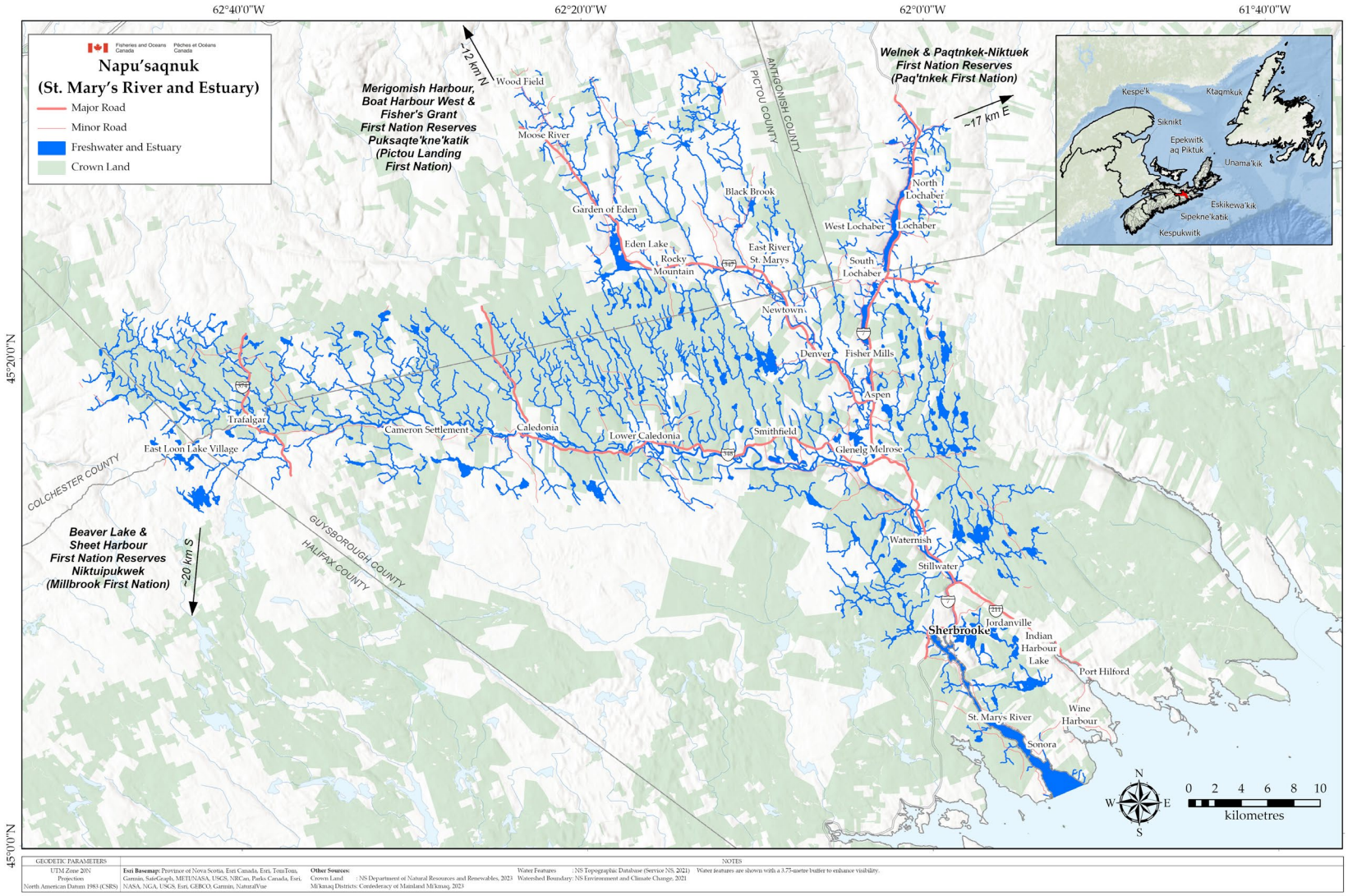

Figure 2. Overview of the Napu'saqnuk / St. Mary's River and estuary Ecologically Significant Area candidate study area.

2 Literature Summary of the St. Mary's River Estuary Ecology

Available peer reviewed literature, grey literature, websites, and other sources that describe the biological components (habitat and species) were reviewed and collated in this section. Napu'saqnuk / St. Mary's River estuary contains important estuarine habitats for many aquatic flora and fauna. Saltmarsh is located along the coastal shores of Napu'saqnuk (Allard et al. 2014, as cited in Jeffery et al. 2020), and eelgrass occurs throughout the estuary (Section 5). Eelgrass has been documented primarily on the mud flats north of the Sonora wharf (Mahar 2022), although to date, the full extent and distribution of seagrasses, macroalgae, or salt marsh have not been well described across the entire extent of the St. Mary's River estuary. Macrophytes in the St. Mary's River estuary likely provide important foraging habitat and refugia for aquatic species, including at risk species such as Atlantic Salmon and Atlantic Cod (endangered, Committee on the Status of Endangered Wildlife in Canada - COSEWIC) and Lumpfish (threatened, COSEWIC) that are known to use these habitat types (Clark et al. 2015, DFO 2019, DFO 2021).

The importance of the St. Mary's River for Atlantic Salmon has long been recognized in the literature, and as a result, Atlantic Salmon are a priority fish species for the St. Mary's River ESA candidate. The St. Mary's River is home to an index population of the Nova Scotia Southern Upland Atlantic Salmon that COSEWIC assessed as endangered in 2010 (COSEWIC 2010); however, is not protected under the *Species at Risk Act*. Atlantic Salmon rely on estuarine habitat during multiple life stages (Able and Fahay 2010, Weitkamp et al. 2014). Salmon smolts are found in estuaries beginning in April where they use ebb tide to help them travel to the ocean (Bowlby et al. 2014). The length of time that smolts remain in estuaries varies and is largely dependent on oceanographic conditions, and the physical fitness and exposure history of individuals while present in freshwater (Bowlby et al. 2014; Halfyard et al. 2013). Smolts are hypothesized to spend longer periods in short and wide estuaries where salt and freshwater mix at faster rates over smaller areas, which poses a greater osmoregulatory demand (Bowlby et al. 2014). Migratory behaviour across the Southern Uplands is largely watershed-specific, with high variability of Atlantic salmon smolt residency times and survival while moving across freshwater-saltwater gradients (Halfyard et al. 2012; Halfyard et al. 2013).

Acoustic telemetry tracking data has shown that smolt survival was overall relatively high in Napu'saqnuk when out-migration occurred, with an estimated survival rate of 98.3% per km of habitat travelled (Halfyard et al. 2012). When averaged, that equated to roughly 83% of smolts reaching the outer Sonora estuary to enter the open ocean after long distances travelled through freshwater habitats (Halfyard et al., 2013, as cited in Gibson et al., 2015). During out-migration, mortality rates and residency time for Napu'saqnuk smolts did not differ depending on habitat type (freshwater, inner estuary, outer estuary, bay), indicating high fitness of individuals and low osmotic stress when encountering the saltwater environment (Halfyard et al., 2012). Estuarine smolt survival ranged from 54 to 89% in other Southern Upland watersheds of the West River Sheet Harbour, LaHave River, and Gold River (Halfyard et al., 2013). Potential contributing factors to largely successful smolt out-migrations in Napu'saqnuk are the extended gradual saltwater-freshwater mixing zone (Halfyard et al., 2012), presence of shallow vegetated mud flats for cover and foraging, and absence of predatory fish such as smallmouth bass (*Micropterus dolomieu*), chain pickerel (*Esox niger*) or striped bass (*Morone saxatilis*; Gibson et al., 2015; Falkegård et al., 2023).

Once smolts reach the ocean, the length of time spent in saltwater varies. Many individuals, known as grilse, will return to spawn in their natal river after overwintering in saltwater for only one winter. Others spend between two and three winters in the ocean, reaching a larger body size with more time spent at sea, before returning to freshwater to spawn (Bowlby et al. 2014).

In the St. Mary's River, the number of multi-sea-winter Atlantic salmon returning to spawn each year has decreased in recent decades, a common trend amongst all Southern Upland watersheds (Bowlby et al., 2014); currently, most Atlantic salmon will spend only one winter season in the ocean before returning as grilse (Gibson et al. 2009, Bowlby et al. 2014). Grilse have been found to remain nearshore during their time in ocean waters (Halfyard et al. 2013). Adult salmon return to their natal river in the spring, summer and fall months, spending from a few days to up to three-and-a-half months in estuaries prior to returning to freshwater (Bowlby et al. 2014). The initiation of upstream spawning migration is linked to river conditions such as temperature and discharge (Thorstad et al., 2008), where cooler water and high flows tend to trigger Atlantic Salmon to return to freshwater (Moir et al., 2003). Adult salmon return rates were modeled for the St. Mary's River (West Branch) using data from 2000 - 2009, with estimated returns at 0.54 - 2.11% for salmon that overwinter at sea for one year (Gibson and Bowlby 2013).

Anecdotally, salmon are showing signs of recovery based on increased numbers of redds near restoration sites and increased adult sightings; however, adult abundance and return rates have not been studied since 2009 to confirm these observations. Electrofishing surveys throughout Napu'saqnuk from 2000 - 2022 recorded stable abundances of Atlantic salmon fry and parr (DFO 2023b). Current numbers of Atlantic salmon using the St. Mary's River estuary annually are not known.

Marine mortality rates for Atlantic salmon are high in estuarine and near-shore environments between the parr-smolt transformation and early smolt phases due to this sensitive life stage (Chaput et al. 2019, Bowlby et al. 2014). During these phases, salmon experience faster growth rates and require abundant and specific food; this environment and their small size make them vulnerable to predation (ASF 2021, Bowlby et al. 2014).

It has been indicated in the literature that the killifish is another important fish species in the St. Mary's River estuary. An asexual clonal hybrid species of killifish has been formed in the St. Mary's River estuary, where the freshwater-preferring Banded Killifish (*Fundulus diaphanous*) and saltwater-preferring Common Killifish (*Fundulus heteroclitus*; often referred to as the Mummichog) have overlapping habitat and interbreed (Hernández-Chávez and Turgeon 2007, Mérette et al. 2009, Dalziel et al. 2020). Hybridization is common between Fundulus species in many locations throughout Canada, but is only known to produce asexual female-only clonal offspring in Porter's Lake and the St. Mary's River estuary, both located along Nova Scotia's eastern shore (Mérette et al. 2009, Dalziel et al. 2020). The rare clonal hybrid killifish in the St. Mary's estuary provides a unique opportunity for scientists to study how fish genomes adapt to environmental change through hybridization and subsequent asexual reproduction (Dalziel et al. 2020).

Diadromous species that are known to be present in the St. Mary's estuary for part of their life cycle include sea lamprey (*Petromyzon marinus*), American eel (*Anguilla rostrata*), sea-run brook trout (*Salvelinus fontinalis*), alewife (*Alosa pseudoharengus*), and blueback herring (*Alosa aestivalis*; Mitchell 2012). Other fish species present in the St. Mary's estuary evident from the literature include Atlantic Silverside (*Menidia menidia*), American Shad (*Alosa sapidissima*) Fourspine Stickleback (*Apeltes quadracus*), Grubby Sculpin (*Myocephalus aenaeus*), and Rock Gunnel (*Pholis gunnellus*; Davis 1976, Mitchell 2012). Species that may also be present based on their known geographic limits and distribution along the Eastern shore of Nova Scotia, but yet to be verified in the St. Mary's River estuary include Atlantic Cod (*Gadus morhua*; Jeffrey et al. 2020), Striped Bass (*Morone saxatilis*; Andrews et al. 2019), and Lumpfish (*Cyclopterus lumpus*; Bundy et al. 2014). As documented in the literature, the estuary also contains some mollusk and crustacean species that play an important ecological and economic role across

coastal environments in the Eastern Shore region and Atlantic Canada more broadly (Jeffery et al. 2020). These include, Atlantic Lobster (*Homarus americanus*), Atlantic Rock Crab (*Cancer irroratus*), Baltic Clam (*Macoma balthica*), Blue Mussel (*Mytilus edulis*), Jonah Crab (*Cancer borealis*), Northern Dwarf-tellin (*Ameritella agilis*), Soft-shell Clam (*Mya arenaria*), and Atlantic Surf Clam (*Spisula solidissima*; Davis 1976, Bundy et al. 2014). The specific interactions and habitat usages of the St. Mary's estuary and near shore environment for most of these species has not been well studied to-date.

3 Physical Oceanography

The physical oceanography of the St. Mary's River estuary was examined using an existing numerical oceanographic model (Finite Volume Community Model, FVCOM; Jabarri et al. 2024) that was further refined, calibrated, and validated with *in situ* data from the estuary. The model is characterized in part by a varying spatial resolution across the model domain, with high spatial resolution in nearshore areas (10 to 100 m) allowing the dynamic nearshore physical processes to be modelled accurately. Below, the model inputs specific to the St. Mary's River estuary, as well as the model structure and preliminary model results for this area are described.

3.1 Model Inputs

3.1.1 River Discharge

The daily mean river discharge data for the St. Marys' River used in the model were collected at the Stillwater Station (01EO001, 45°10'27"N, 61°58'47"W) by the Water office of Environment and Climate Change Canada (https://wateroffice.ec.gc.ca/report/real_time_e.html). River discharge showed a strong interannual variation throughout the time series from 1920 to 2023 (Figure 3). The annual maximum discharge varied from less than 100 m^3 s^{-1} to close to 1000 m^3 s^{-1}. A wavelet analysis revealed that the discharge also showed a strong seasonal and annual variation, with periods of high discharge usually occurring over 1–8 days (Figure 4). Based on the data, the daily mean climatology was calculated using average daily discharge (Figure 5). The discharge in spring and fall was usually higher than that in summer and winter. However, a river flood is possible in any season.

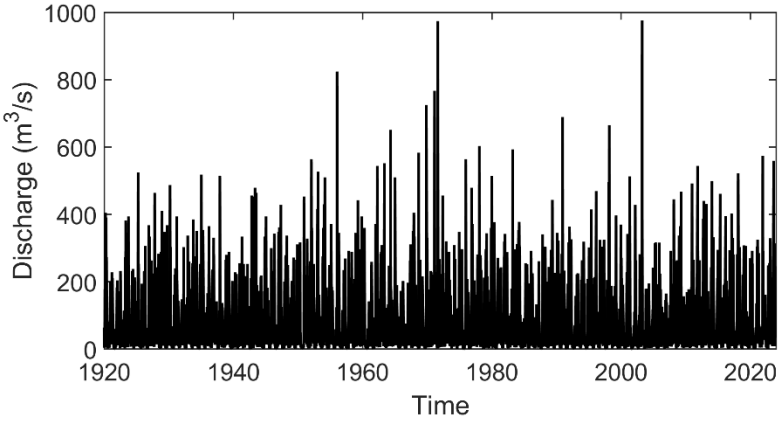

Figure 3. Daily discharge at Stillwater Station from 1920 to 2020.

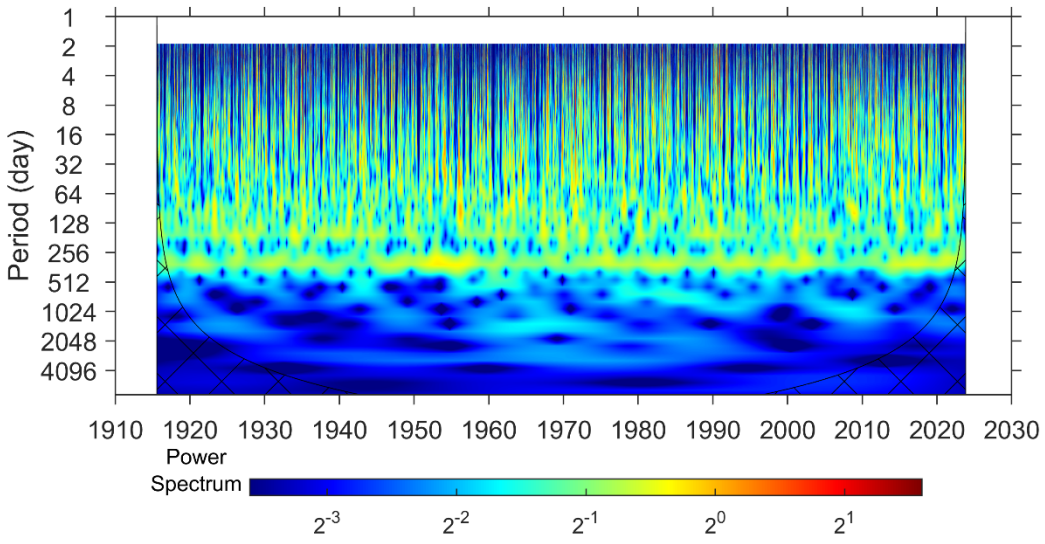

Figure 4. Wavelet analysis of the daily discharge.

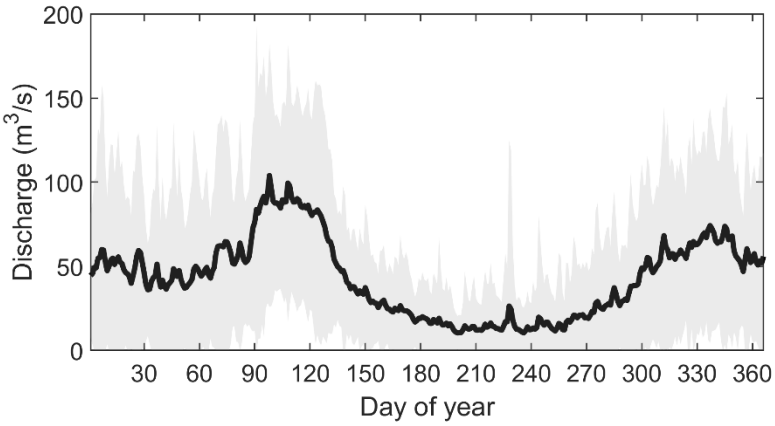

Figure 5. Climatology of daily discharge based on the average daily discharge in 1920–2023.

3.1.2 Water Elevations in the Estuary

Water elevation data were available from two stations (Figure 6), station 7 (upper estuary) and station 35 on the Sonora flats (lower estuary). Data loggers (Onset HOBO Water Level Logger) were deployed on the sea bottom and recorded water pressure in 15 minutes intervals from July to November 2023. Data were used to calculate water depth based on the pressure recording, the standard atmospheric pressure, the density of sea water, and the acceleration of gravity (Wong and Dowd 2021). The river discharge strongly influenced the water elevations at the upper station, especially for the high flood cases (Figure 7A and B). Whereas tidal cycles were an important component for the water elevations at both stations (Figure 7B and C).

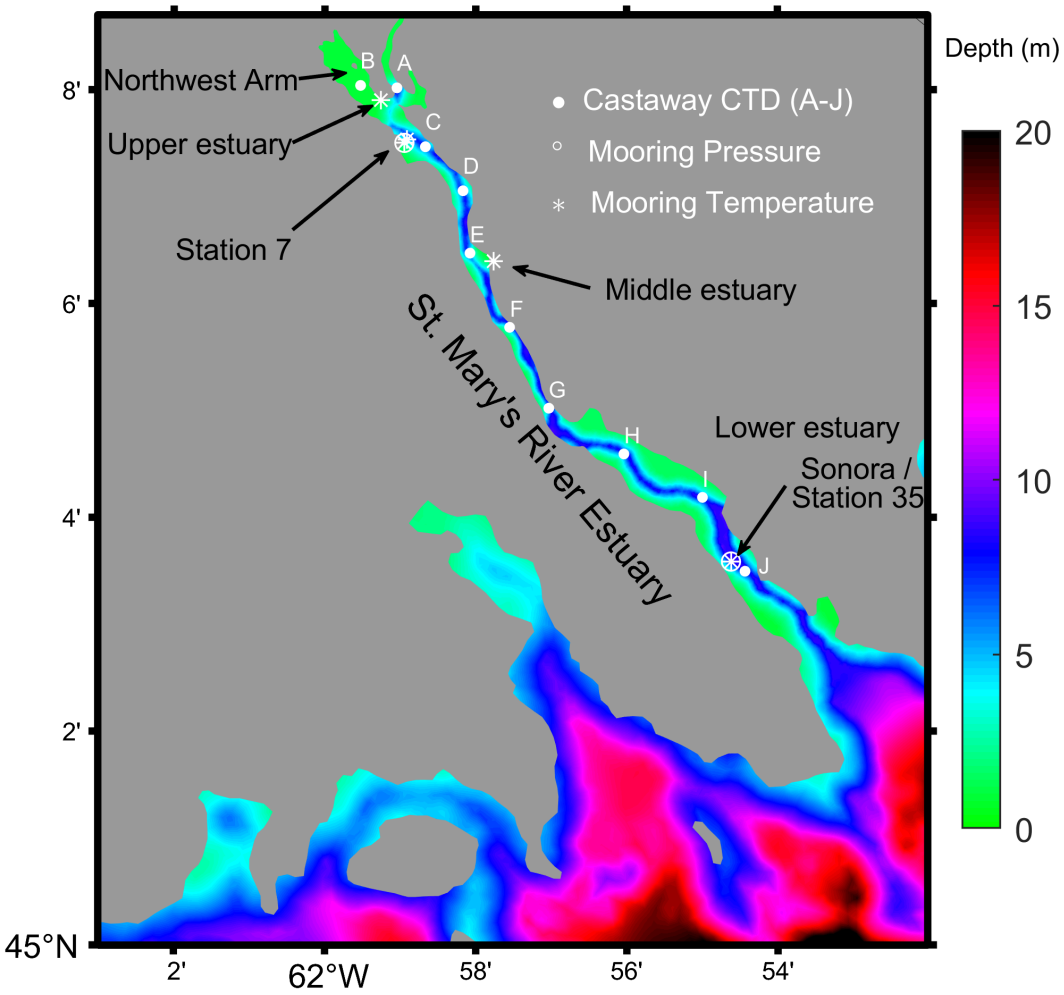

Figure 6. Map showing the depth profile and locations of *in situ* observation data collected in St. Mary's estuary, 2023.

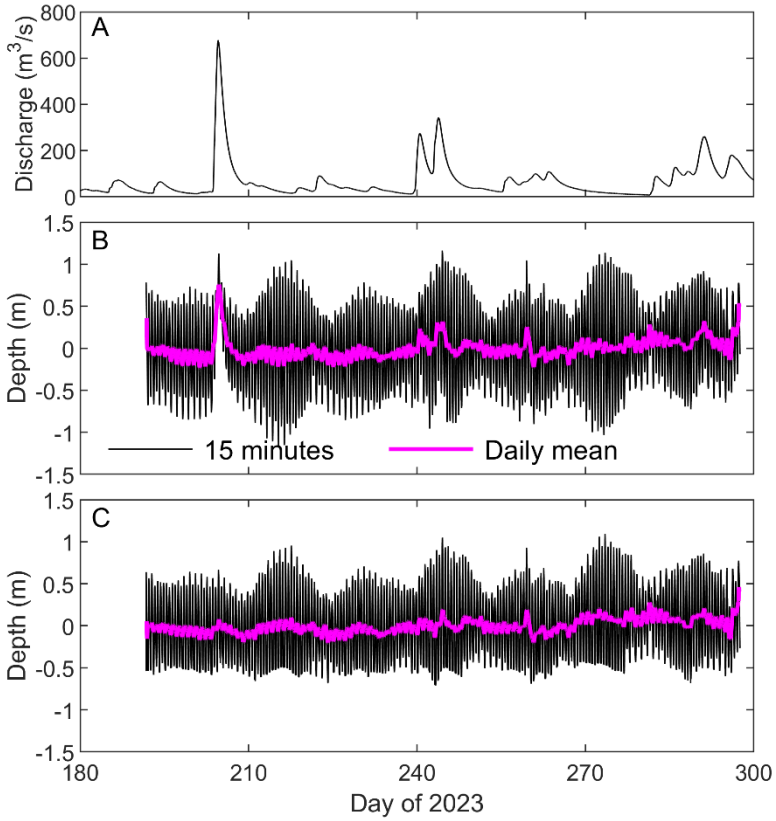

Figure 7. Time series river discharge (A), water elevations at upper estuary (B, station 7), and at the lower estuary(C, station 35/Sonora).

3.1.3 Temperature and Salinity along the Estuary

In situ temperature and salinity time-series data in the river channel and the estuary of the St. Mary's River were not previously available. To provide a temperature time-series, loggers were deployed in 4 different regions of the estuary: the upper estuary, station 7, middle estuary, and lower estuary (Figure 6). Temperature loggers were deployed on the sea bottom and recorded every 15 minutes, from July to November 2023. Time series of the bottom temperature at the four stations show similar features overall across time (Figure 8) except at lower stations, where the variation of the water temperature reaches 10 degrees within one day, especially during spring tides (Figure 7). Variation in water temperature was highest in the middle and lower estuary, reflecting shallower water depths, air exposure at low tide (in lower estuary), and increased tidal influence relative to river discharge.

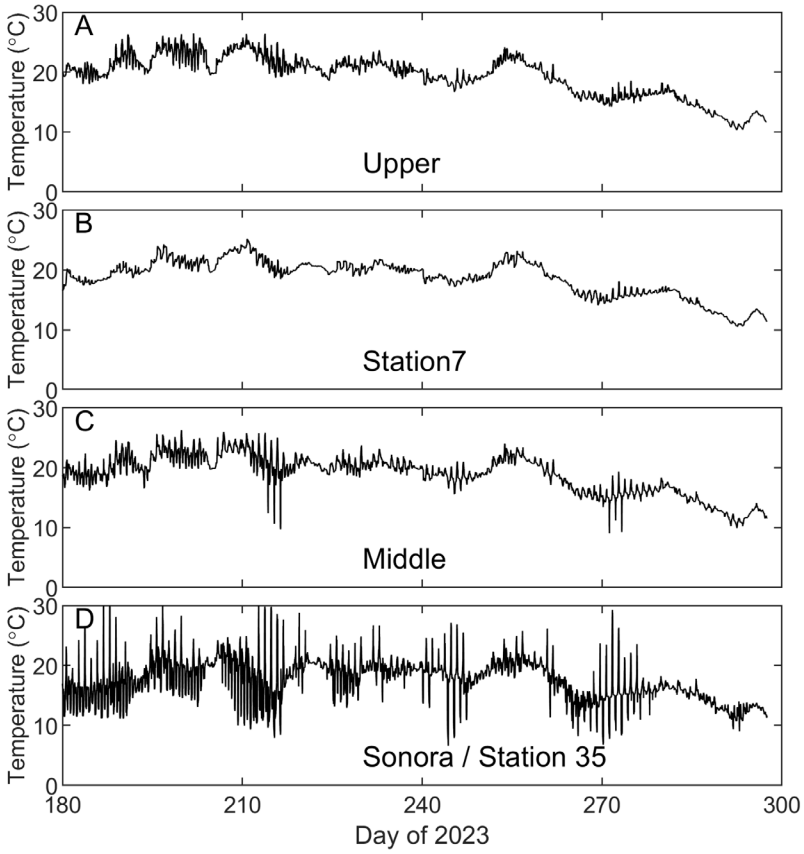

Figure 8. Time series of the bottom temperature at four stations (see Figure 6 for station locations), from the upper estuary to the lower estuary.

Conductivity-temperature-depth (CTD) profiles were also measured across depth at 10 stations (labeled A–J; Figure 9; Table A1) along the estuarine gradient, aiming to characterize temperature and salinity patterns within one tidal cycle. A CastAway®-CTD (SonTek) was used, and profiles were located within the tidal channel. In general, the temperature decreases from the upstream to the downstream (Figure 9), while the salinity shows an opposite pattern, increasing from the upstream to the downstream. This highlights the stronger oceanic influence in the lower estuary while the river discharge dominates the salinity signal in the upper estuary. Strong vertical variations across depth were observed for both the temperature and salinity. The depth of the tidal channel ranged from 4 to 8 m.

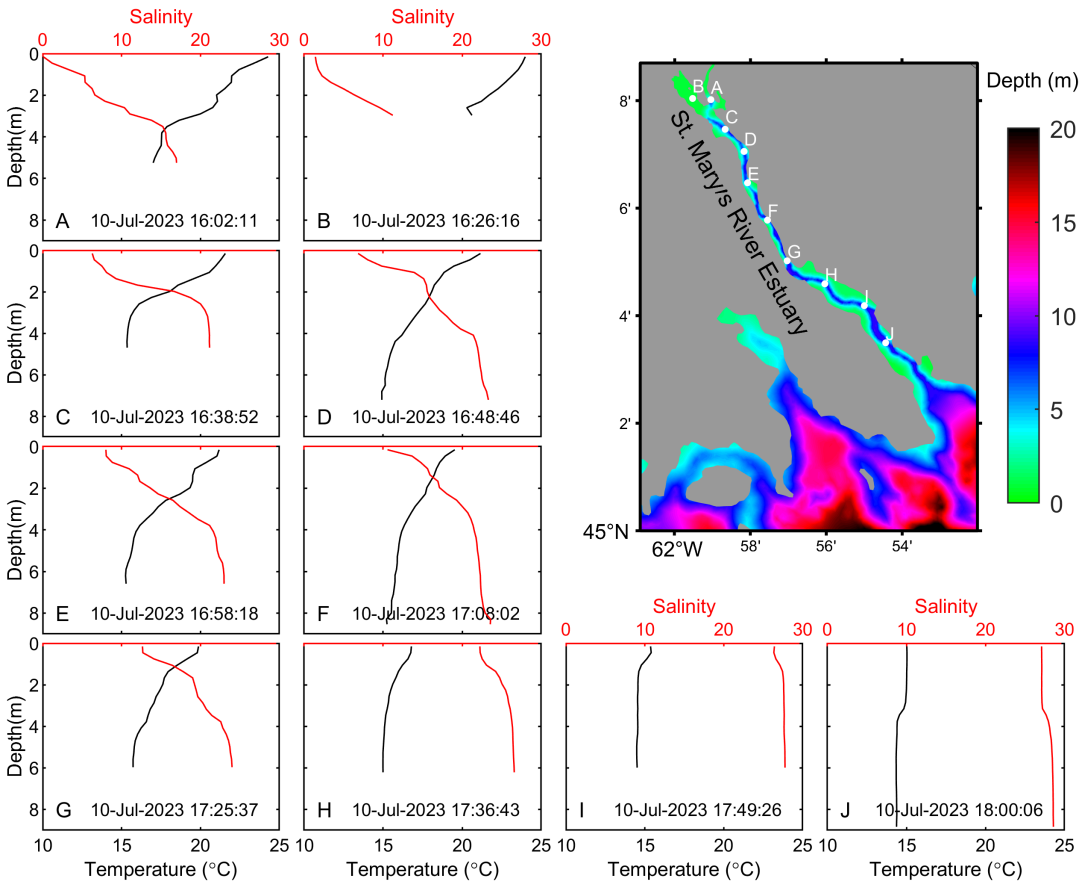

Figure 9. Vertical distributions of water temperature (black) and salinity (red) at 10 Conductivity-temperature-depth (CTD) castaway stations (A-J). Time stamps are in UTC.

3.2 Model Setup

Temperature and salinity in the river channel were preliminarily simulated by adding the river channel in the existing hydrodynamic model based on the Finite Volume Community Ocean Model (FVCOM, Chen et al. 2003). The model uses a triangle grid system, which is spatially flexible to fit complex shorelines. The model domain covers the Gulf of Maine and Scotian Shelf (Figure 10). The model resolution varies from 10 m in the river channel to hundreds of metres in the river estuary (Figure 11). The bathymetry data in the estuary channel are from the Canadian Hydrographic Service (https://open.canada.ca/data/) and corrected with the *in situ* data collected at the CTD stations (Figure 9, Table A1). In the present study, there are 44 vertical layers, which consists of 10 layers with z levels at the surface layer and 5 layers with z levels at the bottom. The interval of the z levels is 5 m in both the surface and the bottom layers. In the water shallower than 220m, the uniform sigma coordinate is used. The open boundary conditions employ a one-way nesting scheme with four variables (water elevations, temperature, salinity and currents) from GLORYS12v1 (Jean-Michel et al. 2021). The tidal components were also included through the nesting; the tidal water elevations and tidal currents of eight major tidal constituents (M2, S2, N2, K2, O1, K1, P1, and Q1) are from the tidal dataset of TPXO9 (Egbert and Erofeeva 2002). Surface atmospheric forcing consists of wind at 10 m above the ocean surface, air temperature at 2 m, relative humidity at 2 m, precipitation, evaporation, shortwave radiation, and longwave radiation. Forcings with 1/4° resolution were

obtained from ERA5 reanalysis datasets from the European Centre for Medium-Range Weather Forecasts. River discharge was used as water input at the river boundary (Silvers Pool, about 20 km northwest to the inlet of the Northwest Arm of the St. Mary's River estuary). The salinity of the river discharge was set to zero, and the temperature of freshwater input was derived from the local air temperature using a linear relationship between air temperature and water temperature at the mooring station in the Northwest Arm (Figure 6) based on the method of Toffolon and Piccolroaz (2015; Figure 12).

3.3 Preliminary Analysis of Model Results

Here the temperature in the St Mary's River estuary is shown as an example of the preliminary oceanographic model results. In general, the movement of freshwater in a river channel is controlled by a horizontal gradient of water elevation, horizontal gradient of density, and vertical mixing. The water elevation upstream is generally higher than that downstream due to river discharge. However, the density downstream is usually higher than that upstream due to the saltier ocean water. The horizontal gradient of water elevation is uniform in the vertical direction, while the horizontal gradient of density usually increases with depth, and reaches a maximum at the bottom. So, the elevation gradient drives the water moving from the upstream to the downstream, but on the contrary, the density gradient drives the movement from the downstream to the upstream. A strong shear usually forms at a subsurface layer, and thus leads to vertical mixing. When the tides are present in the river channel, the tides decrease the velocity in the surface layer and increase the velocity in the bottom layer during the flood phases, while on ebb phases the velocity in the surface layer increases and upstream velocity in the bottom layer decreases. In the study area, controlling mechanisms for the transport of water temperature (Figure 13 A–D) and salinity (Figure 14 A–D) are consistent with the mechanism described above. Warm and fresh water moves quickly from the upstream to the downstream in the surface layer during the ebb phases, while the cold and saltier water in the bottom layer transports from the downstream to the upstream during the flood phase. The saltier water from offshore can reach as far inshore as the Northwest Arm of the St. Mary's River estuary.

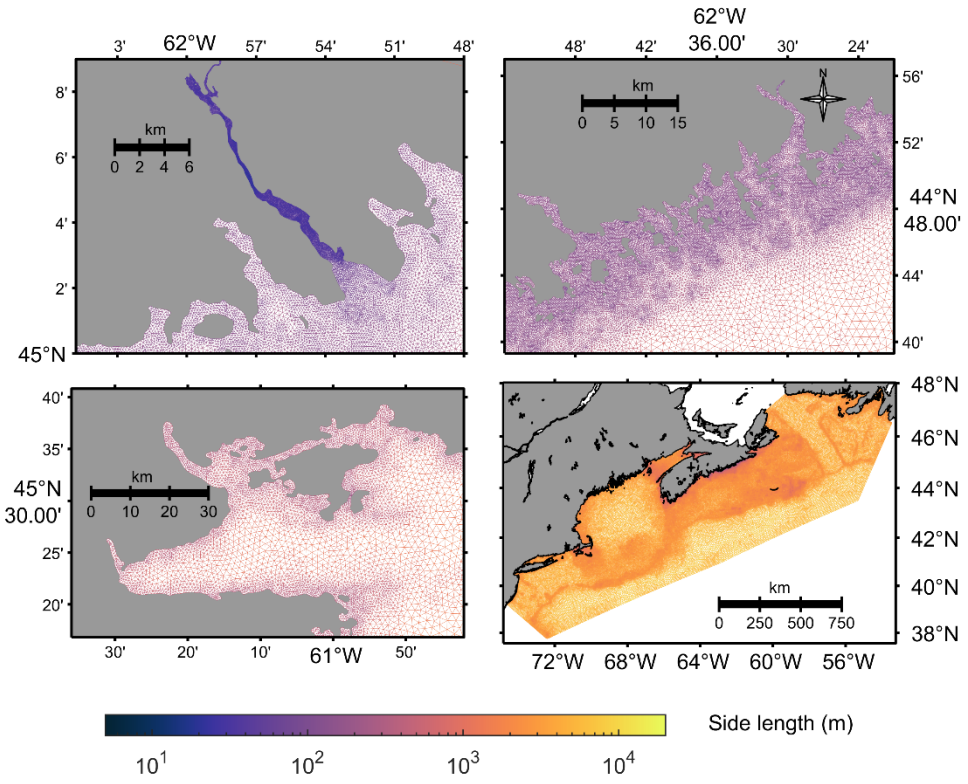

Figure 10. Model domain (right bottom) and model resolution in three subregions of Eastern Shore Island (right top), Canso Strait (left bottom) and the St. Mary's River estuary (left top).

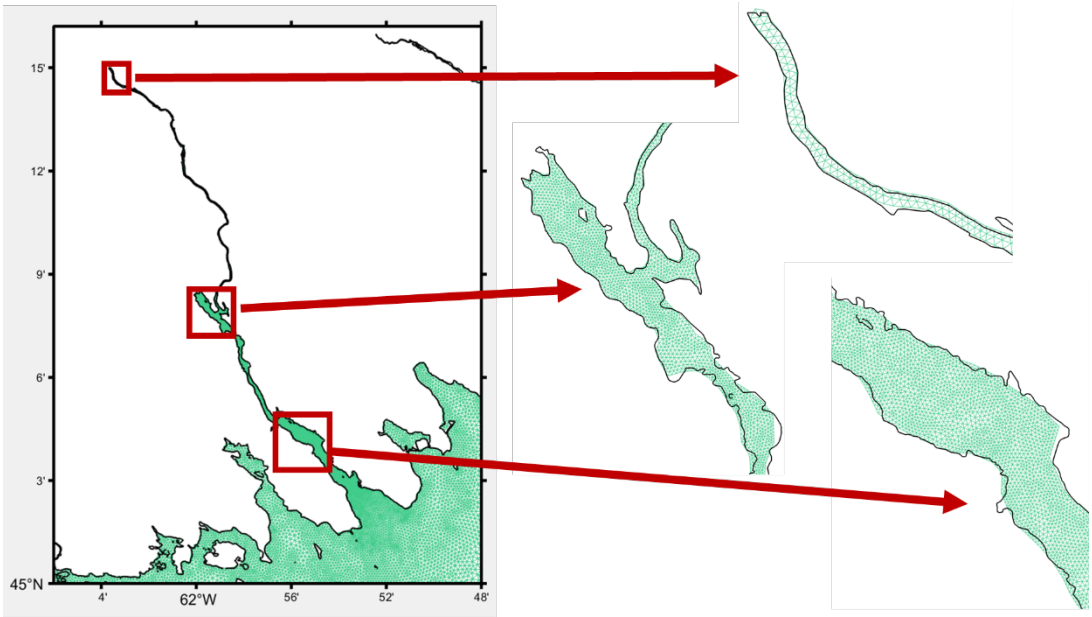

Figure 11. Model mesh in the St. Mary's River channel and estuary.

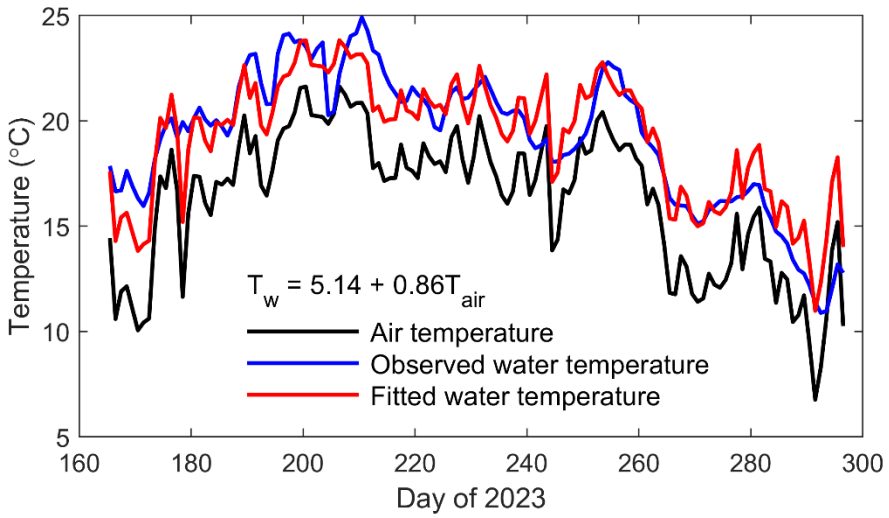

Figure 12. The relationship between air temperature and water temperature at the Northwest Arm of the St. Mary's River estuary (see Figure 6 for location).

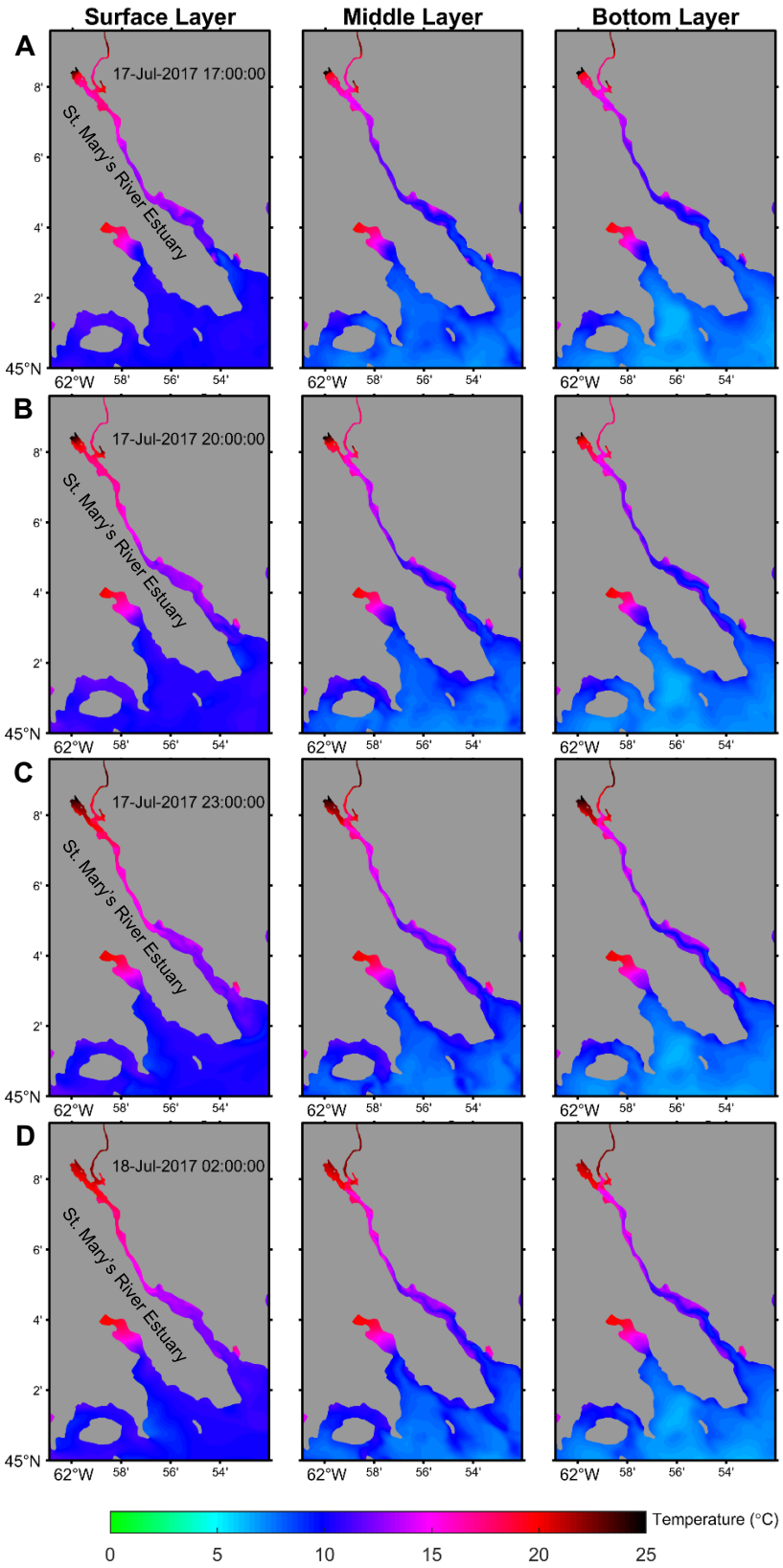

Figure 13. Water temperature at the surface (left), middle layer (middle) and the bottom layer (right) at the start (A) and middle (B) of ebb tide and the start (C) and middle (D) of flood tide.

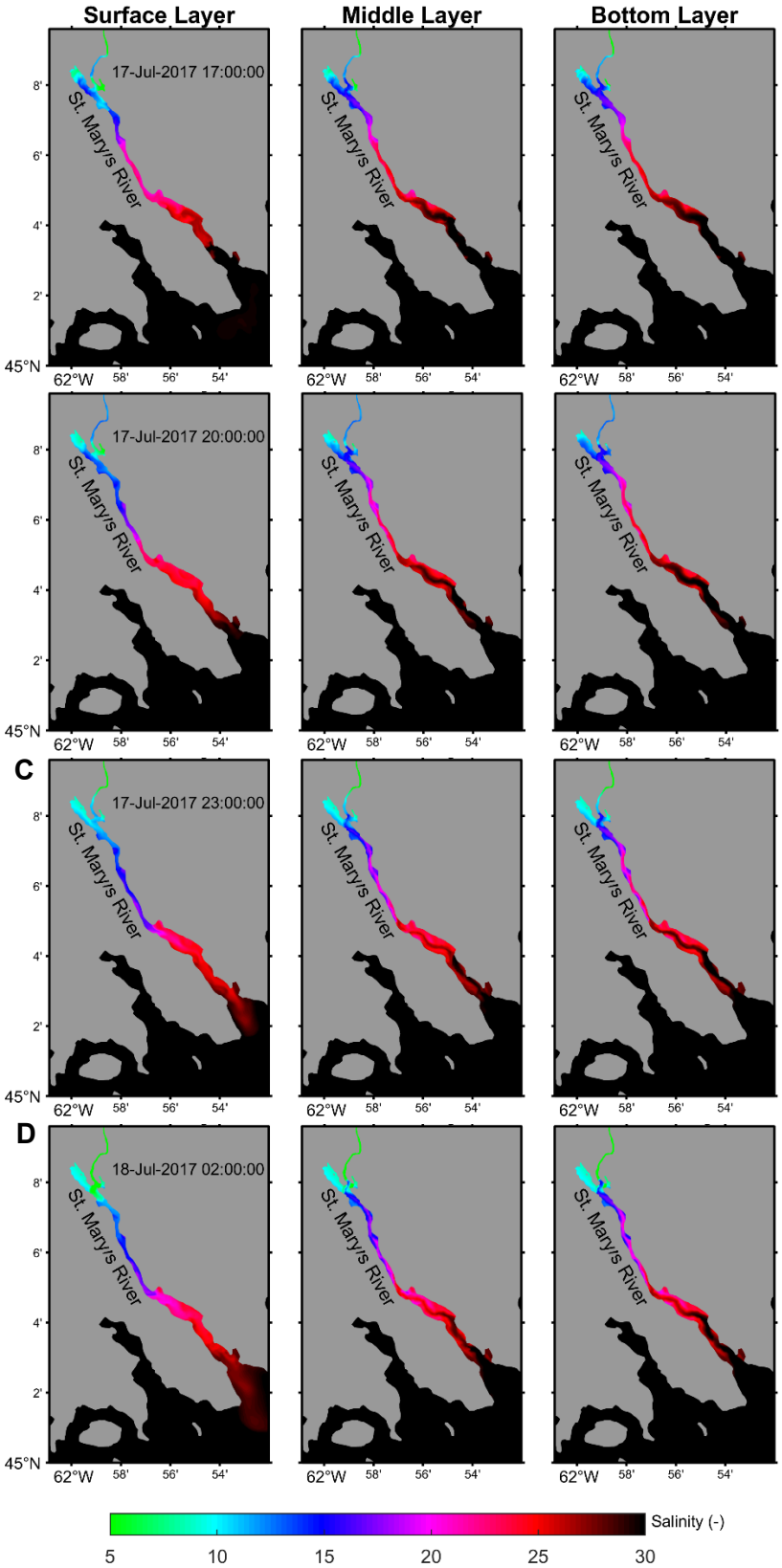

Figure 14. Salinity at the surface (left), middle layer (middle) and bottom later (right) at the start (A) and middle (B) of ebb tide and the start (C) and middle (D) of flood tide.

4 Sediment Dynamics

Sediment composition and dynamics are important for species community composition, benthic habitat provision, nutrient cycling, and water clarity. Sediment dynamics in the St. Mary's River estuary were characterized by examining bottom sediment grain size at stations along the estuarine gradient, deploying instruments to measure turbidity, and measuring water current and wave conditions at the mouth of the estuary.

4.1 Methods

4.1.1 Grain Size

To analyze sediment grain size distributions across the river estuary, sediment samples were collected at 43 stations of the 53 stations along the estuarine gradient, using plastic syringe cores (tips removed; 3-cm-diameter x 5-cm-long) in shallow water or a Petite Ponar grab (Wildco®) in deep water and in coarse sediments (see Figure 15 and Table A2 for numbered station locations). Sediment sampling coincided with drop camera survey locations (see Section 5 below). Sediments could not be sampled at some stations because of the hard bottom. Samples were prepared for Beckman Coulter Laser Diffraction Particle Size (LS 13 320) analysis by drying 10g of each sample at 60 °C for 48 h, then dry sieving the sample on a 2 mm sieve, followed by a 1 mm sieve, to remove the larger size classes (gravel, coarse sand). All sieved size class fractions were weighed and approximately 3 g of the < 1mm fraction was sub-sampled into 30 mL beakers. The sub-samples were then digested with approximately 10 mL of > 50% hydrogen peroxide (H_2O_2) at 60 ºC to remove all organic material. Prior to analysis, sediments were suspended in clean water and sonicated for 1 minute in a sonic bath to disaggregate the particles. The sediment samples were then rinsed with clean water into the sample chamber through a 2000 µm sieve to remove any existing large particles.

The Beckman Coulter LS 13 320, relies on the principles of light scattering to characterize the distribution of suspended sediment over 92 logarithmic channels over a size range from 0.375–2000 µm (Beckman Coulter 2011). Utilizing a Fourier lens and a set of ring detectors to measure the angle of refraction, the instrument generates a scattering pattern of particles within the solution. Each particle's scattering pattern is distinctive to its size; larger particles scatter at small angles, while smaller particles scatter at larger angles. The particle size distribution of the scattering pattern is determined by applying the Fraunhofer theory of light scattering. Particle size distributions are expressed as a weight or volume percent per channel. Grainsize statistics and method of moments (Folk and Ward 1957) are computed by the LS13320 software. For a complete description of the use and results expressed by the Beckman Coulter LS 13320 please see the manual (Beckman Coulter 2011).

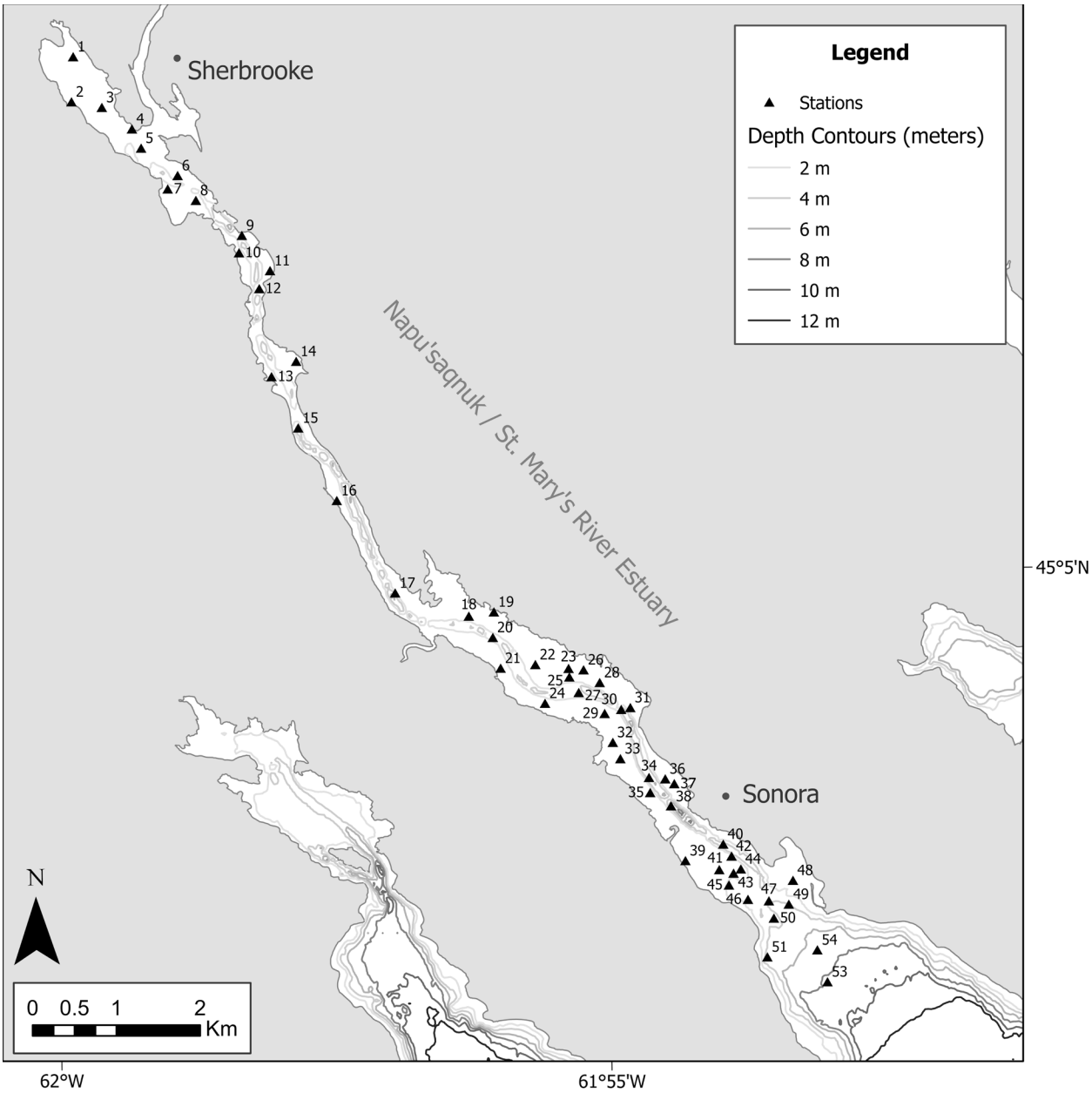

Figure 15. Bottom type survey and sampling stations within the estuary.

4.1.2 Turbidity

Turbidity (Tu) is a measure of the level of suspended particulate matter (SPM) in the water column and is commonly measured as nephelometric turbidity, an index of light scattering by suspended particles (Davies-Colley and Smith 2001). RBR Virtuoso turbidity sensors were deployed at three stations that encompassed the upper and middle to lower part of the estuary system, and slightly offshore (Figure 16), and recorded measurements for 2 minutes every 20 minutes from July to November 2023. Values are reported as average nephelometric turbidity unit (NTU) readings. The Tu sensor used as part of the RBR Virtuoso unit is a Seapoint, auto-ranging sensor, which maintains linearity over values from 0 to 1250 NTU with error less than 2%.

NTU values were converted to suspended sediment concentration. A lab calibration was performed to convert turbidity units into suspended sediment concentration, where bottom sediment from Station 35 was added to a large (20 L) blacked out bucket and stirred constantly while each of the Tu sensors made measurements. An 8-point calibration curve was created with suspended sediment concentrations from 0 to 1000 mg L^{-1} (Figure 17).

4.1.3 Current and Wave Measurements

A Teledyne Sentinel V, 1000 MHz, Acoustic Doppler Current Profiler (ADCP) was deployed to measure currents and waves from a bottom mounted frame that sits on the seabed (Figure 18). Current and wave measurements were recorded for 20 minutes every hour, and the average was used to produce hourly data. Current velocities are expressed in cm s^{-1} with data collected every 0.5 m in the vertical profile, with the first resolvable bin approximately 1.75 m off the seabed. The 1000 KHz, Sentinel V, as configured, can make measurements from roughly the seabed and extending 20 m above the bottom. The ADCP frame was deployed in roughly 15 m of water. Wave statistics (e.g. significant wave height or heights of the average of the largest 1/3 of the waves) were exported from Teledyne software into MATLAB for processing and presentation of results. Additional wave and temperature measurements were made with an RBR TD Duet sensor deployed on the ADCP frame (Figure 18). River discharge for the Saint Mary's River in m^3 s^{-1} was provided by Environment and Climate Change Canada (see Section 3.1.1).

4.2 Results and Discussion

The bottom sediment grain size from the stations in the St. Mary's River estuary ranged from muddy to coarse sands. Generally, the muddy bottom sediments became increasingly coarser with larger median diameters and greater sand fraction when moving from the upper to lower estuary (Table 1, Figure 19). However, bottom sediments with a large sand fraction could also be found throughout the river system at some stations (Table 1). The trapping of mud occurred in some of the mud flat stations located further up the estuary where energy in the system was lower, while stations located towards the mouth routinely had modal sizes well in excess of 100 µm with samples near the middle of the channel being coarse grained (Figure 19, Table 1). These results were similar to those shown by Loring et al. (1996) which reported muddy floc derived material on the mud flats close to eelgrass and sandy coarse samples in the channel.

The concentration of suspended sediments in the St. Mary's River estuary and just offshore ranged from a few mg L^{-1} up to almost 4000 mg L^{-1} at the offshore ADCP station (Figure 20). Typically, suspended sediment concentration (SSC) remained low during the summer with concentrations generally between 5 and 30 mg L^{-1} with values up to 80–90 mg L^{-1}. In fall, SSC generally increased with values on average about twice the ones observed in summer (Figure 20). SSC in the estuary at Station 7 and 35 had the largest increases during times of increased river discharge (Figure 21). SSC in the river over the time of this study remained under a few hundred mg L^{-1} (Figure 21). At the ADCP station, SSC remained high throughout most of the fall (< 250 mg L^{-1}). The Tu sensors deployed in the river and on the ADCP bottom mounted frame sampled the water near the seabed, especially in the offshore station where bottom nepheloid layers of water that contain high concentrations of suspended sediment are present. In addition, the calibration of the Tu sensors was completed using the bottom sediment at Station 35, which despite a significant sand fraction was not as coarse as in the vicinity of the ADCP station.

Thus, SSC would likely be lower if the specific bottom sediment at that station was used to convert NTU to SSC.

Current velocities at the ADCP station generally varied between 5 and 10 cm s^{-1} however, values of 20 cm s^{-1} and above did occur during large wave events (Figure 22). Although wave height was only collected at the offshore ADCP site, we looked at all three sites to evaluate if wave height corresponds to increases in suspended sediment concentration or if waves may have been a factor up in the estuary (Figure 23). Increases in significant wave height are often reflected by increases in bottom shear stress, which can increase the resuspension of bottom sediments into the water column (Figure 22, 23). Changes in significant wave height at the same time as changes in suspended sediment concentration indicate local resuspension, i.e., in the same area as the wave measurements (Jago et al. 2006, Law et al. 2014). Changes in suspended sediment concentration that occur after a wave event is indicative of the advection of sediment to the area (Jago et al. 2006, Law et al. 2014).

Table 1. Grain size data for 43 stations from St. Mary's River estuary. Method of moments statistics are based on Folk and Ward (1957) using the % values in the table for each grain size station and come directly from the analysis on the Beckman Coulter LS13320. Sample volume of 100 ml with minimum detection size of 0.375 micrometres (µm) and a maximum detection size of 2000 µm.

Sample ID	Mean	Median	Mean / Median Ratio	Mode	Std Dev.	Variance	Coeff. of Var.	Skew-ness	Kurt -osis	% < 5 Size µm	% < 16 Size µm	% < 25 Size µm	% < 50 Size µm	% < 75 Size µm	% < 84 Size µm	% < 95 Size µm
1	307.1	296.6	1.0	324.4	190.2	36,190.1	62.0	0.5	0.3	9.51	100.39	188.37	296.57	418.08	486.69	648.44
2	14.1	10.6	1.3	14.9	11.9	141.8	84.7	0.9	0.0	0.85	2.61	4.39	10.57	21.21	27.69	38.24
3	15.3	11.3	1.4	34.6	13.2	174.0	85.9	0.9	0.0	0.82	2.64	4.55	11.29	23.7	30.66	41.86
4	87.4	41.1	2.1	45.8	157.2	24,698.8	179.8	4.0	18.7	1.56	8.15	16.11	41.08	80.06	125.66	383.69
5	136.4	124.8	1.1	185.4	122.7	15,055.5	89.9	1.4	2.5	2.52	13.03	31.48	124.84	196.09	231.57	384.07
6	122.9	108.9	1.1	203.5	103.4	10,687.0	84.1	1.1	2.2	2.63	14.19	33.03	108.86	191.99	224.87	292.99
7	28.6	22.9	1.3	41.7	24.7	611.5	86.3	0.8	-0.1	0.99	3.83	7.15	22.87	44.59	55.7	77.32
8	317.7	283.4	1.1	324.4	247.0	61,002.6	77.7	1.0	1.1	7.31	44.97	135.21	283.37	439.82	545.12	808.64
9	42.3	37.9	1.1	50.2	35.5	1,262.4	84.1	1.6	4.4	1.18	6.97	14.59	37.89	58.77	69.97	104.39
10	33.1	32.2	1.0	50.2	23.3	542.0	70.4	0.3	-0.8	1.07	5.68	11.56	32.2	50.59	58.57	73.41
11	34.5	33.2	1.0	45.8	24.4	595.5	70.7	0.4	-0.6	1.2	6.24	12.62	33.25	51.79	60.77	77.97
13	58.8	54.0	1.1	66.4	42.0	1,760.6	71.4	0.7	0.2	2.02	12.84	26.63	53.95	82.52	100.14	140.78
14	25.2	21.8	1.2	38.0	19.9	394.0	78.6	0.7	-0.3	1.06	4.21	7.84	21.81	38.89	47.06	62.59
15	38.4	39.0	1.0	55.1	25.0	623.3	65.0	0.1	-0.9	1.29	6.96	16.19	38.99	57.26	65.25	79.79
16	57.1	53.7	1.1	60.5	37.9	1,434.5	66.3	0.5	-0.1	2.11	15.08	29.17	53.67	80.35	95.88	128.35
17	72.9	69.8	1.0	80.1	41.9	1,756.9	57.5	0.3	-0.3	3.85	30.89	44.34	69.81	100.61	116.71	147.01
18	89.0	86.8	1.0	105.9	47.4	2,249.8	53.3	0.2	-0.5	7.36	41.3	55.54	86.84	121.96	139.56	172.07
19	29.4	29.7	1.0	45.8	19.0	361.0	64.6	0.1	-0.9	1.1	6.19	12.62	29.66	44.14	50.11	60.8
20	142.0	148.5	1.0	153.8	55.9	3,120.8	39.3	-0.7	0.4	12.63	97.66	117.01	148.55	179.16	193.46	222.69
21	69.1	73.9	0.9	105.9	33.3	1,108.1	48.2	-0.5	-0.8	4.52	30.83	47.07	73.92	97.22	103.7	113.2
22	78.1	74.3	1.1	96.5	47.8	2,280.8	61.1	0.4	-0.4	3.5	27.43	43.6	74.31	110.63	128.71	162.76
23	62.0	61.3	1.0	87.9	37.1	1,374.2	59.8	0.1	-0.7	2.45	18.74	34.87	61.29	89.01	101.48	124.62

Sample ID	Mean	Median	Mean / Median Ratio	Mode	Std Dev.	Variance	Coeff. of Var.	Skew-ness	Kurt -osis	% < 5 Size µm	% < 16 Size µm	% < 25 Size µm	% < 50 Size µm	% < 75 Size µm	% < 84 Size µm	% < 95 Size µm
24	70.9	70.0	1.0	116.3	37.0	1,371.2	52.2	-0.1	-0.8	4.59	32.43	44.99	69.98	100.87	113.46	129.84
25	113.9	117.3	1.0	153.8	55.8	3,115.5	49.0	-0.1	-0.7	11.84	53.47	71.97	117.3	156.02	172.53	202.46
26	40.5	41.0	1.0	55.1	25.5	651.1	62.9	0.1	-0.8	1.34	9.09	19.44	41.02	59.33	67.58	82.96
27	186.9	183.0	1.0	203.5	88.3	7,804.8	47.3	1.0	3.7	34.07	115.14	137.01	183	232.78	257.19	312.3
28	57.1	57.5	1.0	96.5	30.3	918.5	53.0	-0.1	-0.8	3.46	23.98	36.19	57.46	80.5	90.95	105.77
29	67.9	64.5	1.1	72.9	39.0	1,524.3	57.5	0.3	-0.3	3.83	28.98	41.03	64.46	93.77	109.04	137.95
31	85.1	87.0	1.0	127.7	42.9	1,836.4	50.3	-0.2	-0.8	6.64	39.1	53.66	86.96	119.74	131.72	150.75
32	45.4	44.2	1.0	55.1	29.1	846.7	64.0	0.3	-0.6	1.58	11.18	22.62	44.2	65.88	76.47	96.52
33	43.0	43.5	1.0	60.5	26.7	711.5	62.0	0.1	-0.8	1.5	10.03	21.26	43.5	62.93	71.52	87.2
35	92.9	95.4	1.0	140.1	47.2	2,224.1	50.8	-0.2	-0.8	7.82	41.75	57.36	95.39	130.57	143.84	165.79
36	75.7	74.1	1.0	96.5	41.1	1,691.5	54.3	0.1	-0.5	4.81	33.71	47.32	74.13	104.85	119.05	145.34
37	76.2	73.3	1.0	116.3	44.2	1,950.0	57.9	0.2	-0.7	4.13	30.04	43.74	73.29	109.07	124.41	151.82
38	139.5	125.8	1.1	168.9	102.2	10,450.5	73.3	1.6	7.4	6.21	42.42	65.33	125.75	194.68	229.85	309.07
39	140.5	146.6	1.0	153.8	44.6	1,993.2	31.8	-1.1	1.6	38.17	105.87	120.19	146.58	170.87	181.44	200.9
40	158.1	115.5	1.4	153.8	184.3	33,982.3	116.6	2.8	9.8	3.06	22.28	51.83	115.46	183.4	227.56	567.86
43	229.7	177.4	1.3	153.8	182.8	33,409.6	79.6	1.9	5.5	23.51	88.77	115.35	177.38	291.58	382.6	582.75
45	31.3	15.6	2.0	50.2	34.5	1,191.0	110.3	1.3	0.9	0.69	2.51	5.06	15.64	49.02	67.94	106.52
47	177.7	184.1	1.0	203.5	78.4	6,141.0	44.1	-0.4	-0.2	17.46	101.29	132	184.09	232.39	254.72	298.89
48	98.4	100.6	1.0	116.3	46.0	2,111.8	46.7	-0.1	-0.5	11.65	50.76	66.94	100.59	131.16	145.31	172.65
51	821.9	910.4	0.9	993.6	413.9	171,299.0	50.4	-0.6	-0.5	27.76	185.15	634.45	910.37	1,113.08	1,207.53	1,380.96
53	102.0	106.0	1.0	116.3	37.4	1,401.9	36.7	-0.6	0.2	26.03	66.73	81.01	106.03	128.87	138.98	156.56

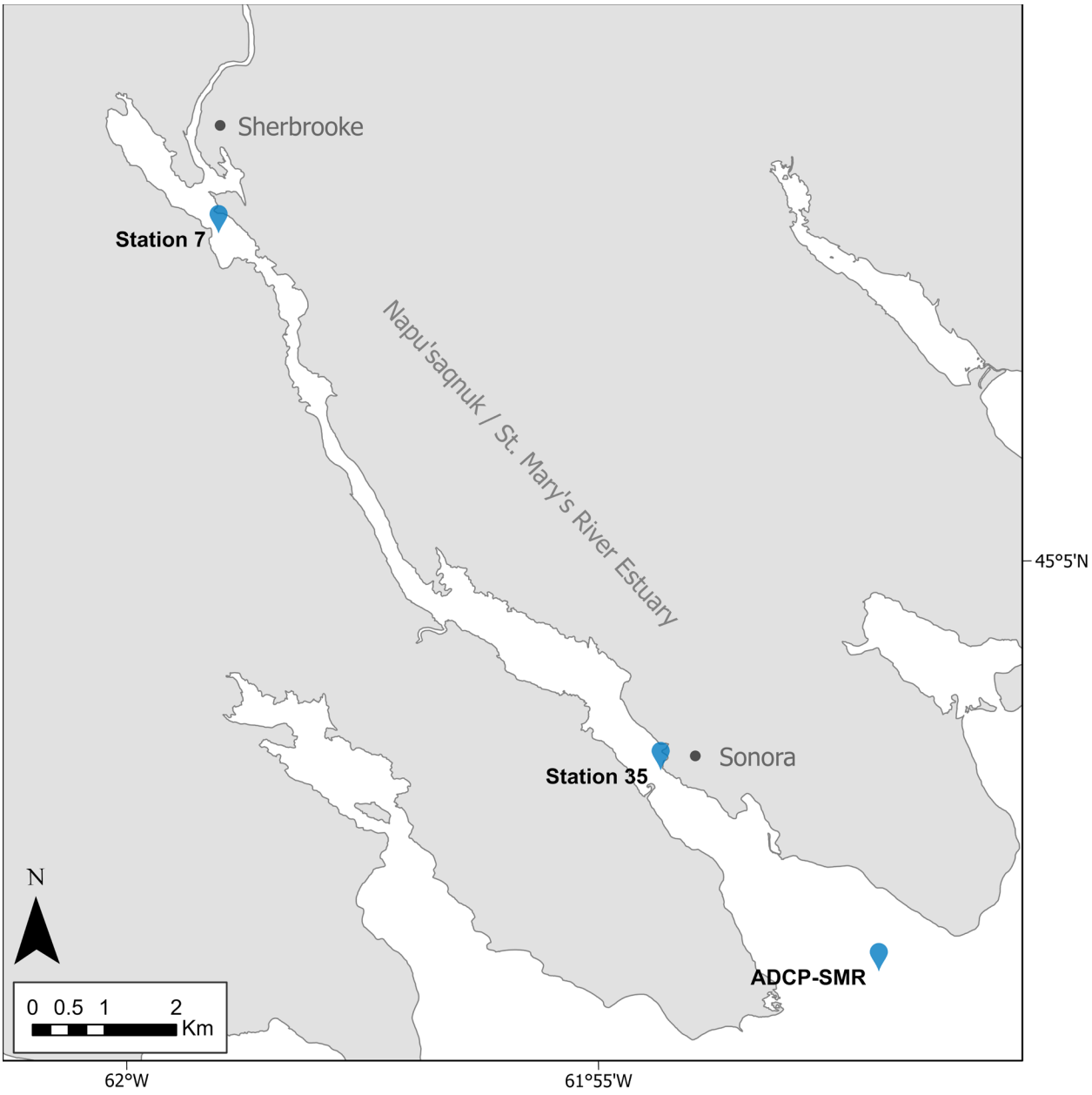

Figure 16. The St. Mary's River estuary with stations of interest marked with a blue pin. At station 7 and 35, RBR turbidity (i.e. Tu) sensors were deployed to measure suspended sediment concentration. At station ADCP SMR, a Teledyne 1000 KHz Acoustic Doppler Current Meter (ADCP) was deployed from a bottom mounted frame looking upward with waves package. The instrument frame also contained an RBR Tu sensor and RBR Duet TD wave sensor.

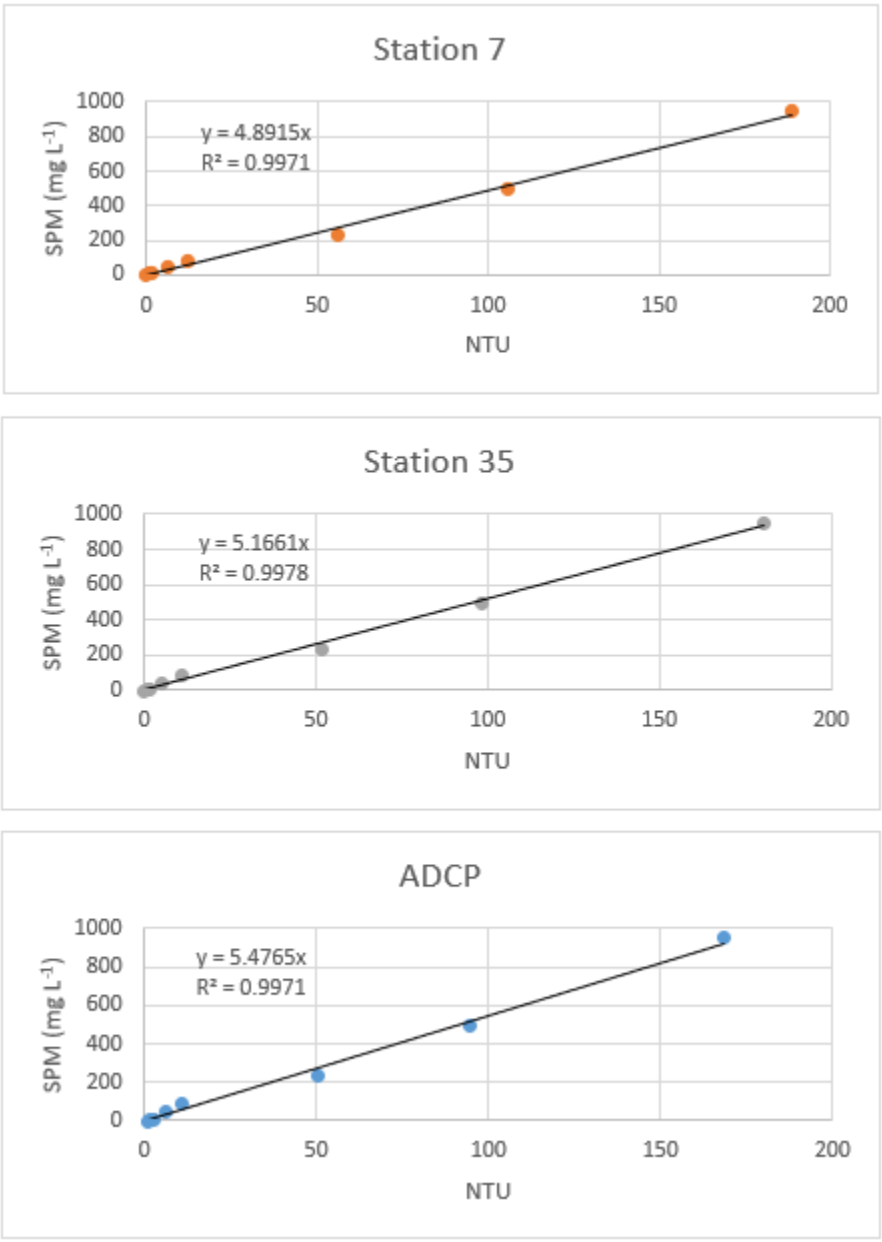

Figure 17. RBR Tu (turbidity) sensor calibration curve from each of the 3 stations in which they were deployed; Station 7, Station 35, and ADCP. RBR Tu sensors were all calibrated using sediment from Station 35 over a range of concentrations from 0 to roughly 1000 mg L^{-1}. The sensors measured in nephelometric turbidity unit (NTU) and values were converted to concentration in mg L^{-1}.

Figure 18. Picture of the ADCP bottom mounted frame place at station ADCP SMR just offshore of the mouth of St. Mary's River estuary. The blue top instrument is the ADCP. The Tu sensor is pointed vertical in white with RBR Virtuoso written on the pressure case. The small horizontal yellow instrument on the top bar of the ADCP frame is the RBR Duet TD wave gauge.

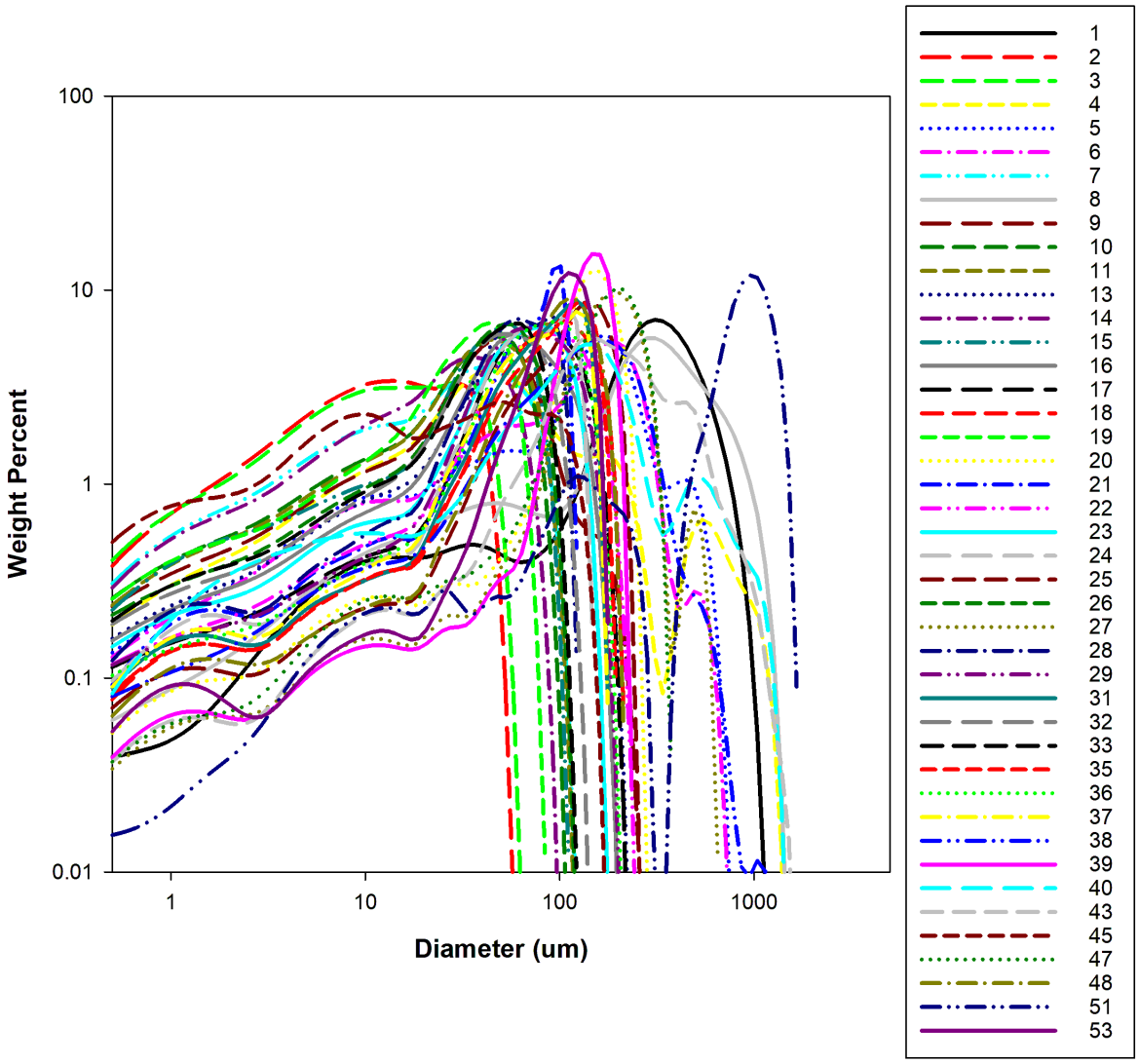

Figure 19. Sediment grain size distributions across the St. Mary's River estuary in 2023 and measured on a Beckman Coulter Laser LS 13320. The graph is a log-log plot of diameter versus weight percent.

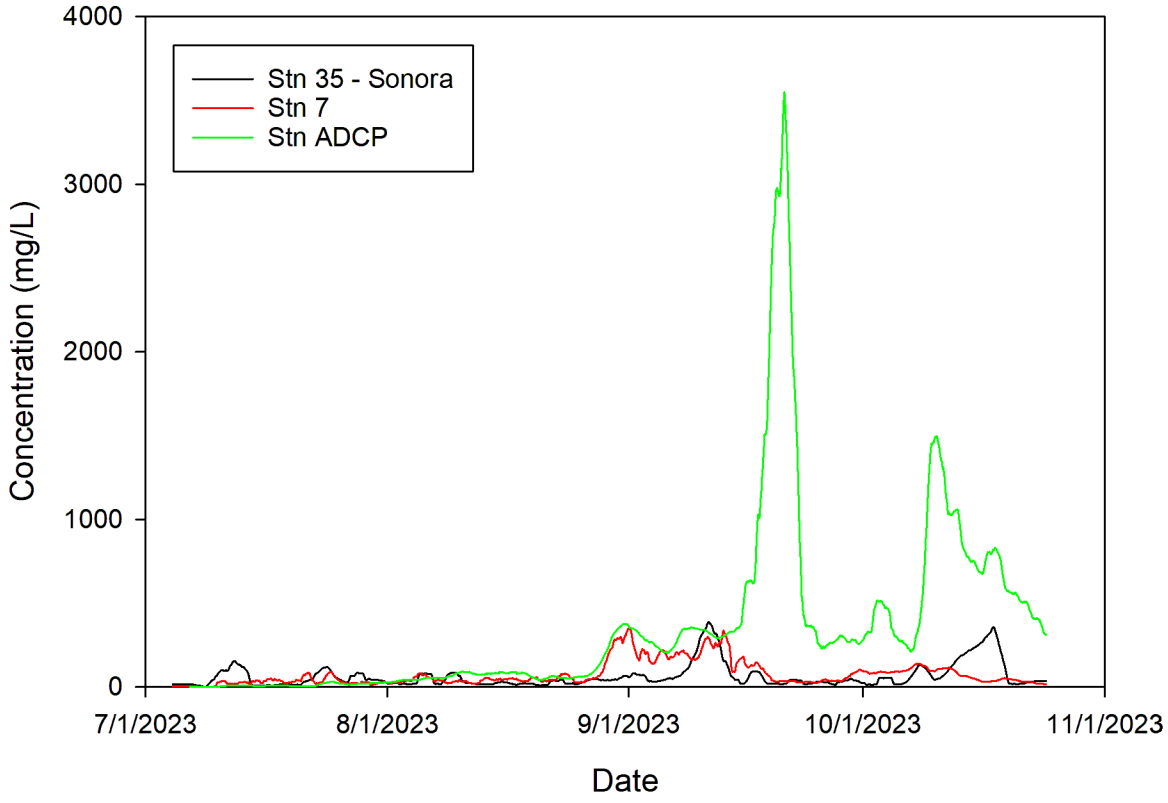

Figure 20. Suspended sediment concentration (mg L^{-1}) from July to November 2023 at three locations across the St. Mary's River estuary (see Figure 16). The highest concentrations (up to 4 g L^{-1}) were observed during an event at the ADCP positioned just offshore. Concentration of suspended sediments in the river at stations 7 and 35 were under 400 mg L^{-1}. Concentration increased at all stations during fall 2023.

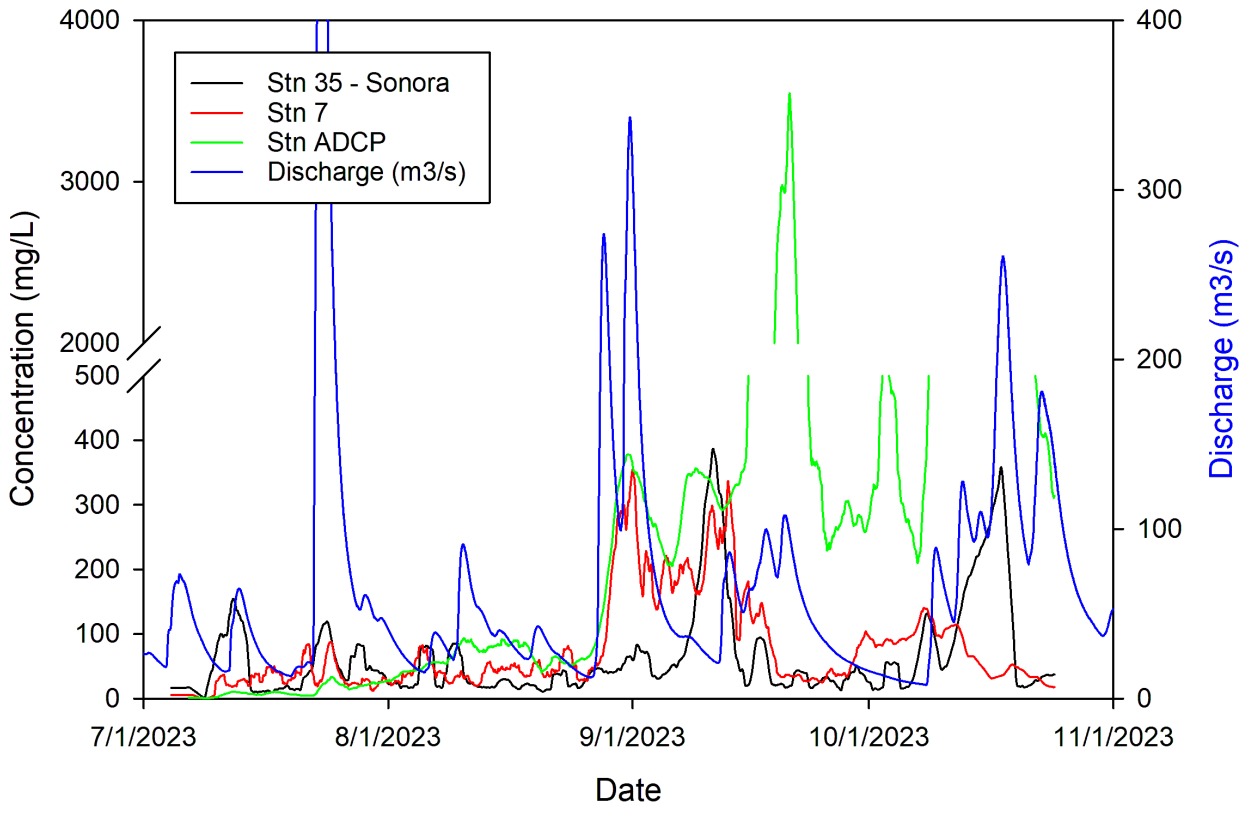

Figure 21. Suspended sediment concentration versus river discharge over the time period the Tu sensors were deployed (July to November 2023). River discharge ($m^3\ s^{-1}$) is gauged by Environment and Climate Change Canada. Suspended sediment concentration at stations 7 and 35 generally increased during times of increased river runoff as seen by spikes in discharge (blue line) and corresponding station data (red, green and black lines).

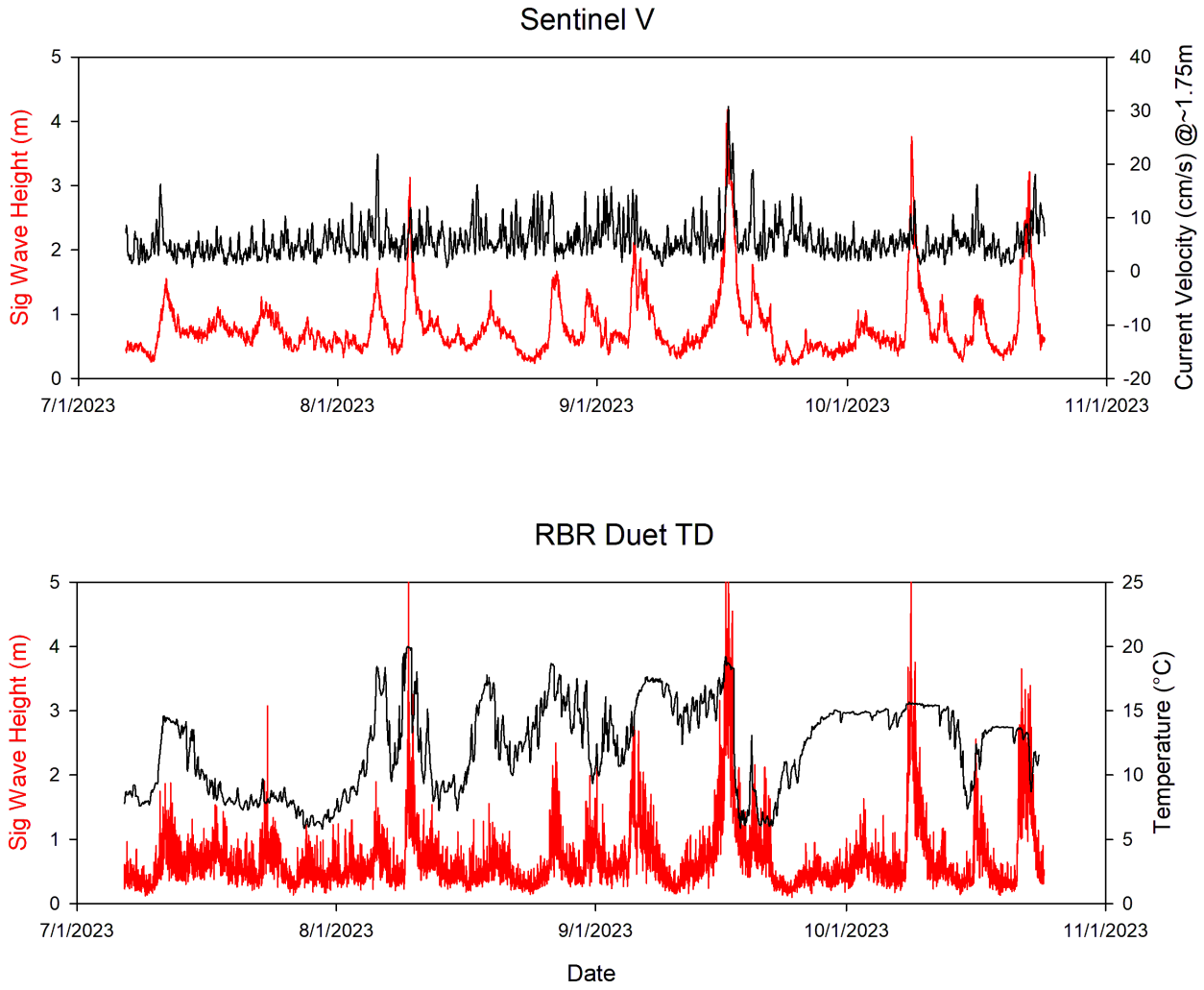

Figure 22. Significant wave height in metres and current velocity in cm s^{-1} at 1.75 m off the seabed from the Acoustic Doppler Current Profiler (ADCP) over the time period from roughly July to November, 2023 (top). Significant wave height and temperature (°C) from the RBR Duet wave gauge sensor that was mounted on the ADCP (bottom). Wave heights from both the ADCP and RBR wave gauge are in good agreement. The temperature record shows drops in temperature of close to 10 °C, corresponding to the largest wave events and likely coastal upwelling events.

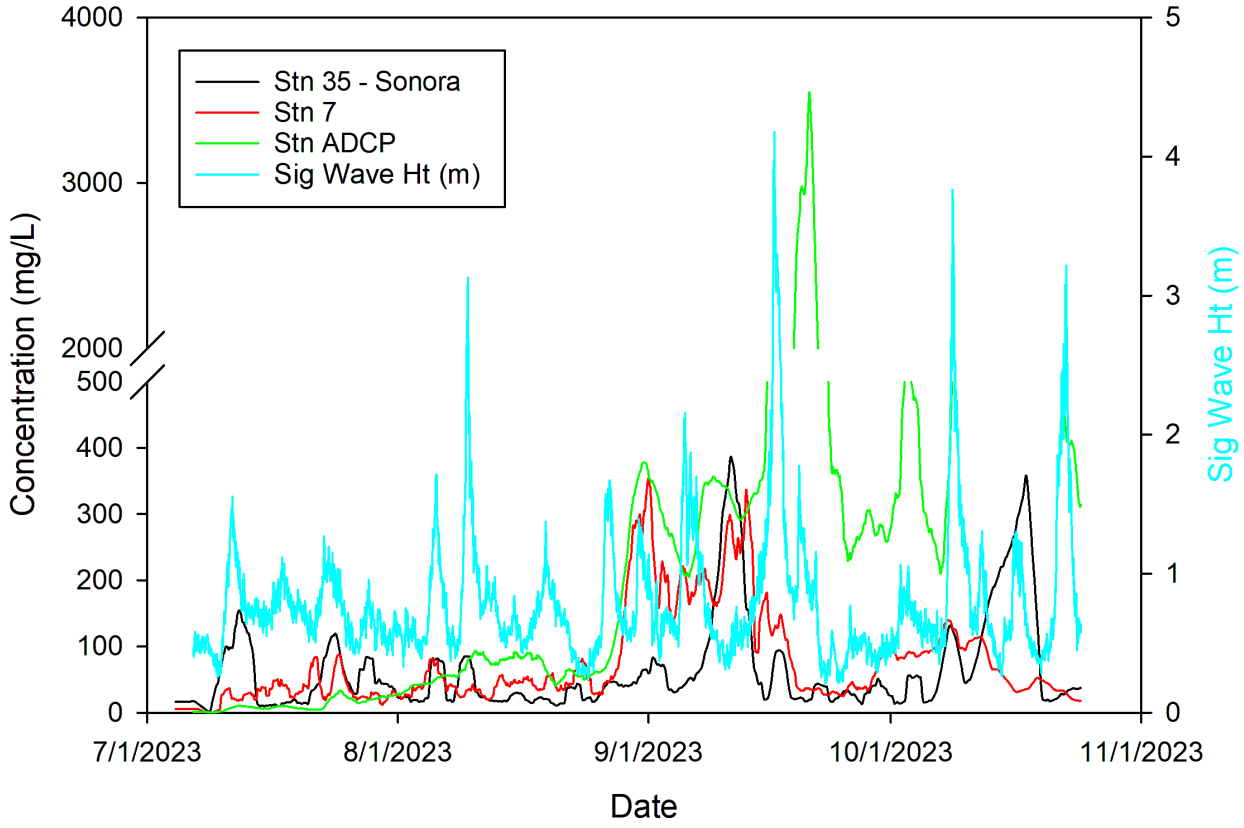

Figure 23. Suspended sediment concentration versus significant wave height from the Acoustic Doppler Current Profiler (ADCP) in July to November 2023. Sharp increases in sediment concentration at the ADCP site generally corresponded with increases in wave height which likely caused the resuspension of sediment locally to the ADCP and continued to increase from local resuspension and advection. Sediment concentration in the river stations sometimes corresponded to changes in wave height at the ADCP location which would be indicative of wind waves at those locations playing a role in the resuspension and transport of sediment in the river stations.

5 Macrophyte Communities

A number of aquatic macrophytes, including eelgrass, other seagrass species, and macroalgae are found throughout the St. Mary's River estuary. These habitats are known to provide key ecosystem services, including maintenance of fisheries, carbon sequestration, water filtration, coastal protection, and sediment stabilization (Barbier et al. 2011; Cotas et al. 2023).To better describe macrophyte prevalence, distribution, and ecological contribution, benthic habitat surveys were conducted along the estuarine gradient using drop cameras, an in-depth seagrass condition survey at two representative stations in the upper and lower estuary, and an analysis of seagrass plant morphology.

5.1 Methods

5.1.1 Field surveys

Drop camera surveys

To characterize macrophyte communities and their distribution in the St. Mary's River estuary, drop camera surveys were conducted at 53 stations (Figure 15, Table A2). Station locations were predetermined and spanned the length of the estuary. Stations accounted for environmental heterogeneity associated with depth (0.5 m–8.5 m) and salinity gradients (see Section 3), both of which were found to later correlate with turbidity and variation in wave exposure (see Section 4). Surveys were conducted on June 13 and 16, July 6, and October 24, 2023. The camera system used to record bottom video at each station consisted of a GoPro® HERO7 camera housed in a SPOT X™ Pro Squid underwater video system (see O'Brien et al. 2022). At each station, the camera was lowered to the bottom and video footage was recorded while the boat passively drifted in the wind and current. A handheld GPS was used to track the boat's location during each video transect. Start and end coordinates of each transect were recorded. During the video recording, the dominant bottom types along the transect were recorded based on field observations, as well as the water depth from the vessel sounder. Video transects varied in length from 3.12 m to 61.8 m and typically recorded 2 minutes of video. Videos were collected in 2.7 k resolution at 30 frames per second, and stored for later image extraction and analysis.

At each station sediment samples were collected to characterize particle size (see Section 4) and organic content. Sediments were collected using plastic syringe cores (tips removed; 3-cm-diameter x 5-cm-long) in shallow water and in soft sediments, or a Petite Ponar grab (Wildco®) in deep water and in coarse sediments. Seagrass plants were also collected when present for further morphological and biomass measurements. Plants were carefully uprooted by hand to ensure above and below-ground material remained intact. Plant and sediment samples were stored in plastic bags and frozen at -20 °C for approximately 1–3 months prior to laboratory processing.

Seagrass condition surveys

In addition to the drop camera surveys, in-depth seagrass condition surveys were also conducted at stations 7 and 35. These stations were selected as they had significant seagrass cover, including both widgeongrass (*Ruppia maritima*) and eelgrass (*Zostera marina*), and represented the upper and lower reaches of the estuary, respectively. Ten quadrats at each station were haphazardly distributed at approximately the same depth and sampled. Quadrats were at least 10 m apart and 2 m from any seagrass-bare sediment interface. Sampling was

conducted using snorkeling on July 13, 2023 during mid to low tide. At each quadrat, water depth was recorded, and the number of eelgrass vegetative and reproductive shoots were counted within a 0.25 × 0.25 m and 0.5 x 0.5 m quadrat, respectively, and widgeongrass vegetative shoots, were counted within a 0.25 x 0.25 m quadrat. Three mature eelgrass vegetative shoots with 5 cm or more live rhizome and three sections of mature widgeongrass shoots with connected belowground tissues were collected. A hand corer (10.8 cm diameter × 12 cm depth) was also used to collect above- and belowground plant biomass. Cores were placed in a mesh bag (10-mm-diameter holes) and rinsed in salt water to remove sediments. Plants and biomass samples were frozen at -20 °C for approximately 3 months prior to laboratory processing.

5.1.2 Data and sample processing

Image analysis

Several images were extracted from each video transect, with the exact number determined by the transect length. Specifically, the average speed (m/s) of the camera drift was calculated from the tracked drift distance (m) and video length (s) and images were extracted at 4m intervals. Images were analyzed to determine the percent cover of different bottom types using the cloud-based Bio-Image Indexing and Graphical Labelling Environment software (BIIGLE 2.0; Langenkämper et al. 2017, https://biigle.de). Each image was overlaid with a 10 x 10 grid of equally spaced points (n = 100). The bottom cover type intersecting each point was categorized and annotated. Cover categories included eelgrass, other seagrass species (i.e., widgeongrass, and horned pondweed *(Zannichellia palustris*)), kelps (Laminariales), other macroalgae (*Fucus*, *Ascophyllum nodosum*, coralline algae, filamentous, foliose and/or cord-like macroalgae), turf algae, detritus (seagrass, algae, or unknown-source), epiphytes, and sediment (bare sand/mud or rock). Categories were later grouped into seven major bottom type categories for data visualization (see Figure 24). Percent bottom cover of each type was calculated as the number of visible and identifiable annotated points for that type, divided by the total number of points (i.e., 100, though in some cases totals were reduced where unknown points were omitted) multiplied by 100. Mean percent cover by bottom type was then calculated for each station by averaging percent cover values across the multiple transect images (n = 2–8).

Sediment analysis

Sediment samples were analyzed to determine organic content at each drop camera station and sediment particle size distribution data (Section 4) was further summarized for biologically meaningful size class fractions. To determine the percent organic matter within sediments, 1g of each sample was dried at 60 °C for 48 h, weighed to quantify total dry mass, combusted at 500 °C for 6 h, and reweighed to determine ash mass (Luczak et al. 1997, Wong 2018). Percent organic matter content was calculated as the ash mass divided by the initial dry mass, subtracted from 1 and multiplied by 100%.

Sediment particle size data obtained from the laser (Table 1) and dry sieving were used to calculate the percent fractions of gravel (≥ 2000 µm), sand (≥ 62 µm–2000 µm), silt (≥ 3.9 µm–62 µm) and clay (< 3.9 µm), where:

$$P_i = 100\% \; x \; \frac{DM_i}{DM_{total}} \quad [Eq.\ (1)]$$

Here P_i is the percent of a sediment size class i from the total sample, DM_i is the dry mass (DM) of size class *i* and DM_{total} is the total dry mass of sample (summed across all particle size classes). Percent sand included data for sediment particles from the 1—2 mm sieved fraction as well as particles > 1mm that were detected by the laser.

Plant morphology and biomass

In the laboratory, seagrass samples were thawed, and plants identified to species (*Zostera marina, Ruppia maritima*, and others, namely, *Zannichellia palustris*). Eelgrass and widgeongrass were further processed for morphology and biomass. For eelgrass, leaf length was measured as the distance from the insertion point to the leaf tip. Leaf width was measured midway along each leaf. Leaves were separated from the shoot, dried individually at 60 °C for 24 h, and then weighed for individual leaf biomass. Leaf biomass per shoot, considered aboveground biomass (AGBM) was calculated by summing across all leaf biomass in that shoot. Rhizome length was measured from the insertion point to rhizome node three (including rhizome internodes 1–3). Rhizome width was measured laterally in the middle of the third rhizome internode. The rhizome section from the insertion point to node three (including any attached roots and rootlets), considered belowground biomass (BGBM), was dried at 60 °C for 48 h and weighed for the belowground dry mass of the shoot.

For widgeongrass, a 'plant' was considered a section of continuous rhizome with a number of individual shoots attached. Shoots were defined by their emergence from a single node or point of attachment on the rhizome, and the number of shoots per plant were counted. The number of leaves per shoot were determined by counting all leaves (broken and full) that were contained within an individual shoot (i.e., emerged from a single node). Maximum leaf length for each shoot was measured as the distance from the node (attachment point on the rhizome) to the tip of the longest leaf. To provide an index of "bushiness", branching shoots were identified as having aboveground nodes with alternately branching leaves, and the proportion of branching shoots per rhizome length was determined as the number of branching shoots divided by the total number of shoots processed at a given station. The longest continuous section of rhizome length, omitting any shorter branching rhizomes, was measured. The aboveground and belowground components of each plant were isolated, collectively dried at 60 °C for 24 h, and weighed. For plants that had more than three shoots, a minimum of three shoots per plant were dried and weighed separately to be able to determine individual shoot weights. The ratio of aboveground to belowground (AGBG) biomass per plant was determined as the sum of the biomass for all individually weighed shoots divided by the full rhizome section.

Biomass core samples collected from each quadrat in the condition survey were thawed and separated into live aboveground and belowground biomass components for eelgrass and widgeongrass. Tissues were dried at 60 °C for 48 h and weighed and the ratio of above to belowground biomass determined. Leaf area index (LAI), leaf area (m^2) per bottom area (m^2) was determined for eelgrass in each quadrat by multiplying the mean total leaf area (one-sided) per shoot by the shoot density.

5.2 Results and Discussion

5.2.1 Benthic habitat characterization

Habitat-forming aquatic macrophytes including seagrasses (various species), kelps and other macroalgae were dominant in various sections of the estuary (Figure 24, Table B1). Seagrasses

were typically located on the elevated flats and shallow waters adjacent to the main channel. 51% of camera station surveys outside of the main channel contained seagrass, with 38% being eelgrass (*Zostera marina*) and 20% being a mix of other seagrass species (widgeongrass (*Ruppia maritima,* and horned pondweed *(Zannichellia Palustris*)). Eelgrass was the dominant seagrass species in the middle to lower reaches of the estuary, including the Sonora flats (stations 23, 24, 26, 28, 29, 32, 33, and 35; Figure 24C, D). At these stations, eelgrass cover ranged from 39 to 98% of the bottom. Generally, more opportunistic seagrass species were observed in the upper estuary (stations 1–7; Figure 24B), where widgeongrass was dominant while horned pondweed was also observed. These seagrasses typically had a patchy distribution, covering 1.9 to 52% of the bottom. Some eelgrass was also observed at the upper estuary stations (stations 6 and 7; Figure 24B) although percent cover was only 1.6 to 32%. The distribution of eelgrass observed along the estuary is typical given the gradients in temperature, salinity, turbidity, depth, and sediment type (see Sections 3 and 4). While eelgrass can survive in a broad salinity range (5–35 PSU (practical salinity units)), thresholds for optimal growth and reproduction are typically 15 PSU and above. Extended exposure to particularly low salinities (5 PSU), such as the freshwater discharging from the river in the upper estuary, can severely reduce seedling germination and shoot survival (Lee et al. 2007, Nejrup and Pedersen 2008). Eelgrass was also likely limited in the upper reaches by high concentrations of coloured dissolved organic matter (CDOM; see Section 6.1) and sediment in the water, which reduced bottom light. Eelgrass typically requires a minimum of 9 to 12 (shallow beds) or 6.4 to 9 (deeper beds) hours of daily photosynthetically saturating light (Lee et al. 2007), and the high CDOM and suspended sediment concentration (SSC) measured (see sections 4 and 6.1) suggest this was likely not always available. Furthermore, warmer water temperatures in the upper estuary from river discharge, shallow depths, and reduced flushing at some locations (stations 1 to 4) likely favored growth of the more temperature tolerant widgeongrass rather than eelgrass (Moore et al. 2014, Richardson et al. 2018, Hensel et al. 2023).

Throughout the estuary, bottom cover at stations in the deeper, more dynamic, main channel was characterized mainly by bare sand/mud or rock and the absence of seagrasses. While eelgrass can inhabit a range of water flows and has more significant belowground biomass that allows stronger plant anchoring compared to widgeongrass, higher flow rates cause more patchy and fragmented eelgrass beds (Fonseca and Bell 1998, Fonseca et al. 2002). Field studies have shown that seagrass percent cover (%) declines with increasing current speeds, where measured current speeds above 40 cm s^{-1} correlated with areas of zero seagrass cover (Fonseca et al. 1998). Although water currents could not be measured directly in the main channel, observations during field work suggest flows in the deep channels were upwards of 0.65 m s^{-1}, which would not support seagrass presence. While turf algae and macroalgae can tolerate more dynamic conditions and high water flows, these were also not observed in the main channel. Rather, turf algae were sporadically present throughout the estuary, typically co-occurring with areas of bare sand/mud and/or detritus and epiphytes. Kelp and other macrophytes were only found at the mouth of the estuary (stations 41-54) in full marine waters where sediments were coarser and more rocky, providing hard substrates for macrophyte attachment (Figure 24D).

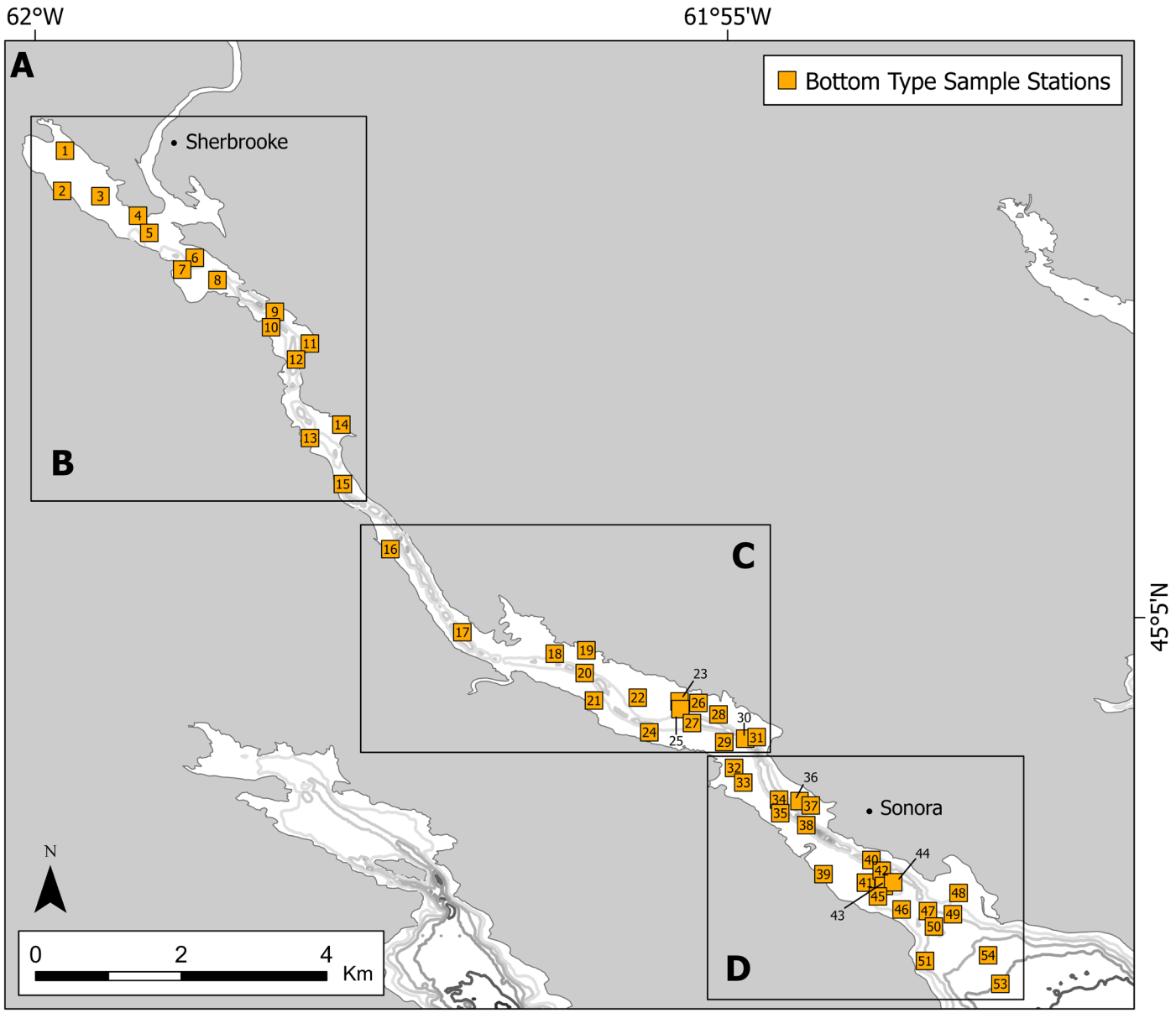

Figure 24A. Drop camera survey station locations across the St. Mary's River estuary (**A**) and outlines of inset areas in the (**B**) upper, (**C**) middle and (**D**) lower regions of the estuary.

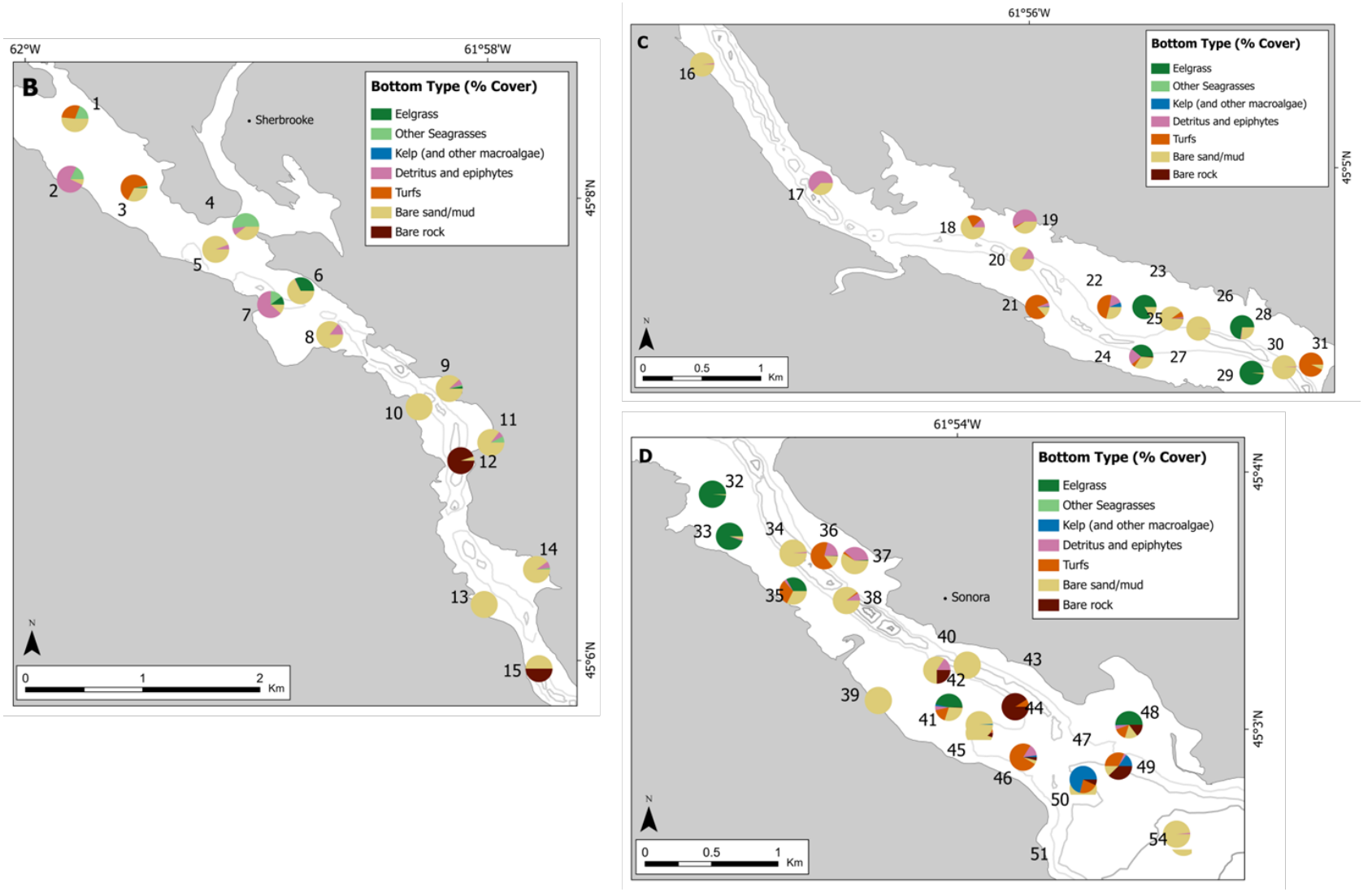

Figure 24B. Percent (%) cover of bottom type characterized through drop camera surveys at stations spanning the (**A**) St Mary's River estuary, (**B**) upper, (**C**) middle and (**D**) lower regions. Numbers on maps correspond to surveyed station ID numbers.

5.2.2 Sediment type

The percent sediment clay and silt content, collectively categorized as mud (< 63 µm), ranged from 3–98% in the St Mary's River estuary (Figure 25A, Table B2). Percent organic matter sediment content ranged from 0.37–17.9%, with station 2 (upper estuary) and 51 (lower estuary) containing the maximum and minimum organic content, respectively (Figure 25B). There was a general trend of increasingly sandy sediments (i.e., higher particle size) with lower organic content when moving from the upper estuary to the open ocean (Figure 25). Organic content decreased with percent sand content as expected (linear regression, $R^2 = 0.25$, $F_{1, 36} = 11.87$, $p = 0.0015$). Gravel was sporadically observed, only exceeding 1% at six stations throughout the estuary (stations 5, 6, 21, 40, 45 and 51, Table B2).

The absence of eelgrass in highly organic muddy sediments (stations 2 and 3) is not surprising, as high sediment sulphide concentrations are often found in these conditions. Although eelgrass can oxidize sulphides in its tissues or by oxygen leakage around its roots, these processes can be inhibited in low light and high temperature conditions (Koch et al. 2007). Eelgrass plants have a lower threshold tolerance towards sulfide compared to widgeongrass, likely given differences in species' root structure and permeable surface areas for oxygen loss (Pedersen and Kristensen 2015). Chronic exposure to these high sulfide concentrations can ultimately reduce eelgrass growth and survival, and plants are often not found in these sediment conditions (Goodman et al. 1995, Pedersen and Kristensen 2015).

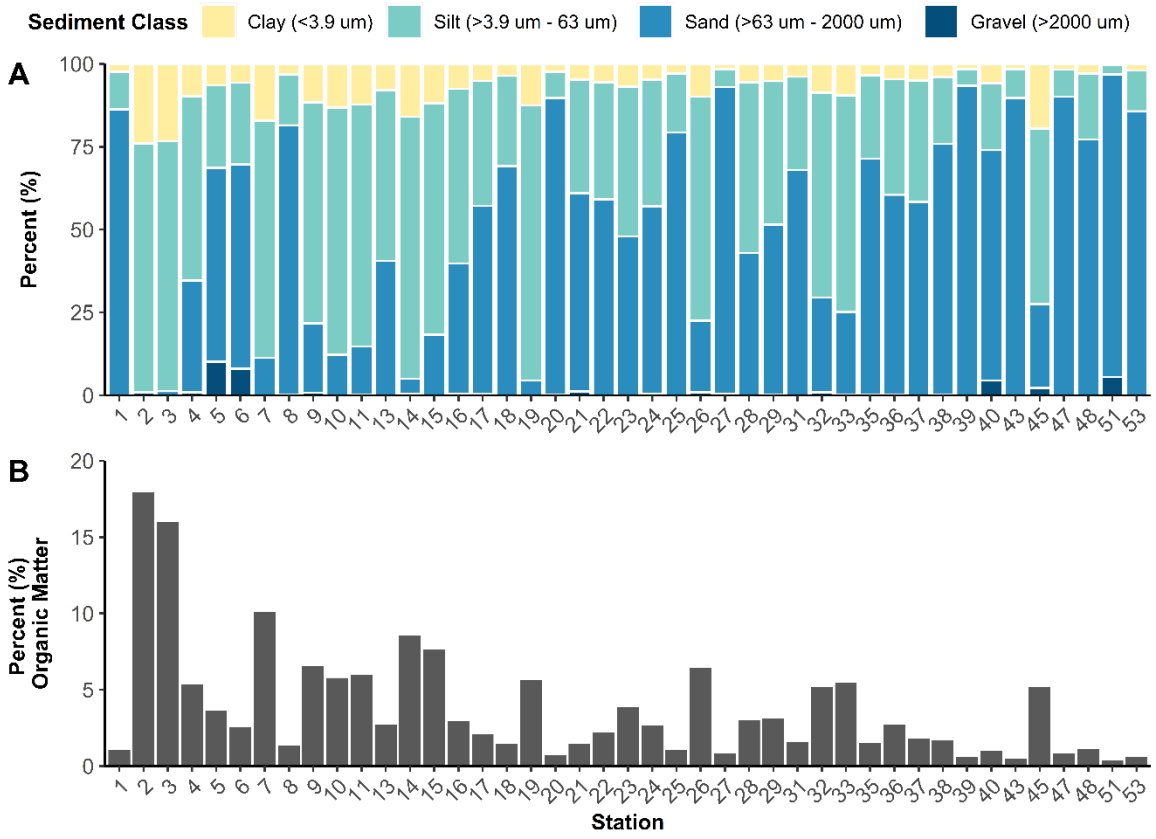

Figure 25. Sediment type in the St. Mary's River estuary characterized by percent (%) particle size (**A**) and organic matter content (**B**).

5.2.3 Seagrass density, biomass, and morphology

Eelgrass

Mean *Zostera marina* (eelgrass) vegetative shoot density determined from the condition surveys was 84.8 ± 26.8 and 1089.6 ± 116.7 shoots per m^2, at stations 7 and 35, respectively (mean ± SE). Total shoot density (vegetative and reproductive) was quite variable at both stations, ranging from 0–288 shoots m^{-2} at station 7 in the upper estuary to 516–1664 shoots m^{-2} at station 35 in the lower estuary in July 2023 (Figure 26A). Shoot density would likely show typical phenological patterns for temperate seagrasses across the year, with lowest densities during overwintering, increasing density with spring growth, peak densities during the summer, and reduced densities in the fall with senescence (Wong and Dowd 2023). As discussed above, the low salinity conditions at station 7, combined with limited bottom light from high CDOM and sediment concentrations in the water column, likely reduced eelgrass shoot density and its ability to grow in these conditions (Lee et al. 2007, Nejrup and Pedersen 2008, Enríquez et al. 2019).

Leaf morphologies were measured on plants collected from both the camera survey and condition surveys. Leaf lengths were longest at station 7 (Figure 26B), while leaf widths were fairly consistent across all stations (Figure 26C). Eelgrass plants typically grow longer leaves in light-limited conditions, related to either deeper depths or, as in this case, high light attenuation in the water column from CDOM and suspended sediments (Enríquez et al. 2019). Longer leaves provide more photosynthetic tissue to improve light capture and support photosynthesis (Enríquez et al. 2019). Although seagrass leaves will also grow wider in low light conditions, this was not observed here (Figure 26C). Interestingly, LAI was lowest at station 7 and highest at station 35, this trend mirrored differences in shoot density despite the much longer leaves at station 7 (Figure 26E). Correspondingly, the denser beds in the lower estuary would likely be the most productive.

Eelgrass aboveground dry biomass (AGBM) per shoot (0.025–0.251 dry g, Figure 26D) was variable across stations, although stations with longer leaves tended to have higher AGBM, as expected. Similar patterns were also observed for rhizome length (8.86–55 mm, extending from nodes 0–3, Figure 26F) and belowground dry biomass (BGBM; 0.003–0.048 dry g), where longer rhizomes were heavier. Rhizome width (Figure 26G) increased from the upper to lower estuary, which is further reflected in the belowground dry biomass (Figure 26H). The shoot-level aboveground to belowground biomass ratio tended to decrease from the upper to lower estuary, indicating the relative importance of aboveground tissues in the higher estuary relative to lower (Figure 26I). These patterns in biomass are consistent with previous studies where eelgrass rhizome thickness and total belowground biomass are lower in more silty, warm, shallow protected waters compared to sandy, cooler, more exposed waters (Krumhansl et al. 2021, Wong and Dowd 2023). Seagrass plants will typically reduce allocation into belowground tissues under stressful conditions, when reduced light, high sulphide concentrations, or warm temperatures, cause increased respiratory burden. These conditions were prevalent in the upper estuary, where river discharge caused reduced light and water temperatures were warmer (see Figure 13 for temperature and Section 6.1.2 for coinciding coloured dissolved organic matter prevalence), so the observed trend in aboveground to belowground (AGBG) biomass ratio is not surprising. Energy allocation into aboveground tissues supports neutral or

higher production to respiration ratios to support continued growth and survival (Marsh et al. 1986, Lee et al. 2007).

Eelgrass biomass patterns were also evaluated from hand cores collected from stations 7 and 35 during the condition surveys. Eelgrass AGBM was much higher at station 35 (lower estuary) than station 7 (higher estuary), despite shoot biomass showing the opposite pattern for AGBM. The AGBG biomass ratio was highest at station 7, similar to the ratio calculated from shoot biomass. The ratio was close to zero at station 35, indicating an even allocation of energy into both aboveground and belowground plant tissues (Figure 27A–C). These bed-scale characteristics in aboveground and belowground biomass reflect similar patterns to those observed per shoot, although the trends are not as strong. This is likely because the core sampling introduces additional variation related to shoot density (Figure 26A), as well as detritus in the sediments, thickness of the rhizome matte, and inadvertent sampling of plants outside of the core (i.e., rhizomes of plants adjacent to the core are sometimes difficult to break and end up being included in the sample).

Widgeongrass

Widgeongrass was observed only at eight stations (1–4, 7, 9, 11, and 14), relatively fewer stations than eelgrass. All of these stations were in the upper reaches of the estuary that experienced lower salinities, higher temperatures and more light-limited conditions (see Sections 3, 4 and 6). Widgeongrass vegetative shoot densities ranged from 0–384 shoots m^{-2} across quadrats at station 7 (Figure 28A). The number of shoots per plant varied across stations, with station 2 exhibiting the highest values (Figure 28B). The number of leaves per shoot and maximum leaf length were relatively consistent across stations, although they tended to be higher at station 7 (Figure 28C, D). While BGBM was also consistent across stations, aboveground biomass per shoot was highest at station 7 (Figure 28F). This resulted in a high AGBG ratio at station 7 although a high ratio was also observed at station 1 (Figure 28G). The high AGBG ratio at station 7 coincided with plants there having the greatest proportion of branching shoots, where 70% of sampled shoots categorized as branching (Figure 28H). Prevalence of branching shoots suggests provision of a highly structured habitat, although these data may have been influenced by the different collection dates (July 13, 2023 for station 7 and June 13, 2023 for remaining bottom type survey stations). No reproductive structures were observed on the widgeongrass collected in this study. However, while widgeongrass does employ both sexual and asexual reproductive strategies, salinity has been identified as an important driver of reproductive strategy of this species, where more annual populations are well-adapted to areas with low salinities in early spring that facilitate rapid germination and seedling establishment (Mayer and Low 1970, Richardson 1980).

Cores collected for the condition survey only contained widgeongrass at station 7 (Figure 27D-F). AG and BG biomass patterns were similar to those observed at the shoot level, with generally a greater allocation to AG components resulting in AG:BG biomass ratio ranging from 0.59–4.17 (Figure 27F). When considering the differences in the absolute biomass of each species, there is a clear dominance of eelgrass within the estuary where mean eelgrass AG biomass was 30.87±5.88 g m^{-2} across stations and widgeongrass averaged 3.23 ±2.15 g m^{-2}, and was only present in the upper estuary (mean ±SE; Figure 27A, D).

Eelgrass and widgeongrass vary substantially in structure and life history strategies, with widgeongrass being a smaller-form brackish water seagrass species with shorter, thinner

shoots and less robust below ground components compared to eelgrass (Moore and Duffy 2016, French and Moore 2018). Widgeongrass also has more opportunistic life history traits including widespread sexual reproduction within months of germination and hardy seeds with high germination rates (Hensel et al. 2023, Mayer and Low 1970, Richardson 1980, Strazisar et al. 2016). Eelgrass employs mainly asexual reproduction in Atlantic Canada, although low variable sexual reproduction can be evident (Vercaemer et al. 2021). These differences likely influence the ecosystem functions and services that each seagrass species provide in the estuary (Moore and Duffy 2016, French and Moore 2018, Hensel et al. 2023, Hensel et al. 2024). Comparative studies in Chesapeake Bay, United States have shown that widgeongrass' habitat structural complexity supports higher faunal abundance and diversity than eelgrass because its thin, branching shoots increase surface area to volume ratio compared to eelgrass' single, ribbon-like shoots, while eelgrass beds tend to support larger predator individuals such as blue crabs (*Callinectes sapidus*) (Hensel et al. 2024). In contract, in the Nauset Marsh system in Cape Cod, Heck et al. (1995) found that faunal richness, abundance, and biomass were highest in eelgrass beds relative to widgeongrass habitat located in neighbouring marsh pools. However, marsh pools were highly anoxic and likely did not support high invertebrate production (Heck et al. 1995). These differences in habitat provision by seagrass species will also vary seasonally given documented differences in species' peak biomass phenology and tolerance to anomalous summer heat events, largely defined by differences in their temperature tolerance (Johnson et al. 2003, Moore et al. 2014, Richardson et al. 2018, Hensel et al. 2023, Hensel et al. 2024). Structural differences between the two seagrass species also explain major differences in primary production, where total biomass per area is significantly lower, and belowground biomass is reduced in the smaller bodied widgeongrass compared to the larger bodied eelgrass (Hensel et al. 2023, Hensel et al. 2024). This presents potential implications for future blue carbon sequestration capacity within the estuary (Nguyen et al. 2021).

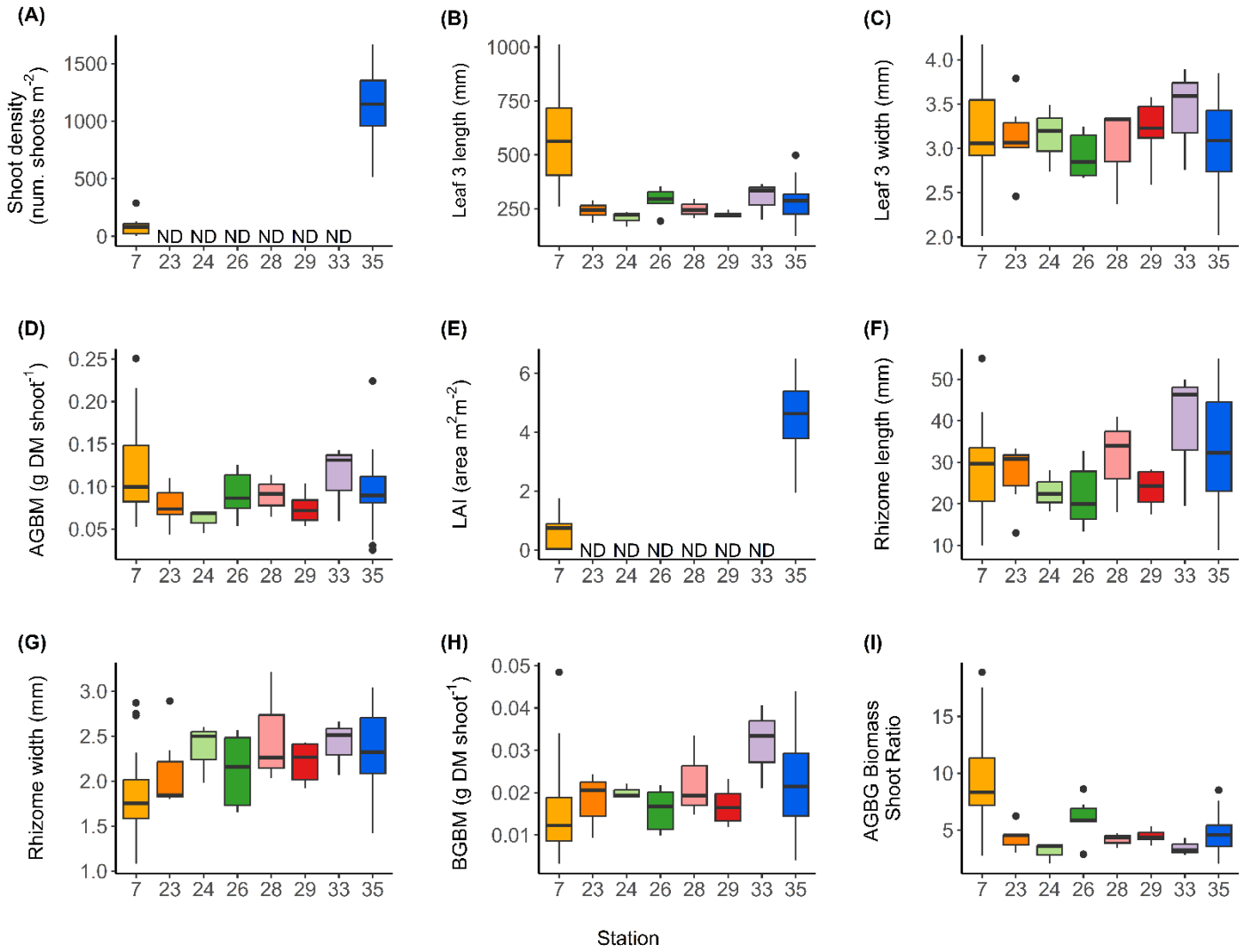

Figure 26. Biological characteristics *Zostera marina* at each sampling station where it was found, described by (**A**) shoot density (number of shoots m^{-2}), (**B**) leaf 3 length (mm) and (**C**) width (mm), (**D**) aboveground biomass (AGBM, g dry mass (DM) per shoot), (**E**) leaf area index ((LAI), area m^2 m^{-2}), (**F**) rhizome length (mm) from insertion point to node 4 (first three internodes), (**G**) rhizome width (mm, internode 3), (**H**) belowground biomass (BGBM, g DM per shoot, for first three internodes), and (**I**) aboveground:belowground (AGBG) biomass ratio by shoot. Shoot density and LAI could only be calculated from the condition survey samples. Boxes indicate median± upper and lower quartiles, whiskers indicate minimum and maximum values. ND, no data. n = 6–30.

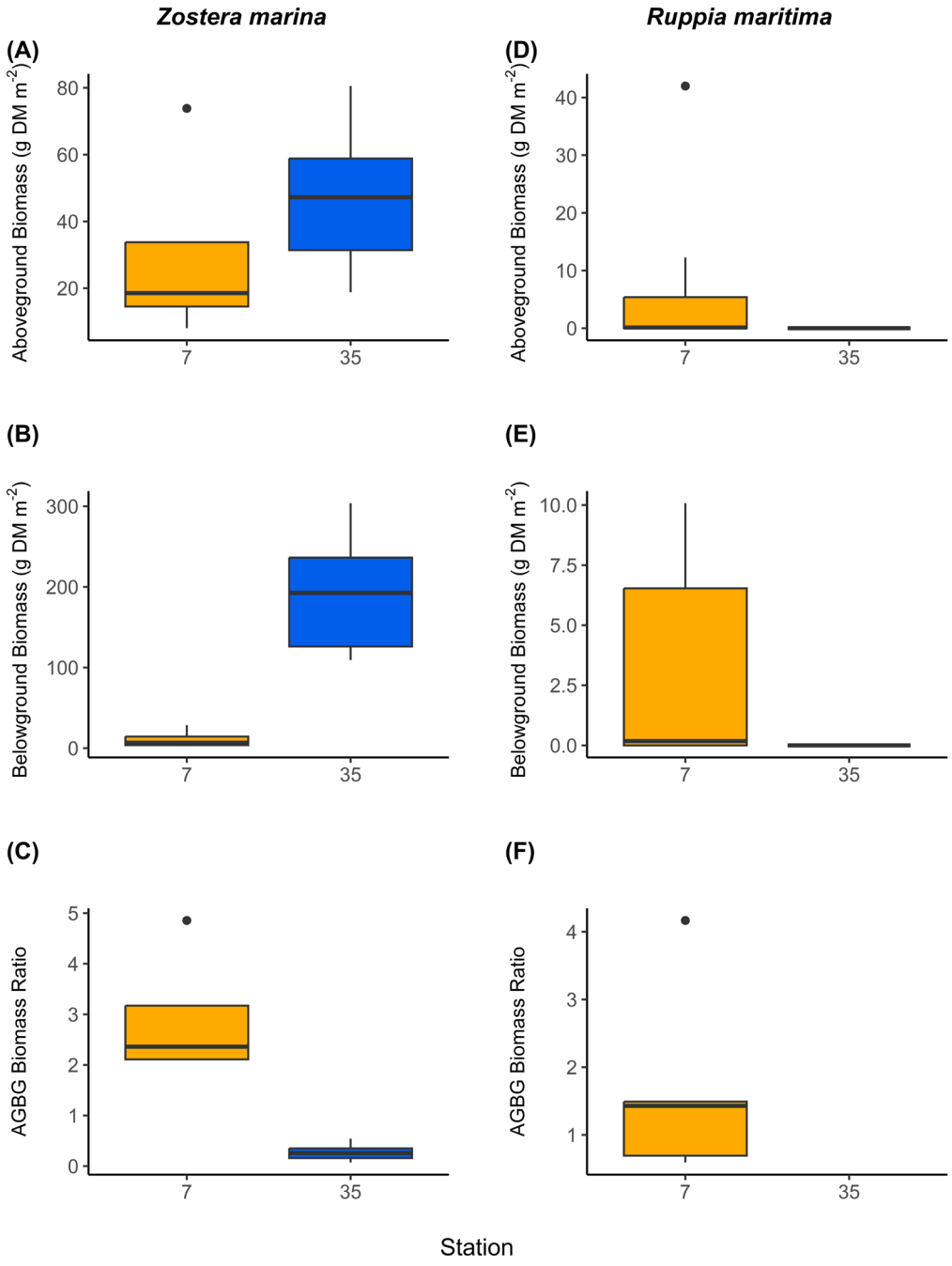

Figure 27. Seagrass aboveground, belowground and aboveground:belowground (AGBG) biomass ratio for (**A–C**) *Zostera marina* (n = 4–10) and (**D–F**) *Ruppia maritima* species (n = 5).

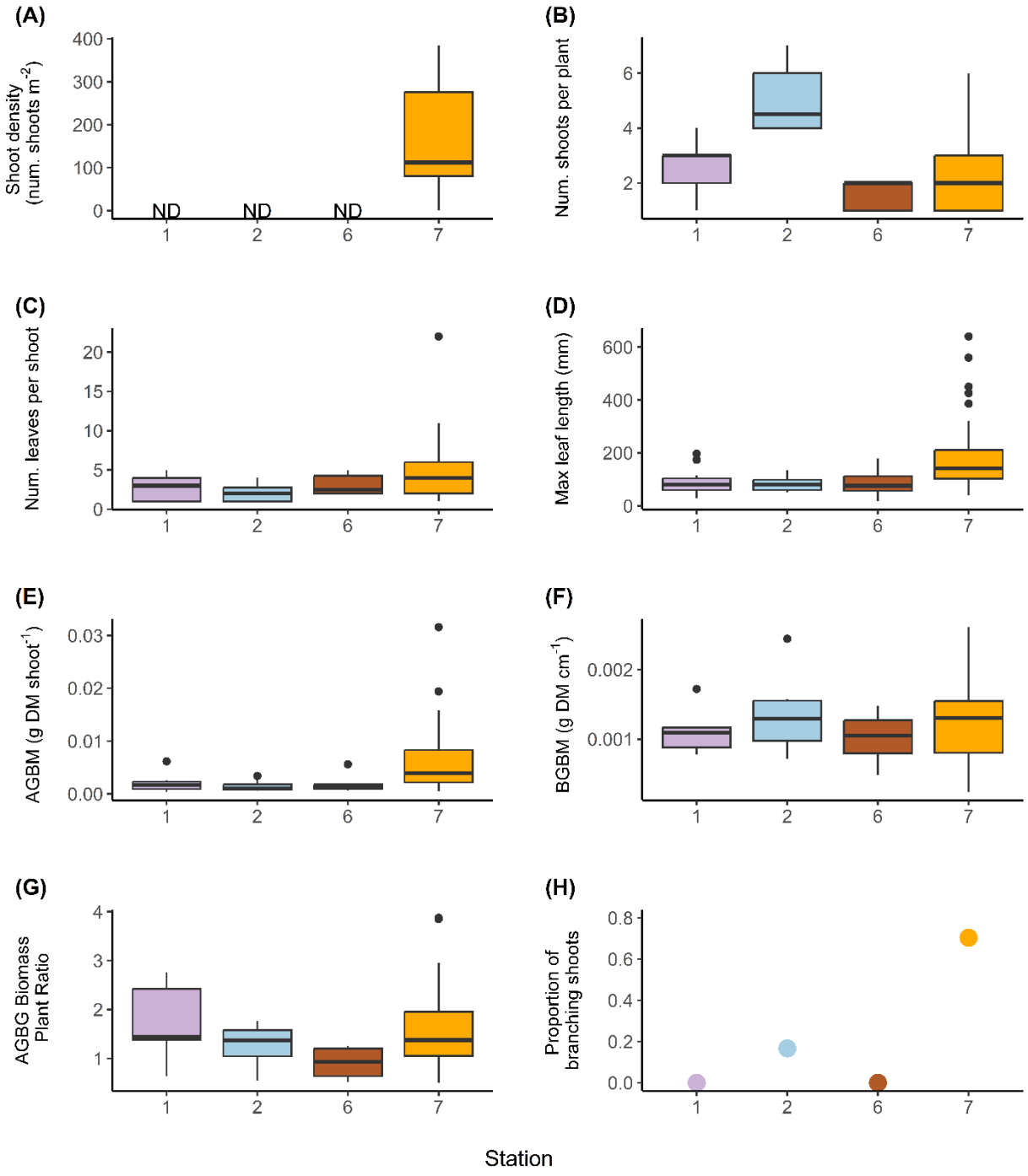

Figure 28. Biological characteristics of *Ruppia maritima* at each sampling station where it was found, described by (**A**) shoot density (number of shoots m^{-2}), (**B**) number of shoots per plant, (**C**) number of leaves per shoot, (**D**) maximum leaf length within a shoot (mm), (**E**) aboveground biomass (AGBM, g dry mass (DM) per shoot), (**F**) belowground biomass (BGBM, g DM per plant), and (**G**) aboveground:belowground (AGBG) biomass ratio by plant, and (**H**) proportion of branching shoots. Shoot density could only be calculated using samples from the condition survey. Boxes indicate median± upper and lower quartiles, whiskers indicate minimum and maximum values. ND, no data. n = 5–30.

6 Satellite Mapping of Macrophyte Communities

Passive remote sensing techniques were used to map marine macrophyte distribution within the St. Mary's River estuary. These techniques are regularly applied to understand the large scale distribution of macrophytes (Kutser et al. 2020). Yet, passive remote sensing is limited to regions where water clarity is high enough for sunlight to reach the sea floor and be reflected back to the sensor. The strong contribution of river discharge in the estuary (see section 3) results in extremely high concentrations of coloured dissolved organic matter (CDOM) within the water column. This manifests as a "darkening" of the water and increases the attenuation of light. Consequently, an understanding of CDOM dynamics in St. Mary's River estuary is required to understand where passive remote sensing derived techniques can be accurately used to quantify macrophyte distributions.

6.1 Coloured Dissolved Organic Matter

CDOM consists of water-soluble biogenic, heterogeneous organic substances that are yellow to brown in colour and is the portion of the dissolved organic matter pool that is light absorbing (Aiken et al. 1985). CDOM may originate from several sources in coastal areas including rivers, sewage, saltmarshes, terrestrial soils, macrophytes, or biological production (Clark et al. 2008, Chen et al. 2004). CDOM influences visibility and light attenuation in the water column, with implications for the detectability of submerged aquatic vegetation (SAV) by satellites. CDOM levels also have a direct effect on light available for photosynthesis by macrophytes, and can be used as a proxy for dissolved organic carbon concentrations (Mannino et al. 2008, Massicotte et al. 2017).

6.1.1 Methods

To measure CDOM, seawater was collected from the boat at 1 m depth with a Niskin bottle from ten sites along a salinity gradient in St. Mary's River estuary on July 7, 2023 (Figure 29). Seawater collections were made over the course of two hours, starting at high tide (Site 1) and progressing through to ebb tide (Site 10). These sampling stations corresponded to the CTD profile transect (described in Section 3.1). Seawater was filtered within 12 hours of collection through a 0.2 µm polycarbonate filters, which were first rinsed three times with ultrapure (Milli-Q) water using a vacuum pump with less than 10 PSI pressure to remove potential impurity on the filter. Seawater was then pulled through the same filter and the flask received an additional three seawater rinses before final filtration. Samples were stored in glass amber bottles in the dark at 4 °C until analysis. Samples were brought to room temperature before absorbance was measured at 2 nm interval from 200 to 724 nm on an UltraPath^{TM} (World Precision Instrument) instrument using liquid waveguide spectroscopy and either a 2 or 10 cm pathlength (Mannino et al. 2019). CDOM absorbance was converted to absorption (m^{-1}) using the following equation (Eq. 2):

$$a(\lambda) = 2.303 * A(\lambda) / l \quad [Eq. (2)],$$

where, l is the pathlength and A(λ) is the CDOM absorbance. CDOM absorption was offset so that the average absorption at wavelengths >700 nm was zero (Mannino et al. 2019). CDOM absorption coefficients are provided at 250, 350, and 443 nm. The first two wavelengths are common reference wavelengths to report CDOM absorption coefficients. The third wavelength (443 nm) corresponds to peak phytoplankton absorption with important implications for ocean colour. CDOM slope was calculated using a linear regression on logarithmically transformed

absorption values over two spectral ranges: 275–295 and 350–400 nm to provide information on water source. Where low slope values are associated with terrestrial sources, and higher slope values are associated with photobleached oceanic waters (see for instance Helms et al. 2008).

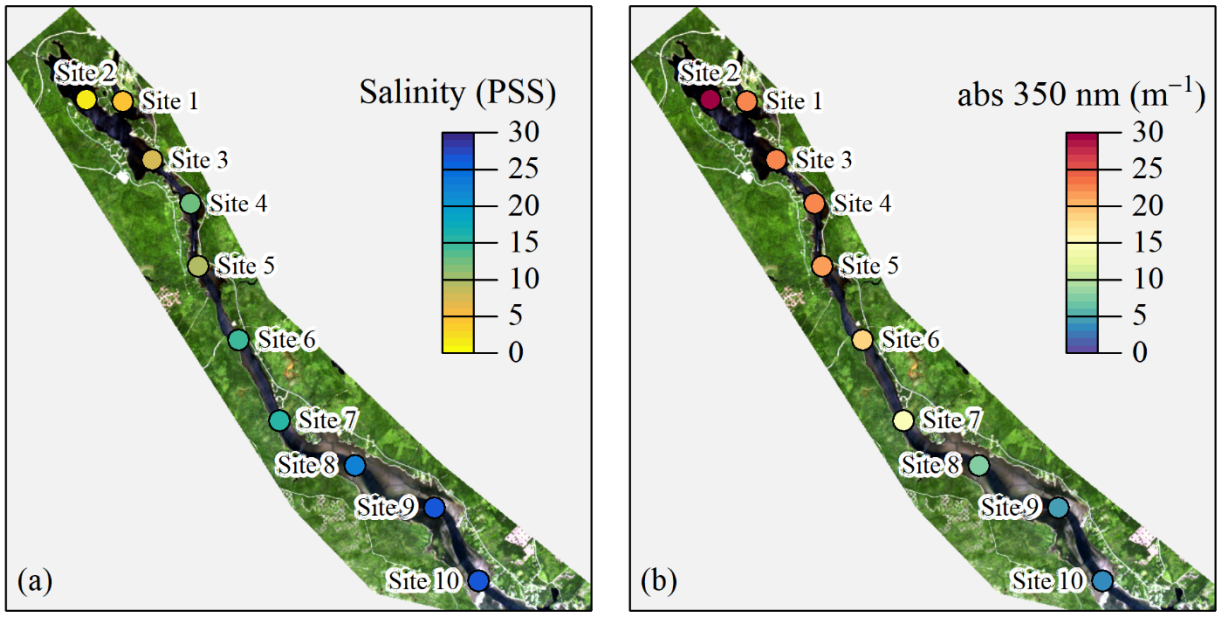

Figure 29. Map showing the gradient of salinity (a) and coloured dissolved organic matter (CDOM) absorption (abs) at 350 nm (b) in St. Mary's River estuary measured on July 7, 2023. Base map is a Planet Scope image collected on July 23, 2022.

6.1.2 Results and Discussion

The slope at 275–295 nm increased from inner to outer estuary, with the slope at 350–400 nm following an inverse relationship (Table 2; Figure 30). CDOM absorption across all wavelengths was maximum at Site 2 (104 m^{-1} at 250 nm) and reached a minimum at Site 9 and 10 (17 m^{-1} at 250 nm) with an approximate 142–149% difference in absorption coefficients between these two sites at 250, 350, and 443 nm (Table 2 and Figure 31). There was a strong negative relationship (R^2 = 0.92) between both salinity and 275-295 slope with the CDOM absorption at 350 nm (Figure 32), supporting the use of CDOM absorption to retrieve salinity and identify water origin. Consequently, the relative terrestrial input of CDOM is highest in the inner estuary and decreased towards the open ocean in the St. Mary's estuary as expected. However, the high absorption at 350 nm along the river transect suggest non-negligible contribution from the river water at stations 9 and 10 (i.e., $a_{CDOM}(350) > 4\ m^{-1}$). For instance, CDOM absorption at 350 nm at the Atlantic Zone Monitoring Program (AZMP) high frequency monitoring Halifax Station 2 (about 30 km offshore) ranges from 0.3–0.5 m^{-1} based on data collected from 2021 to 2023 during the AZMP missions, and ranged between 1–4 m^{-1} in the Bras d'Or lake in 2022-2023 (Devred, unpublished data). The high CDOM absorption measured at St. Mary's estuary prevented the bottom optical signal to reach the surface and therefore limits the use of satellite-based bottom-habitat mapping to the exposed mud flats and southern regions of the estuary where the water is clearest (see Section 6.2).

Table 2. Slopes of coloured dissolved organic matter (CDOM) absorption coefficients between 275 and 295 nm, and between 350 and 400 nm, slope ratios and absorption coefficients for CDOM (a_{CDOM}) at 245, 350 and 443 nm in St. Mary's River estuary.

Station	Slope 275-295 nm (m^{-1})	Slope 350-400 nm (m^{-1})	Slope Ratio	a_{CDOM} 250 nm (m^{-1})	a_{CDOM} 350 nm (m^{-1})	a_{CDOM} 443 nm (m^{-1})
Site 1	0.0128	0.0164	0.785	81.70	23.06	5.13
Site 2	0.0124	0.0160	0.774	103.55	30.23	6.97
Site 3	0.0125	0.0156	0.801	77.91	22.65	5.32
Site 4	0.0122	0.0151	0.811	78.38	23.26	5.67
Site 5	0.0130	0.0154	0.843	77.07	22.27	5.30
Site 6	0.0125	0.0149	0.834	64.25	18.89	4.72
Site 7	0.0124	0.0153	0.815	52.89	15.36	3.64
Site 8	0.0131	0.0156	0.838	29.87	8.33	1.88
Site 9	0.0149	0.0150	0.989	17.28	4.56	1.08
Site 10	0.0146	0.0153	0.960	16.76	4.38	1.01

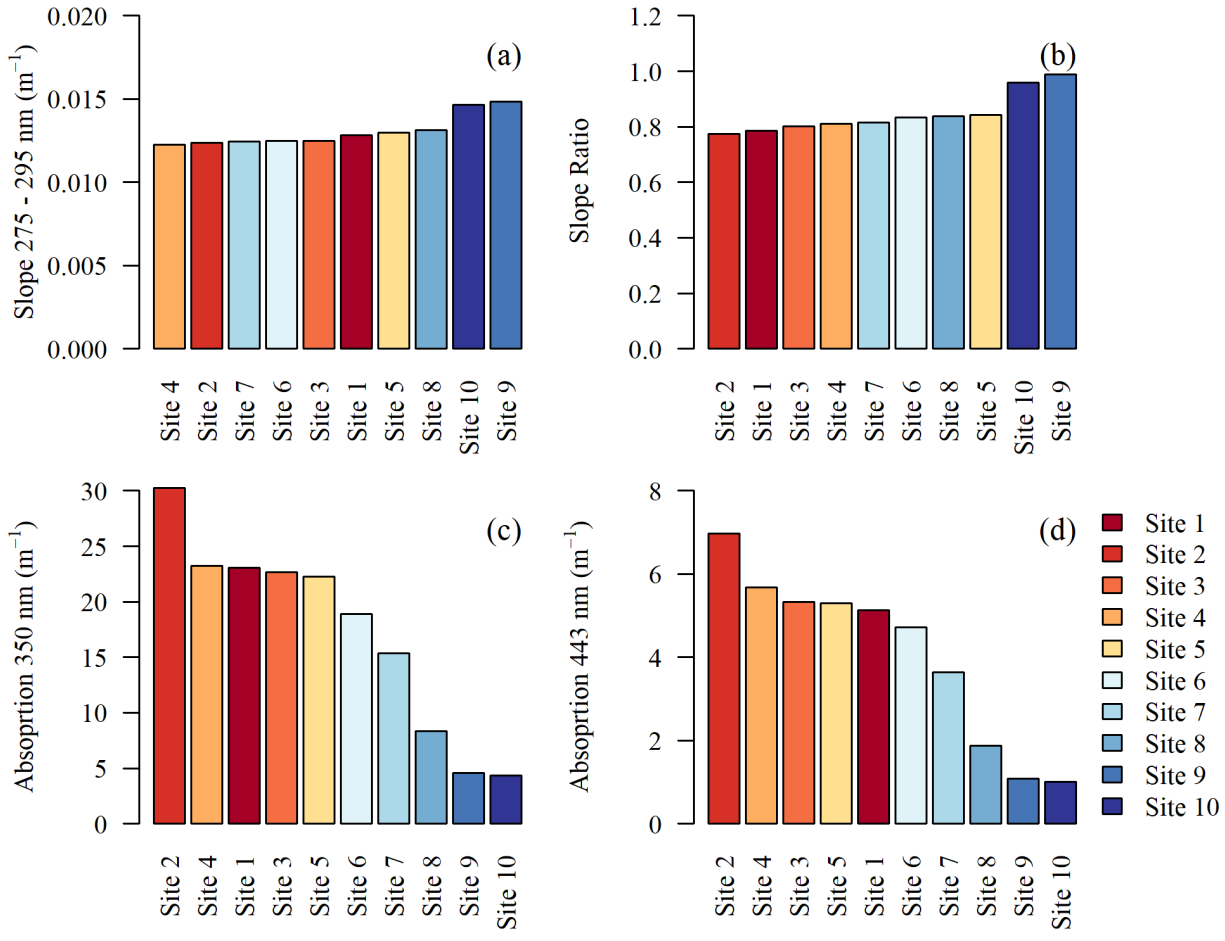

Figure 30. Slope ratios and absorption coefficients for coloured dissolved organic matter (CDOM) in St. Mary's River estuary, colour coded by site.

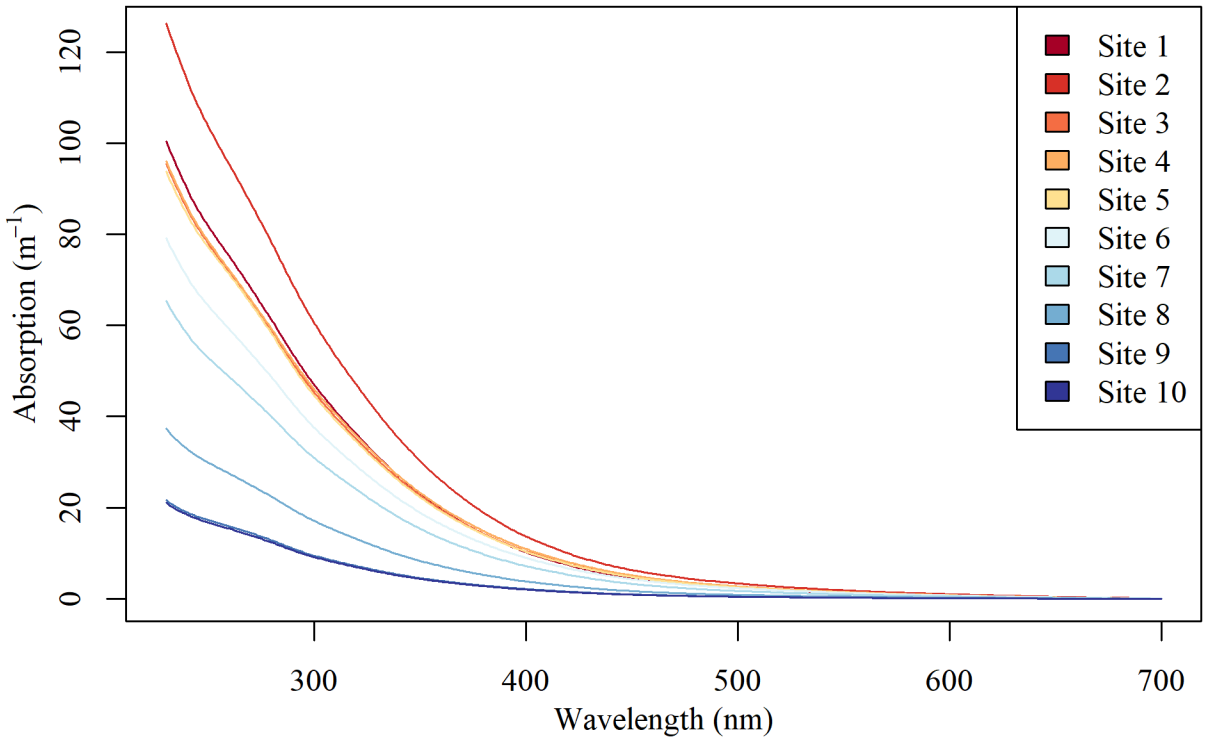

Figure 31. Coloured dissolved organic matter (CDOM) absorption curves for all wavelengths and sites in St. Mary's River estuary.

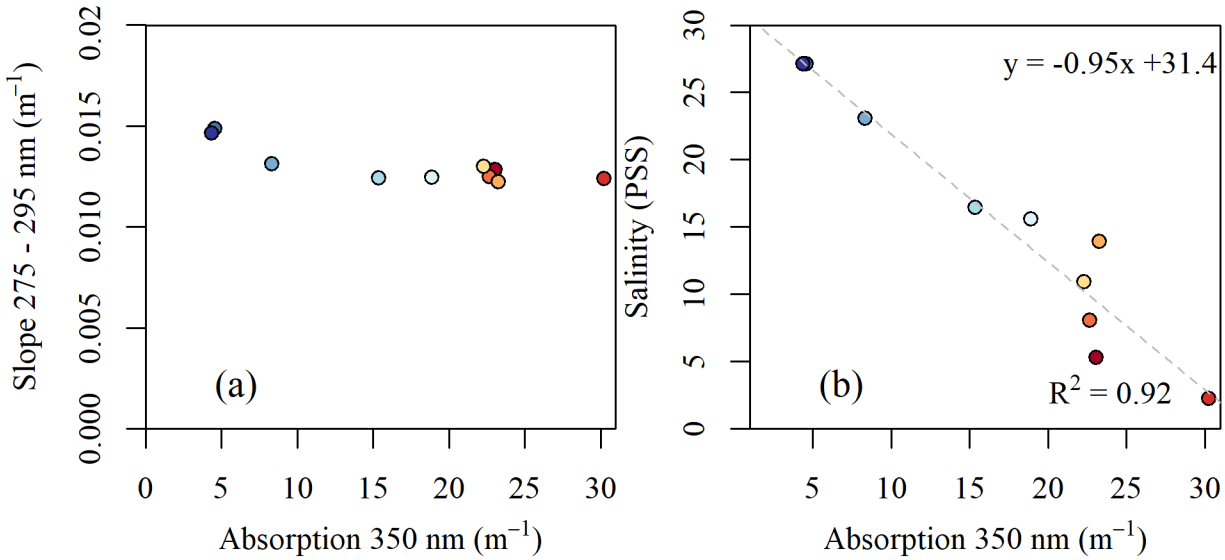

Figure 32. Relationship between the slope at 275–295 (a) and salinity (b) to coloured dissolved organic matter (CDOM) absorption at 350 nm in St. Mary's River estuary, colour coded by site. See Figure 31 for site legend, where colours run from red to blue for collection sites 1–10.

6.2 Bottom Habitat Mapping

Marine macrophyte distributions can be mapped using passive remote sensing when water clarity is sufficient to allow sunlight to reach the seafloor and be reflected back to the sensor. Using information on coloured dissolved organic matter (CDOM) dynamics from Section 6.1, macrophyte distribution was mapped along the shallow sand flats, and outer estuary using aerial and satellite imagery. High CDOM concentrations precluded the ability to produce bottom habitat maps in the upper estuary, and along the channel that runs the length of the estuary. Each imagery type has different resolutions and benefits. Satellite imagery is routinely captured at set time intervals and was used to inform on the general stability of macrophyte beds across time since the launch of the respective satellites. Aerial imagery is captured at select snap shots in time, at very high spatial resolutions, and was used to create maps of SAV which were validated with *in situ* data. Both satellite and aerial imagery can be used to begin to understand the large scale distribution of macrophytes in St. Mary's River estuary since 2008 across years and seasons.

6.2.1 Methods

In Situ Data

Drop camera surveys performed in July 2023 (see Section 5) were used as *in situ* data for model training and validation (Figure 33). Various sites were visited throughout the estuary and the percent cover of bottom habitat was recorded. Note that the dominant vegetation type was seagrass (*Zostera marina* (eelgrass) and *Ruppia maritima (widgeongrass)*) in the inner estuary (black dashed box in Figure 33) with a transition to a seaweed and seagrass community in the ocean-exposed regions. The habitat percent cover was used to label a point as vegetated (>60% seaweed or seagrass) or non-vegetated. Polygons were drawn along the drift tract points and any pixel extracted within the polygon was used in model building and validation.

Aerial Imagery

The Nova Scotia Orthophotomap Database was examined to find aerial imagery overlapping the St. Mary's estuary (https://nsgi.novascotia.ca/datalocator/indexing/; accessed on March 20, 2024) and aerial orthorectified RGB imagery was purchased from 2008 and 2019 for six sheets at a 25 cm resolution. These sheets were merged into a single layer and cropped to the St. Mary's River estuary bounds (Figure 33). The 2008 imagery was a mosaic of 3 flights that occurred between July 12–16, 2008, and the 2019 imagery was collected during one flight on August 6, 2019.

No atmospheric correction was performed on these images due to the limited spectral information (i.e., three broad spectral bands), and since only image-based classification methods were used. Furthermore, due to the limited spectral information, and high spatial resolution (25 cm), land was masked by first buffering a bathymetric layer with a 30-m spatial resolution by a 200 m buffer to ensure no land or sea boundary pixels were mistakenly masked. The shoreline was then manually traced and masked out. The deep-water channel with high CDOM absorption (see Section 6.1 above) was additionally masked out of the image by removing all water pixels with a Digital Number lower than 20. Patchiness in the channel mask was removed by applying a 4 m buffer combined with some manual masking to further remove dark channel pixels. A deep-water mask was defined based on the 5 m depth contour in ocean exposed section of the estuary using a high-resolution bathymetry dataset (Section 3; Canadian

Hydrographic Service bathymetry data, https://open.canada.ca/data/, updated in upper estuary with *in situ* depth readings, Figure 9). Finally, due to extremely high CDOM and strong sun glint in the 2019 image, the upper estuary was also masked. The final land, channel, deep water and CDOM/glint mask was applied to both the 2008 and 2019 image (Figure 33).

Satellite Imagery

The Sentinel-2 (10 m resolution; 2016–2024) and Planet Scope (3 m resolution; 2016–2024) archives were examined to qualitatively look at shifts in seagrass coverage in a small region of the estuary where the largest seagrass beds were found during the 2023 field survey (pink box in Figure 33). Winter and summer true colour composites were visually analyzed to assess the general stability of the seagrass beds across season and years (Table 3) and to assess if the 2023 field data could be used to train the 2019 aerial imagery. The comparison between satellite imageries, years, and seasons was further done to identify and understand potential differences between the two aerial images collected 11 years apart but in the same season.

Table 3. Dates of representative Sentinel-2 and Planet Scope images captured in winter and summer from 2016–2024.

Year	Winter Sentinel-2	Winter Planet Scope	Summer Sentinel-2	Summer Planet Scope
2016	3/27/2016	N/A	9/13/2016	N/A
2017	N/A	2/23/2017	8/4/2017	8/4/2017
2018	3/27/2018	3/26/2018	9/23/2018	8/7/2018
2019	3/27/2019	3/18/2019	9/8/2019	8/14/2019
2020	3/6/2020	3/18/2020	9/7/2020	8/28/2020
2021	3/6/2021	3/21/2021	9/17/2021	8/15/2021
2022	3/11/2022	2/11/2022	9/7/2022	8/4/2022
2023	3/11/2023	2/15/2023	7/29/2023	N/A
2024	2/19/2024	2/9/2024	N/A	N/A

Bottom Habitat Classification

The 2019 bottom habitat maps were created using random forest models following the methods detailed in Wilson et al. (2020; 2022) in R version 4.3 (R Core Team 2021) using the *caret* (Kuhn 2020)*, terra* (Hijmans et al. 2024)*, irr* (Puspendra 2019)*, and randomForest* (Breiman et al. 2022) packages. The three RGB bands (red, green, blue) were used as predictor variables from the aerial imagery. The imagery was further processed to be water-column corrected using depth invariant indices (Lyzenga 1978) and principal component analysis (PCA) on the three RGB bands. The RGB bands, depth invariant indices, and principal components were all used as predictor variables. The pixels extracted from the field polygons were divided into 5 folds repeated ten times. Each data partition was used to build a random forest model and the withheld data was used to generate confusion matrices understanding, producer, user, and overall map accuracy as well as the Kappa coefficient. Final accuracy metrics are the average of the 50 cross-validation runs. The final habitat map was built by summing the 50 cross-validation maps, and converting to a percentage to define the probability of vegetation habitat map. Each cross-validation map was filtered using a 3x3 modal filter to reduce salt and pepper effects before producing the final map.

Due to large habitat shifts between 2008 and 2023, the 2008 aerial imagery was classified using an unsupervised k-means cluster analysis. Furthermore, due to differences in the imagery from the mosaic of multiple image dates (July 12–16, 2008) the analysis was carried out only in a subregion of the area of interest (e.g., pink box, Figure 33). This subregion was chosen as it corresponded to the largest seagrass beds observed in 2023, and there was minimal interference of the multiple image dates. The water column was relatively homogenous across the image with some slight glint salt and pepper pattern on the northern side of the deep channel around site 22/23. To account for this, the image was smoothed using a 3x3 median filter to reduce the slight glint speckling.

As bright sand is an easily identifiable bottom habitat type, all pixel values with a Digital Number > 130 in the green band were labelled as bare habitat (no vegetated macrophyte habitat observed). A k-means cluster analysis classified the remainder of the imagery using the *terra* (Hijmans et al. 2024) package and clusters were labelled based on the dominant habitat type using the RGB. The optimum number of clusters was defined using the *NbClust*() function from a package by the same name (Charrad et al. 2022), whereby the Euclidean distance was tested on the k-means method for between 4 and 8 clusters on 10,000 random pixels on all 30 indices (see Charrad et al. 2022 for details on the indices). This step was repeated 25 times to ensure the randomly selected pixels were representative of the entire dataset. The modal value across all indices and repetitions was 4 clusters which was defined as the optimal number of clusters to represent habitat type. The mean and median cluster number was 4.5 and 4.8, respectively. The final habitat map was denoted as three classes: bare, low-density vegetation, and high-density vegetation based on merging the k-mean clusters through comparison with the image RGB. The delineation of low to high density was based on both the colour of the RGB and the spectral shape in the low-density class which were in between the bar and high density class.

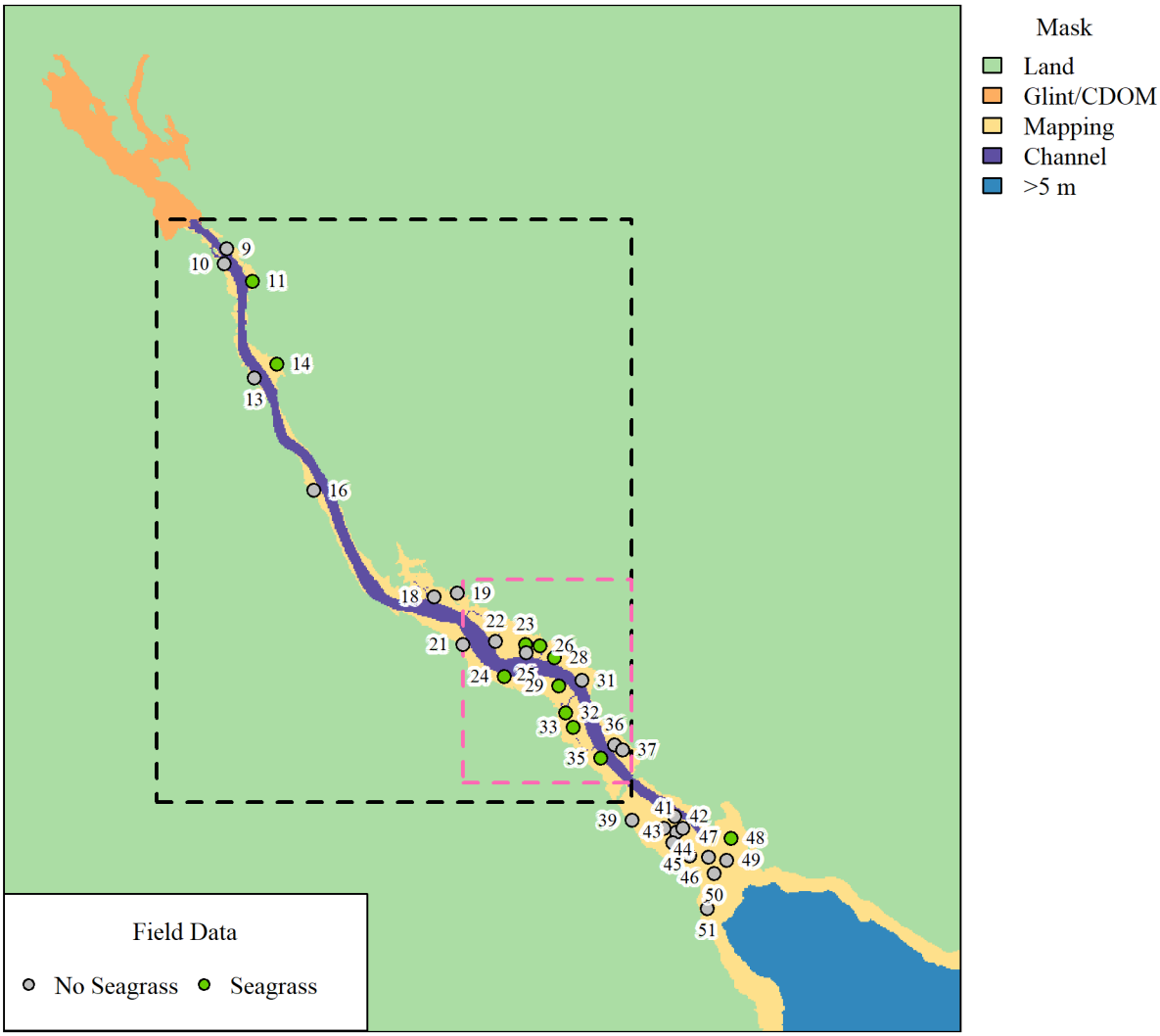

Figure 33. Different masks layered on the mapping region in St. Mary's River estuary showing the location of the field survey data used in model training and validation. Dashed black box indicates the region where seagrass was the dominant macrophyte. Pink dashed box indicates the region where the largest seagrass beds occurred and satellite time series was qualitatively examined. Numbers indicated field survey site locations.

6.2.2 Results and Discussion

Satellite Imagery

True colour composites of Sentinel-2 (10-m resolution) and Planet Scope (3-m resolution) were visually analyzed to understand if the large scale seagrass distribution remained consistent since the launch of the two different satellite platforms (2016) within a small region of St. Mary's estuary (Figure 33). The "best" representative summer image, defined as an image acquired in August or September to match typical seagrass maximum extent, was examined for each year between 2016 and 2023 (Figures 34 and 35). Additionally the best winter image, defined as an image acquired in February or March, was also examined (Figures 36 and 37). As each representative image was collected at varying tidal height, some images appeared "darker" than others due to the impact of the overlaying CDOM rich waters.

The summer seagrass distribution extent remained consistent between 2016 to 2023 (Figures 34 and 35). A large seagrass bed persisted within the yellow polygon, as well as a smaller bed across the channel to the north and to the east. Small fluctuations in bed extent (shifts in bed edge by 10's of metres) are highlighted by the orange arrows in Figures 34 and 35, which reach a maximum in 2023. In contrast to summer, the winter seagrass distribution was slightly reduced in 2016 and 2017 compared to the peak summer distribution (Figures 36 and 37). From 2018 to 2023 the winter distribution matched the summer habitat. However, the entire above ground biomass of seagrass appears to have disappeared by February 2024 (Figures 36h and 37h). Consequently, this visual analysis suggests larger interannual variations in the seagrass bed extent in winter than in summer.

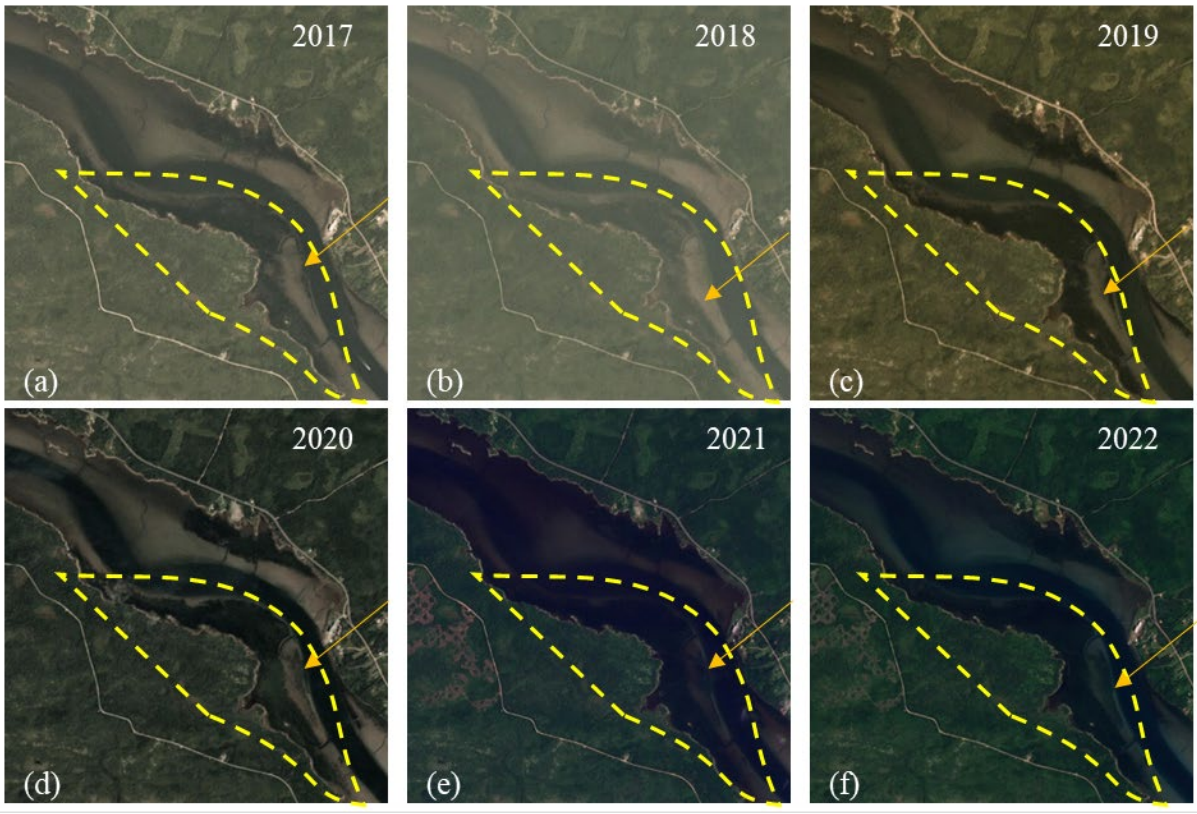

Figure 34. Representative cloud free Planet Scope images acquired in summer from 2017 to 2022. Yellow dashed polygon highlights one large seagrass bed known from field surveys, orange arrow in the same location for all images. No cloud free image was available in 2016 or 2023. Polygon is a rough approximation to orientate between images with varying atmospheric and water optical conditions and includes some land and channel.

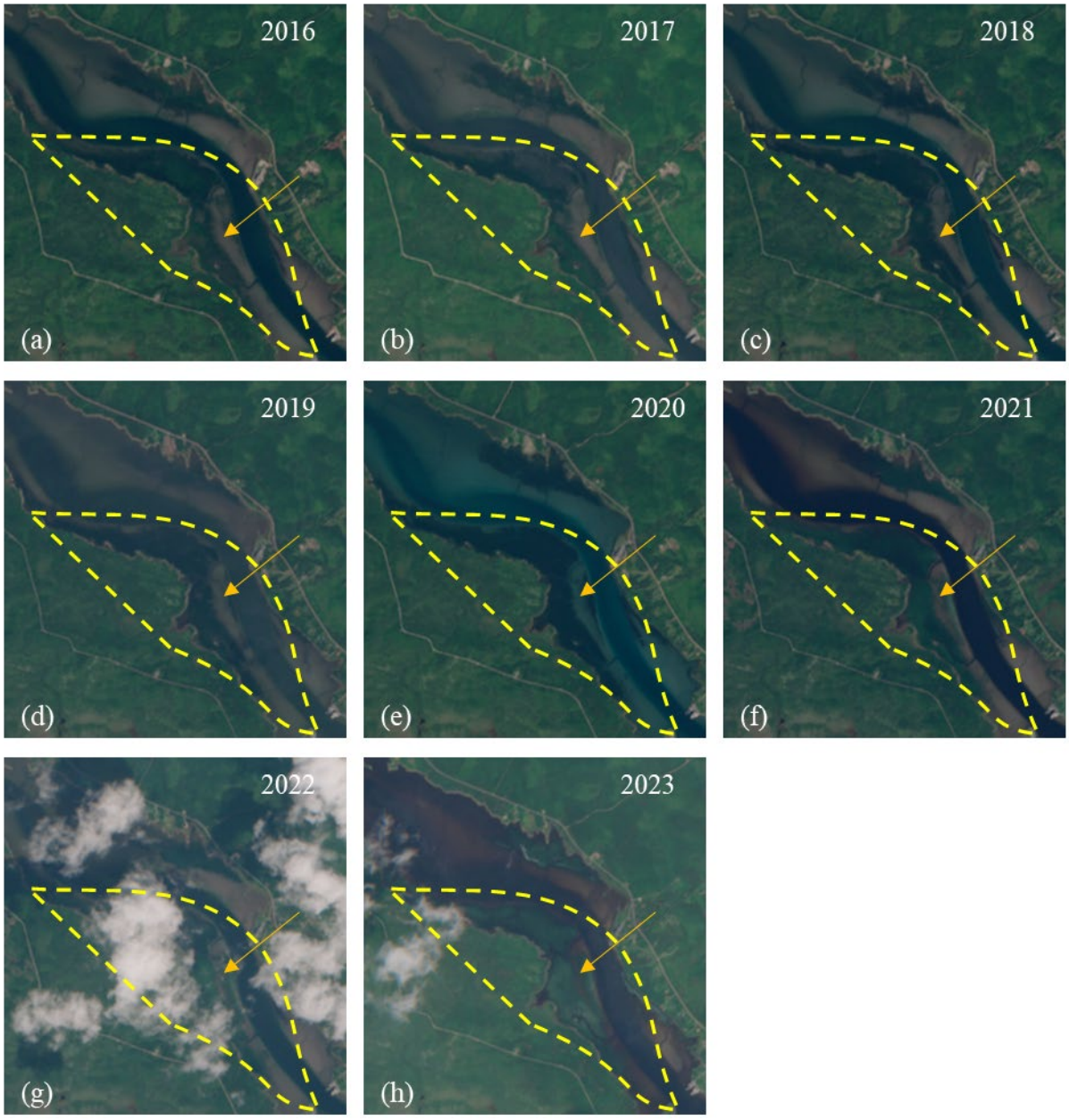

Figure 35. Representative cloud free Sentinel-2 images acquired in summer from 2016 to 2023. Yellow dashed polygon highlights one large seagrass bed known from field surveys, orange arrow in the same location for all images. Polygon is a rough approximation to orientate between images with varying atmospheric and water optical conditions and includes some land and channel.

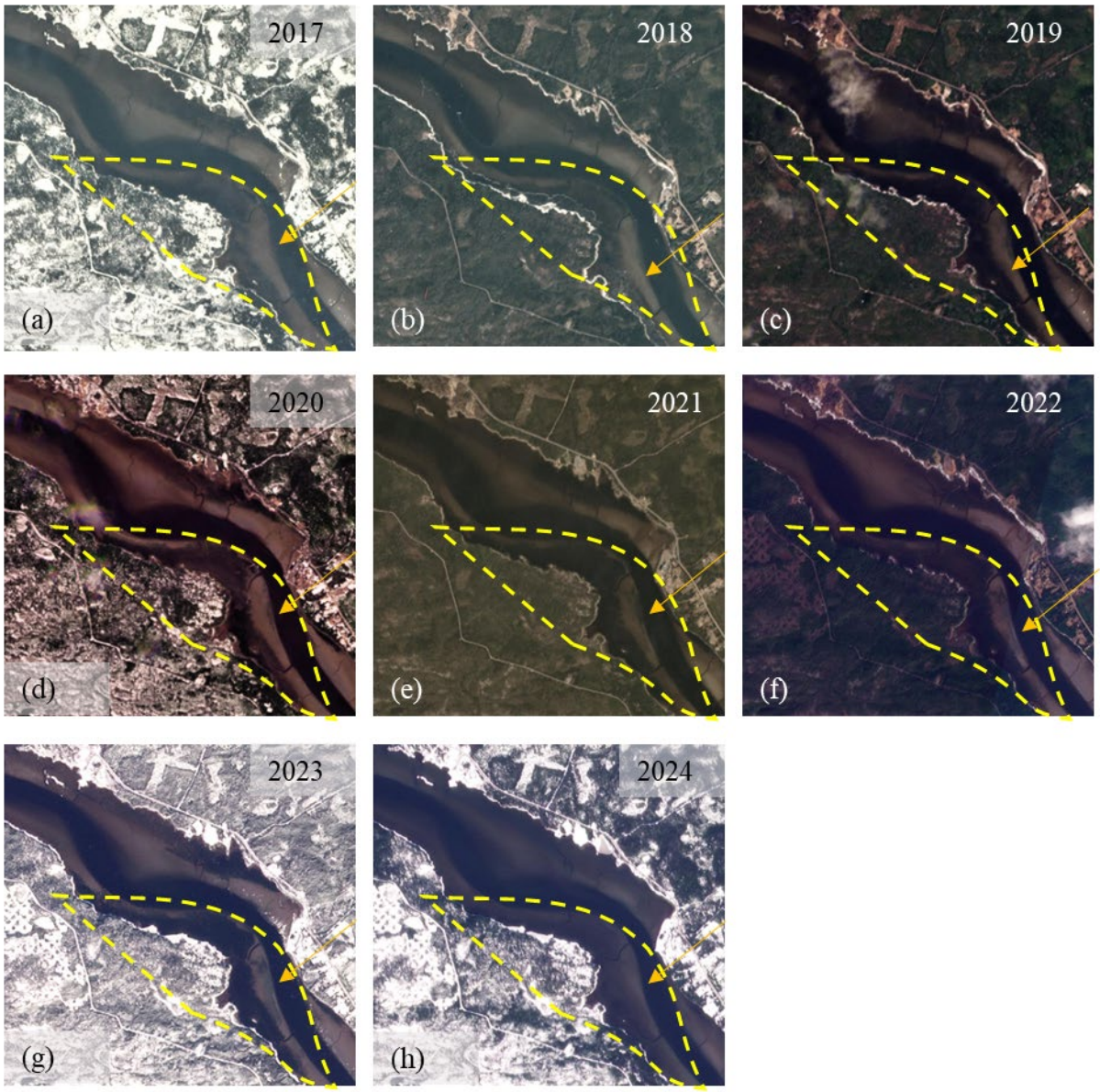

Figure 36. Representative cloud free Planet Scope images acquired in winter from 2017 to 2024. Yellow dashed polygon highlights one large seagrass bed known from field surveys, orange arrow in the same location for all images. Polygon is a rough approximation to orientate between images with varying atmospheric and water optical conditions and includes some land and channel.

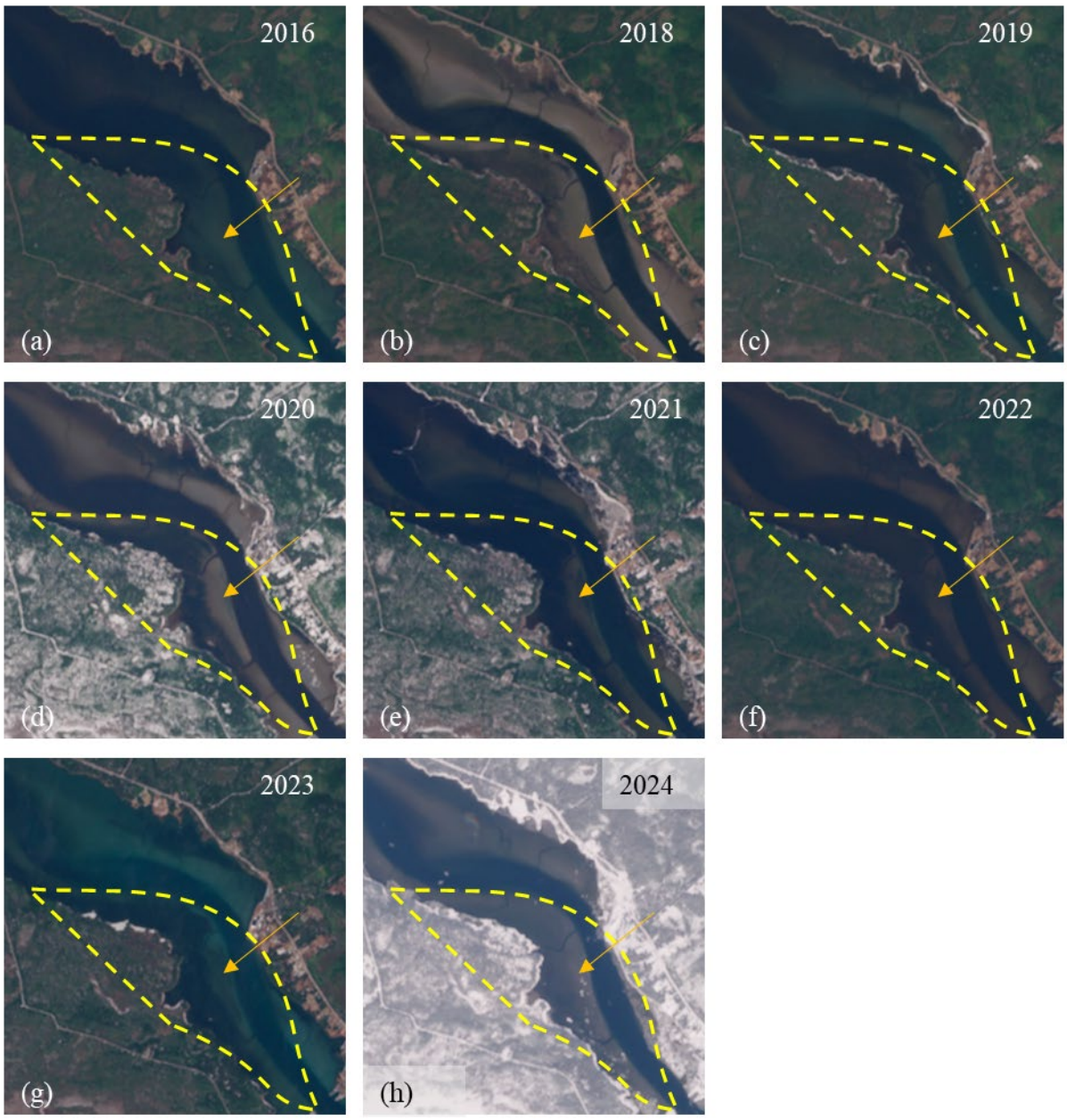

Figure 37. Representative cloud free Sentinel-2 images acquired in winter 2016, 2018 and 2019 to 2024. Yellow dashed polygon highlights one large seagrass bed known from field surveys, orange arrow in the same location for all images. Polygon is a rough approximation to orientate between images with varying atmospheric and water optical conditions and includes some land and channel.

Aerial imagery

The visual satellite analysis found that summer seagrass extent was relatively constant from 2016 to 2023. As such, the summer 2023 field data was used to train and validate the random forest classification on the 2019 summer aerial imagery. The 2023 field data was quality controlled to ensure the same habitat type was observed at the same location across both years. In most instances there was very good agreement between the two datasets. For example, Site 37 was defined as a soft sediment habitat in the 2023 field data, and the 2019 imagery reflected this habitat type (Figure 38a–c). Furthermore, the large eelgrass bed at Site 29 was present in both 2019 and 2023 images (Figure 38d–e). Seagrass cover in general was greatest in the central estuary (pink box; Figure 33). Even with the limited spectral bands of the aerial imagery, the digital number spectra were very different between these two sites in both shape and magnitude (Figure 38a). This resulted in a bottom habitat map classification with an average overall map accuracy of approximately 98% (Table 4). The image-based average vegetated habitat probability was low for sites with high bare substrate percent cover, and high for sites with high vegetation percent cover (circles; Figure 39). The 2019 random forest classification on the aerial imagery classified approximately 4.9 km^2 of coastal habitat (Table 5). Of the mapped region, approximately 2 km^2 was classified as vegetated habitat, among which at least approximately 0.5 km^2 was seagrass dominated habitat based on the pink inset region (Figure 33).

Following the quality control of the 2023 field data, nine of the 34 field survey sites which overlapped the mapping area were omitted from model training (triangles; Figure 39). Sites 49 and 51 were omitted as they occurred along bed edge transitions from vegetated to bare, with average percent covers of approximately 50% vegetated. However, the map classification accurately defined these transition points (Figure 40a–c), and the probability of vegetated habitat maps reflected these intermediate percent cover values (Figure 39). Furthermore, two additional sites exhibited a decrease in vegetated habitat coverage between 2019 and 2023 and were omitted from model training/validation. The first one, Site 14 was located near the inner estuary and the aerial imagery in 2019, while quite dark, suggested that patchy vegetation was present in 2019 but field data showed that vegetation was mostly absent in 2023. The second was Site 39 which field surveys indicated as 100% sandy habitat while the 2019 aerial imagery suggested the presence of a large macrophyte bed (Figure 40d–e). Four Sites (42 to 45), located at the start of the seaward side of the estuary were highly heterogeneous environments with highly varying sediment types (mud/sand vs rock) and vegetated types (seagrass vs seaweed; percent cover based on the 2023 field survey information). This is an extremely difficult area to map using remote sensing techniques and the map classification identified very patchy vegetated habitat with a moderate probability (Figure 40a–c). For similar reasons, Site 35 in the inner estuary was excluded as it was located in a very patchy seagrass/seaweed environment with a wide range of percent cover.

Following the quality control of the 2023 field data, some field survey points had their polygons drawn slightly away from the field data location. The two circles with high vegetation coverage (> 60%) but low habitat probability (approximately 0, Figure 39b) correspond to the edges of seagrass habitat where slight shifts in seagrass coverage, or GPS inaccuracy (typical accuracy +/- 3-5 m but pixels are 25 cm) resulted in the specific field site coordinates overlapping sandy habitat. In this instance the training polygon was drawn slightly away from the field points in a continuous habitat section to avoid mixed habitat in model training (Figure 41d–e). Finally, some

turf dominated seaweed habitat points were changed to bare habitat points (diamonds; Figure 39) as the largest differences between the aerial imagery and field data occurred with turf seaweed habitats which encompass a small proportion of the vegetated community in St. Mary's River estuary relative to seagrass. For instance, while a turf/seaweed vegetation was observed at Site 31 in both 2019 and 2023 (Figure 42d–e), Site 36 presented as soft sedimentary habitat in 2019 (Figure 42a–c) based on comparisons with the spectra of other bare habitat sites (Site 38; Figure 38a–c). These shifts are not surprising as turf algae are more ephemeral than the habitat forming vegetation (seagrass/kelp) and the RGB and habitat map suggests the turf habitat may have shifted slightly west of the station in 2019 relative to 2023 (Figure 39, 42).

The 2008 aerial imagery was classified using an unsupervised k-means cluster analysis as there were large shifts in habitat distributions between 2008 and 2023. Three habitat types were denoted from the k-means analysis: bare, low-density vegetation, and high-density vegetation (Figure 43). The bare habitat class included all bare sediment habitat, and the high-density vegetation class included habitat that was likely dense seagrass habitat. The low-density vegetation class was a more mixed class that presented reflectance characteristics along the borders of the two other classes, and with intermediate reflectance between the bright sand and dark seagrass. This class likely contained vegetated habitat that was dominated by turf habitat, low-density seagrass habitat and/or dark sediments. As such, it may overestimate the extent of vegetated habitat coverage. The low-density class made up approximately 26% of the inset region, with only approximately 14% of the region being covered with high-density vegetation class (Table 6).

Large shifts in the distribution of vegetated habitat were observed between 2008 and 2019 (Figure 43). There was a large increase in the extent of the seagrass bed around Site 29 (Figure 33) between 2008 and 2019 (Figure 43). Examining the satellite imagery, this increase occurred prior to 2016 (Figure 34 and 38) and the bed remained stable into 2023 when field surveys occurred. There was a notable shift from low-density vegetation class in the northwest of the inset region in 2008 to bare in 2019 (Figure 43). On the northern side of the channel, the low-density class transitioned to high probability vegetated from 2008 to 2019. In general, the habitat extent in 2008 was patchier than in 2019 with non-continuous beds, whereas in 2019 the vegetated beds were larger and more continuous than in 2018, albeit slightly smaller in scale.

To quantify these habitat shifts, the 2019 bottom habitat map was thresholded to become a binary vegetated/bare habitat map and two scenarios were considered. The first indicated a "Low" vegetated habitat coverage scenario in 2008 where the low-density and bare class were merged into one bare habitat class, and the vegetated class represented only by the high-density vegetation class. This scenario indicated a conservative estimate of vegetation coverage in 2008. The second indicated a "High" vegetated habitat coverage scenario in 2008 where the low-density and high-density vegetation classes were merged into one vegetated class and indicated a maximum estimate of vegetation extent in 2008. The 2008 and 2019 classifications were then overlaid to understand where changes occurred between years (Figure 44).

In the "Low" scenario approximately 61% of the pixels were classified as bare habitat across both years (blue; Figure 44a). Approximately 30% of the pixels experienced a habitat shift which was dominated by a gain in vegetation from 2008 to 2019 (beige and gold; Figure 44a). This vegetated habitat gain was most evident around Site 29 and 28 (Figure 33) into a large

continuous vegetated habitat (gold; Figure 44b). This gain resulted in a total increase of vegetated habitat by 0.297 km^2 from 2008 to 2019 (Table 6; Figure 45).

In the “High” scenario approximately 48% of the pixels were classified as bare habitat across both years (blue; Figure 40a) and the total vegetated surface area was comparable from 2008 to 2019 (0.05 km^2 decrease; Table 6; Figure 45). While there was a minimal shift in total vegetated surface area, there was a larger pixel-wise shift of habitat type across years (beige and gold; Figure 40a). Where, approximately 16% of the 2008 vegetated habitat was lost by 2019, largely in the northwest and southeast of the inset region (beige; Figure 44c). There was still a large gain in vegetated habitat in the centre by Site 29 (gold) with more continuous vegetated habitat predicted along the southern shoreline.

Consequently, following this exploratory change detection analysis of seagrass/vegetation extent in St. Mary’s River estuary, it is likely that there has been an increase in summer seagrass habitat extent within the inset region since 2008. While the maximum predicted increase in the “Low” scenario was small (approximately 0.3 km^2), it represented a maximum of a 170% increase in total surface area. This increase had the highest certainty in the centre of the region around Site 29. Based on examining aerial and satellite imagery, this increase happened prior to 2016 and summer seagrass extent since 2016 has been relatively stable. Further work is required to understand why there was such a large change in summer distribution in 2008, and why seagrass habitat decreased in some winters but not all. Understanding any shifts in seagrass habitat is important to quantify, as it will impact the multitude of essential ecosystem functions and services seagrass provides.

Table 4. Average confusion matrix giving the accuracy metrics (%) from the 2019 random forest calculation. Overall map accuracy is bolded, kappa significance at 0.05 indicated with an asterisk.

Field Data	**Habitat Map**		**Producer Accuracy**	**Kappa**
	Bare	**Vegetated**		
Bare	1037.66	18.96	98.21	—
Vegetated	13.74	516.84	97.42	—
User Accuracy	98.69	96.46	**97.94**	0.95*

Table 5A. Proportion of map cells and total surface area of vegetated habitat by probability for the inset region for 2019 (see Figure 34 for map).

Min Probability	Max Probability	Number of Cells	Proportion of Cells (%)	Surface Area (km^2)
0	9	12900089	61.00	0.806
10	19	146994	0.70	0.009
20	29	98924	0.47	0.006
30	39	83448	0.39	0.005
40	49	73213	0.35	0.005
50	59	73242	0.35	0.005
60	69	83301	0.39	0.005
70	79	105285	0.50	0.007
80	89	152665	0.72	0.010
90	100	7429049	35.13	0.464
TOTAL	N/A	***21146210***	***100.00***	***1.322***

Table 5B. Proportion of map cells and total surface area of vegetated habitat by probability for the full mapped area for 2019 (see Figure 34 for map).

Min Probability	Max Probability	Number of Cells	Proportion of Cells (%)	Surface Area (km^2)
0	9	44164512	56.49	2.760
10	19	390342	0.50	0.024
20	29	334279	0.43	0.021
30	39	214323	0.27	0.013
40	49	356188	0.46	0.022
50	59	222490	0.28	0.014
60	69	251745	0.32	0.016
70	79	468694	0.60	0.029
80	89	854638	1.09	0.053
90	100	30927565	39.56	1.933
TOTAL	N/A	***78184776***	***100.00***	***4.887***

Table 6. Proportion of map cells and surface area of vegetated habitat for the pink inset region (Figure 33) in 2008 and 2019 by habitat type.

Year	Class	Number of Cells	Proportion of Cells (%)	Surface Area (km^2)
2008	Bare	12795627	60.51	0.800
2008	High Density Vegetation	2822384	13.35	0.176
2008	Low Density Vegetation	5528128	26.14	0.346
2019	Bare	13564435	64.15	0.848
2019	Vegetation	7581704	35.85	0.474

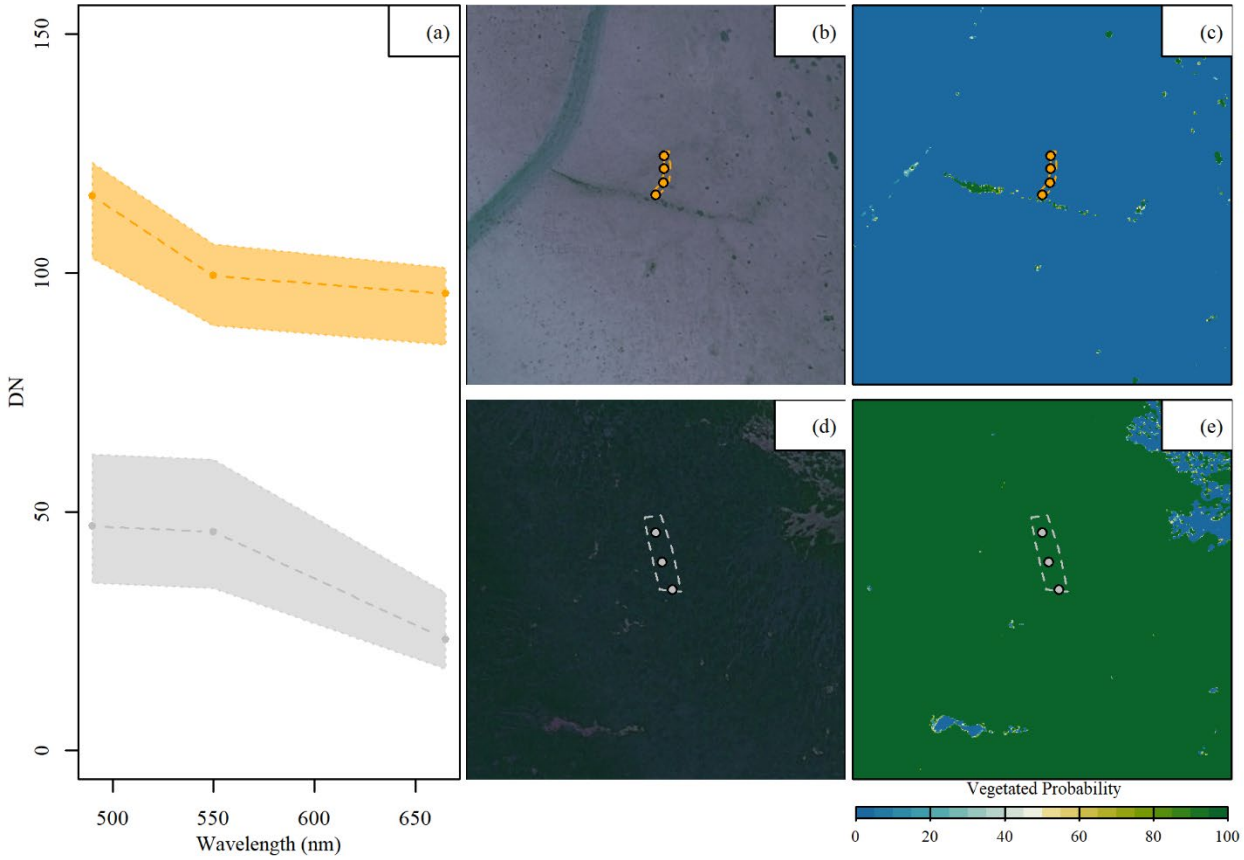

Figure 38. Example bare sediment (top row; Site 37; orange) and eelgrass bed (bottom row; Site 29; grey). Spectral signature (left column) based on the digital number (DN) showing the average (dashed line) and range (shading). Aerial imagery red green and blue (RGB) (middle column; b, d) showing the 2023 field drift survey sampling location (points) and the dashed lines show the polygon used to extract the spectral signatures. Final map classification (right column; c, e) where green colours are vegetated habitat and blue colours are bare sediment).

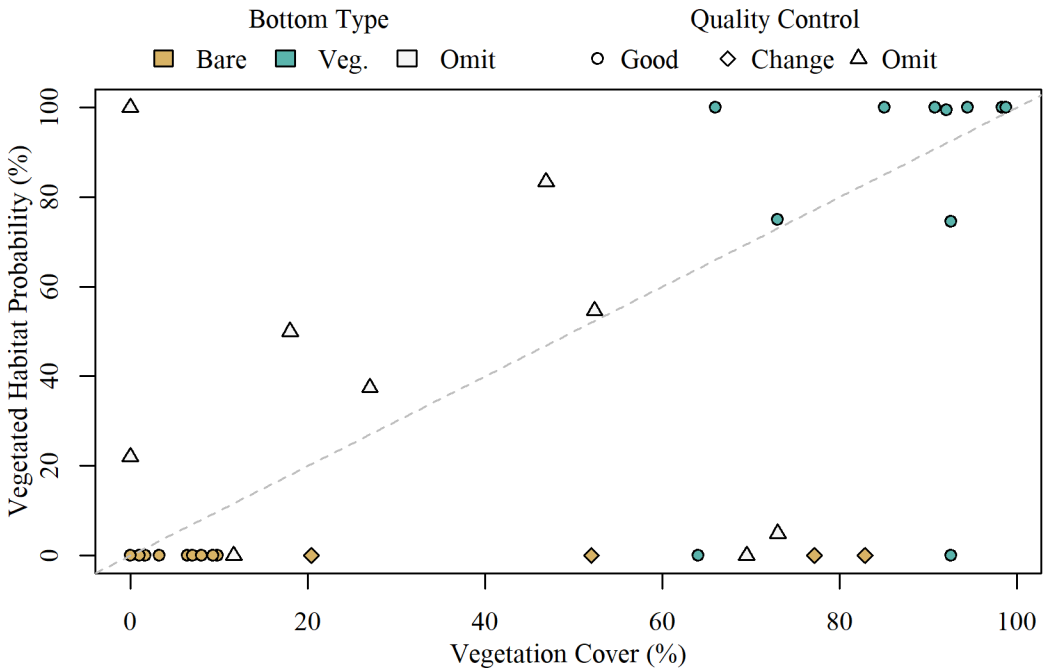

Figure 39. Average vegetated habitat probability from the 2019 aerial imagery versus the average percent cover the field data collected in 2023 showing vegetated habitat cover. Colour indicates what habitat label was given to a point in the random forest classification, shape indicates the quality control check performed on the data. Grey dashed line shows the 1:1 line.

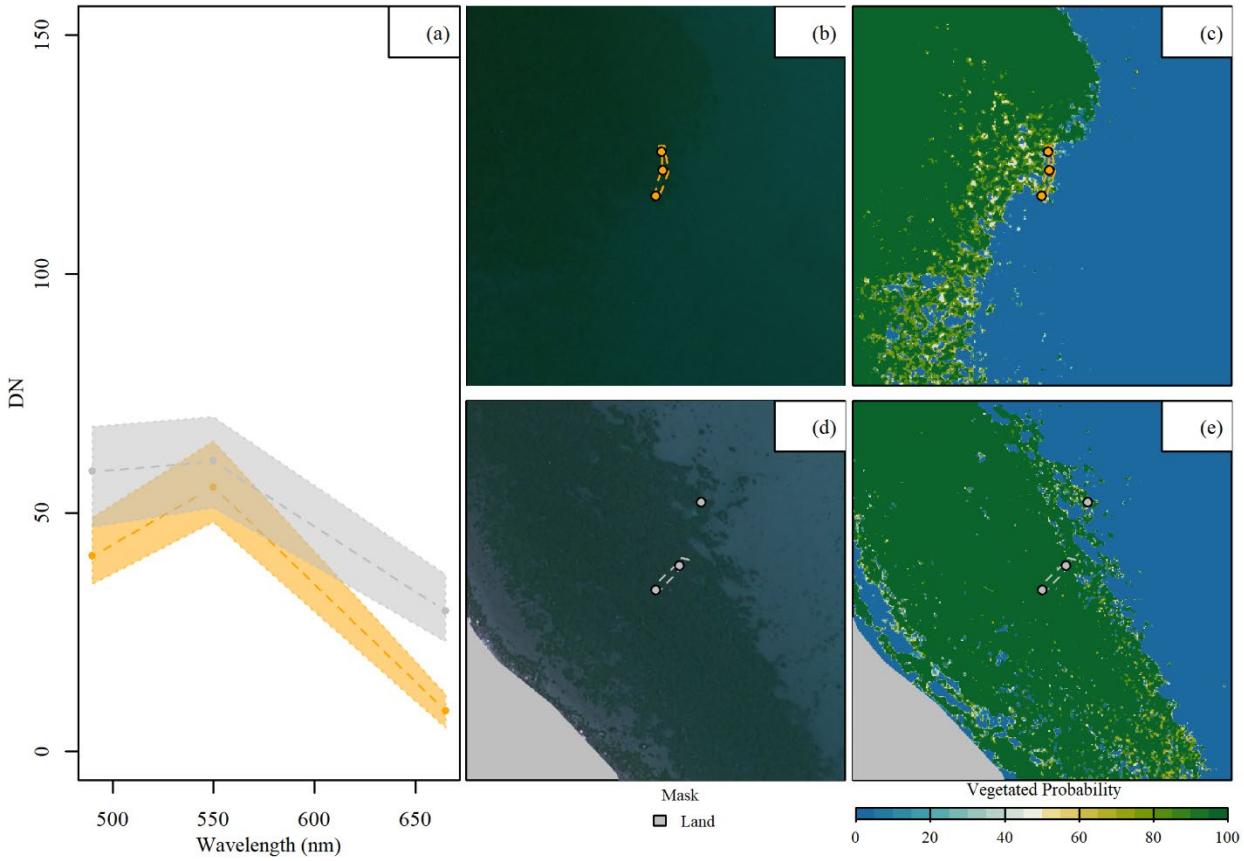

Figure 40. Example bed edge transition from vegetated to sand (b, e; Site 51: orange) and habitat shift between 2019 and 2023 (d, e; Site 39; grey). Spectral signature (a) based on the digital number (DN) showing the average (dashed line) and range (shading). Aerial imagery red green blue (RGB) (b, d) showing the 2023 field drift survey sampling location (points) and the dashed lines show the polygon used to extract the spectral signatures. Final map classification (c, e) where green colours are vegetated habitat and blue colours are bare sediment).

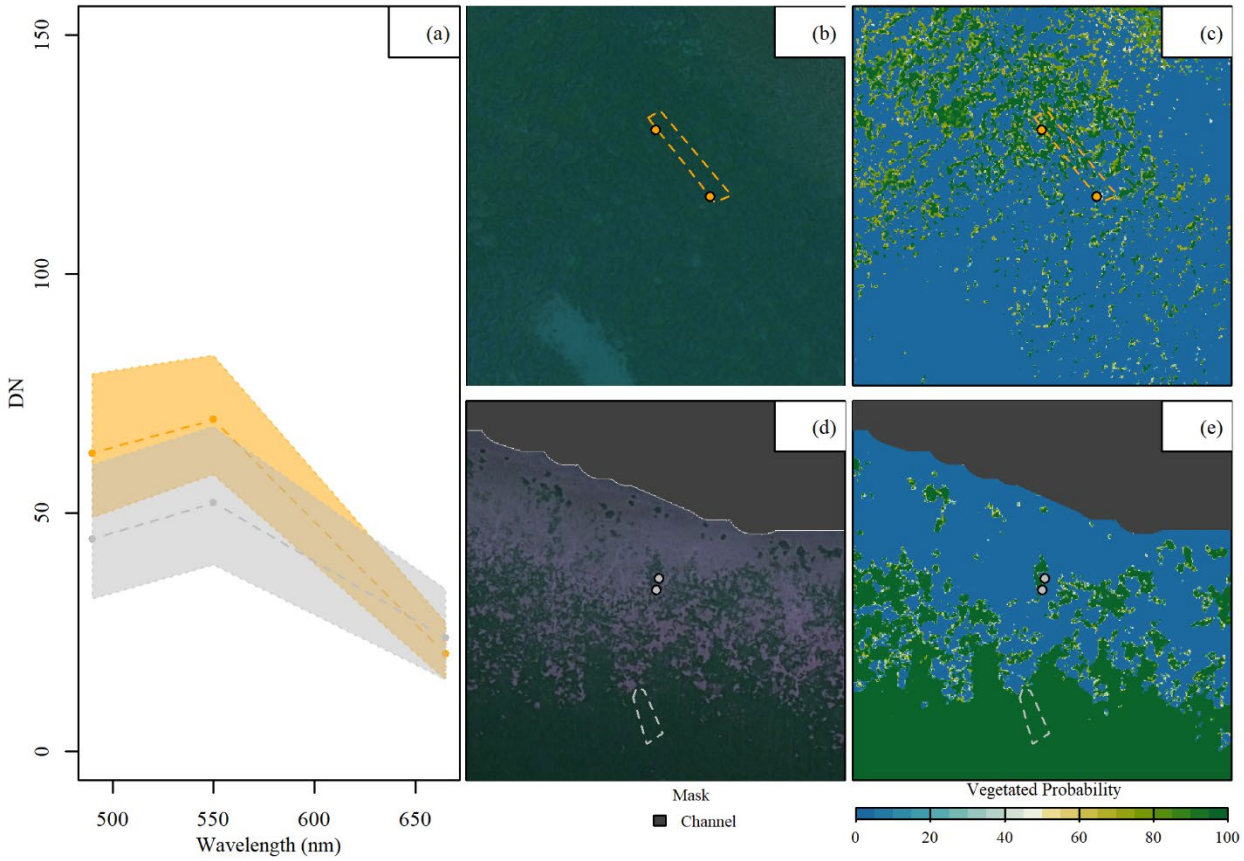

Figure 41. Example heterogenous habitat (b, c; Site 43; orange) and eelgrass bed (b, e; Site 24; grey). Spectral signature (a) based on the digital number (DN) showing the average (dashed line) and range (shading). Aerial imagery red green blue (RGB) (b, d) showing the 2023 field drift survey sampling location (points) and the dashed lines show the polygon used to extract the spectral signatures. Final map classification (c, e) where green colours are vegetated habitat and blue colours are bare sediment).

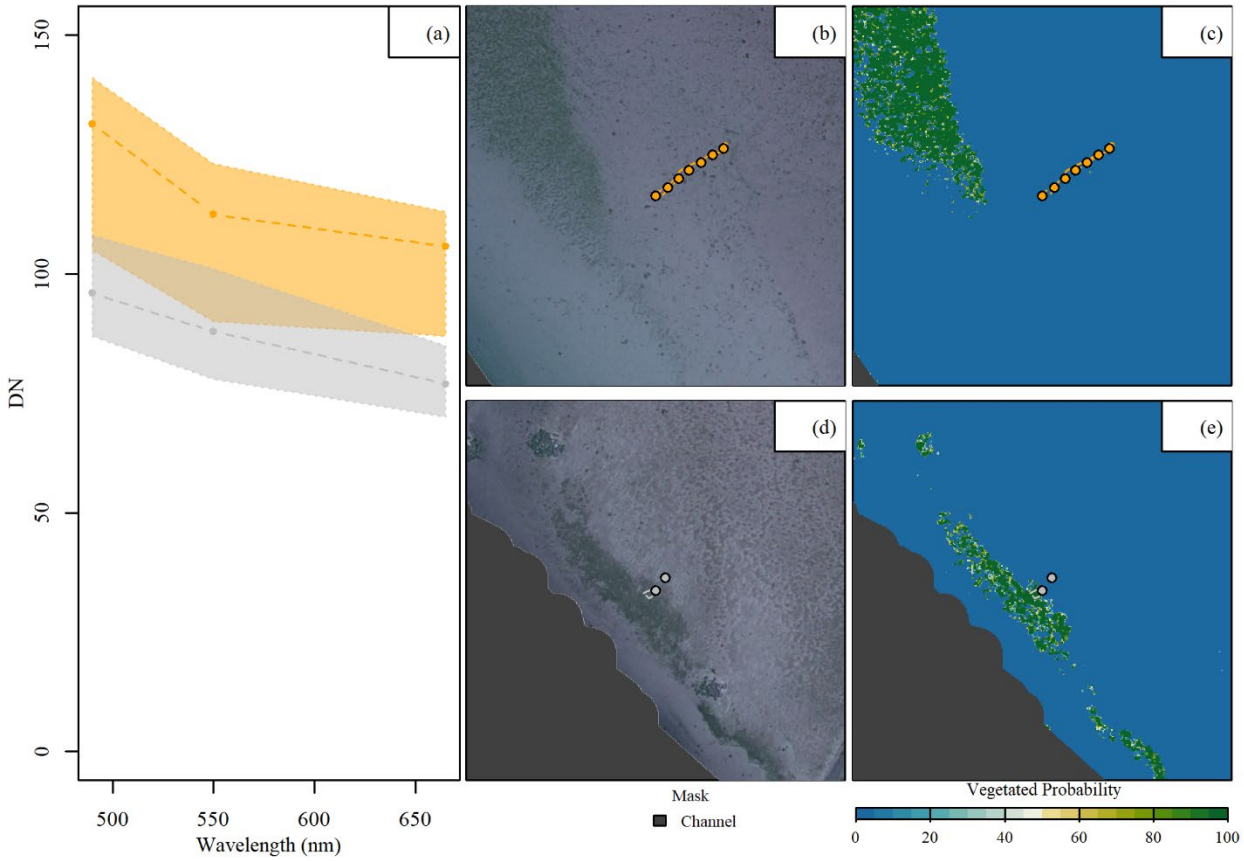

Figure 42. Example bare sediment (b, c; Site 36; orange) and turf habitat (d, e; Site 31; grey). Spectral signature (a) based on the digital number (DN) showing the average (dashed line) and range (shading). Aerial imagery red green blue (RGB) (b, d) showing the 2023 field drift survey sampling location (points) and the dashed lines show the polygon used to extract the spectral signatures. Final map classification (c, e) where green colours are vegetated habitat and blue colours are bare sediment).

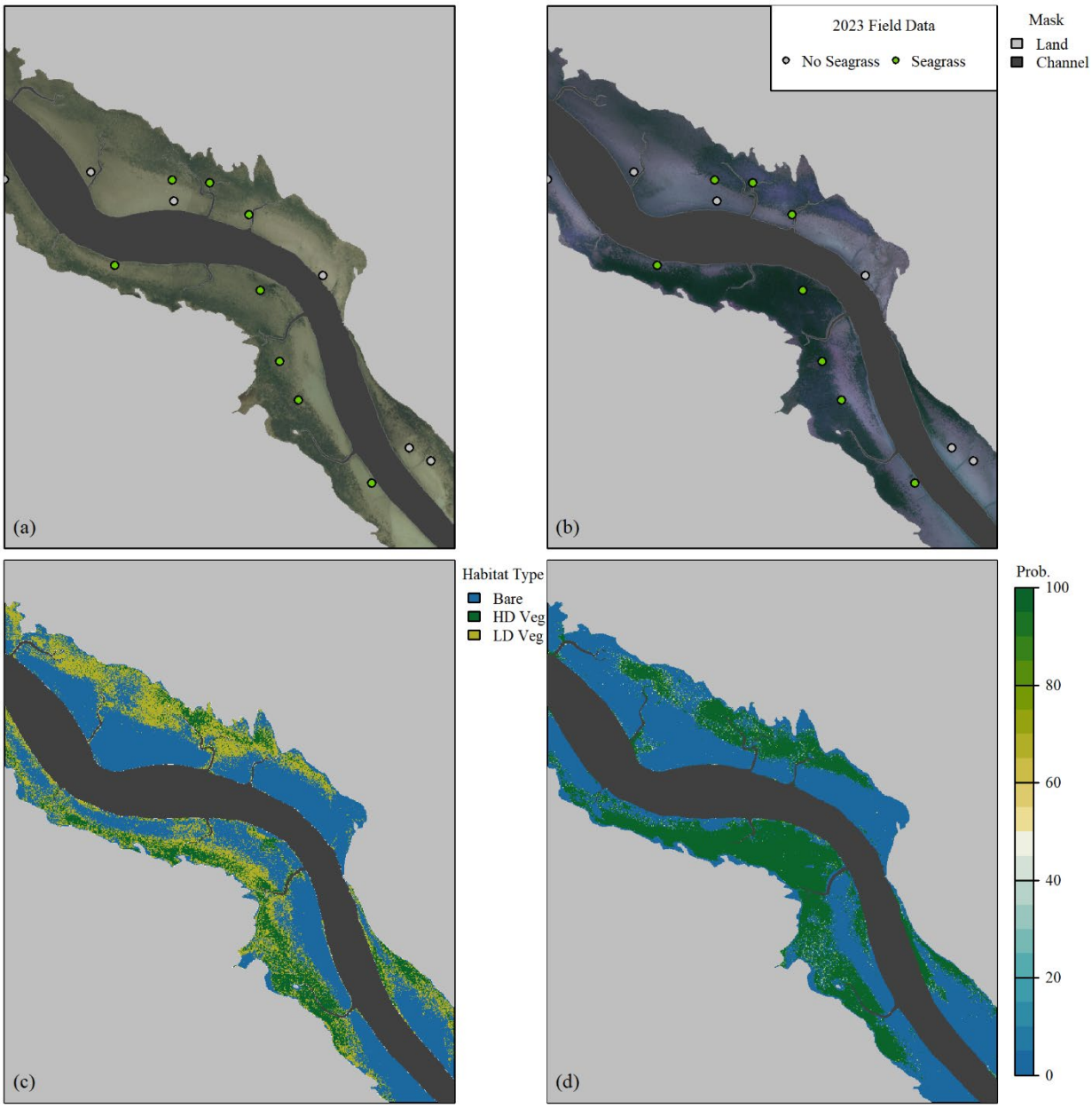

Figure 43. Aerial imagery acquired in 2008 (a) and 2019 (b) within the pink polygon inset region from Figure 33 showing the locations of the large seagrass beds observed in 2023. The 2008 k-means cluster analysis indicating the dominant bottom habitat type of bare, low density vegetation (LD Veg), and high density vegetation (HD Veg; c) compared to the 2019 random forest classification showing probability of vegetated habitat (Prob.; d).

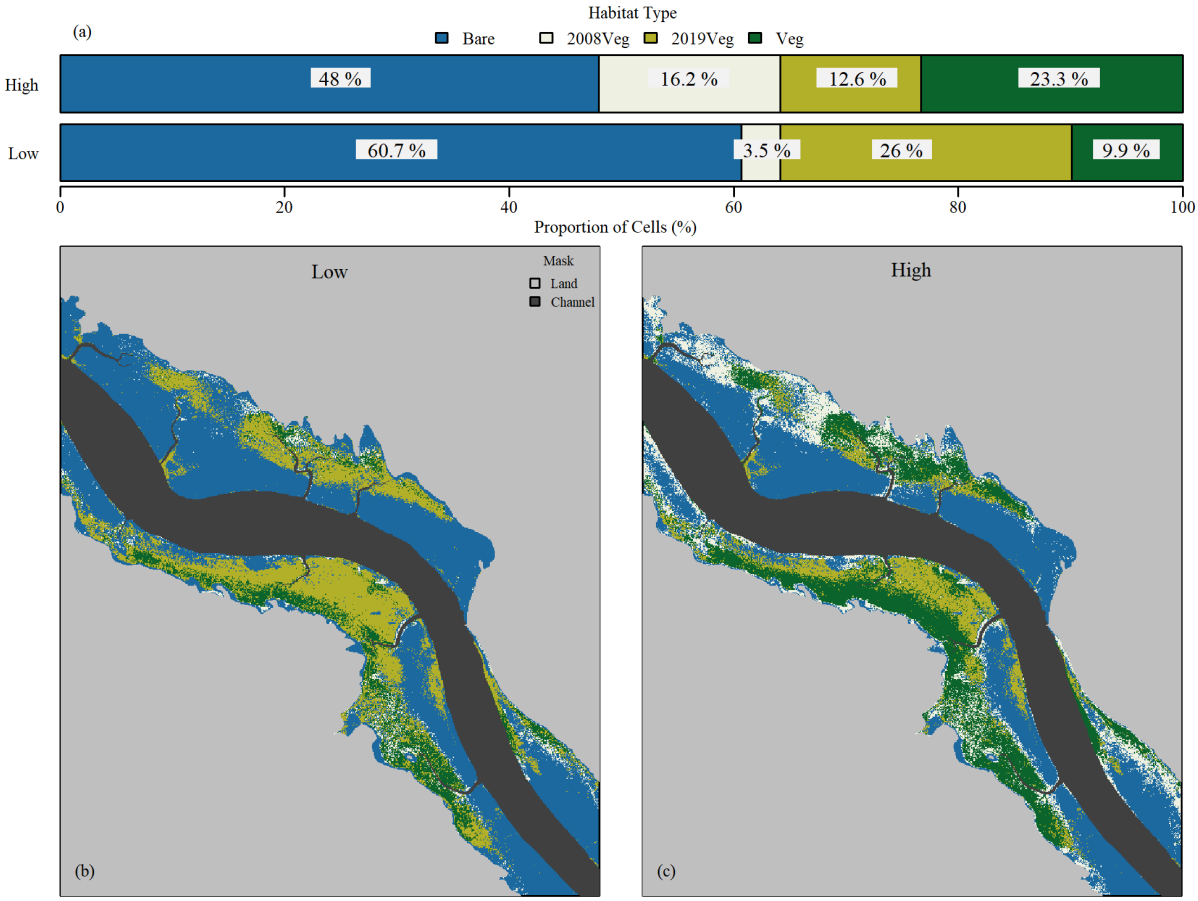

Figure 44. Comparison of bottom habitat maps between 2008 and 2019. Proportion of cells that agreed or disagreed across years where bare/vegetated was bare/vegetated in both 2008 and 2019 (a). Bare cells in 2008 but vegetated (Veg) in 2019 are labelled “2019Veg”. Vegetated cells in 2008 but bare in 2019 are labelled “2008Veg”. The “low” habitat map is the conservative habitat map in 2008 where only the high density vegetation cluster was labelled as vegetated habitat (c). The “high” habitat map is the maximum distribution as it included the low density and high density vegetation clusters (c).

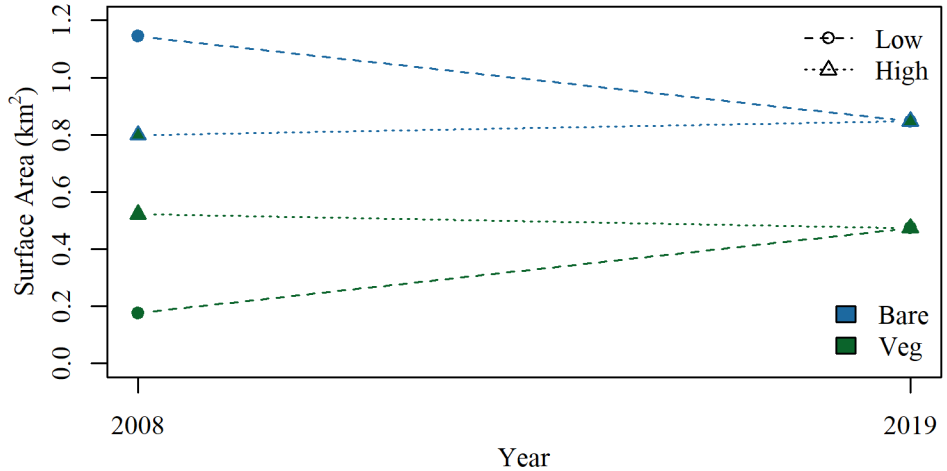

Figure 45. Surface area for the low and high estimate by habitat type and year.

7 Faunal Communities

The Canadian Parks and Wilderness Society – Nova Scotia Chapter (CPAWS-NS) received funding from DFO Science to conduct marine biodiversity surveys and community outreach in areas of interest for the establishment of Marine Protected Areas (MPAs) or Other Effective Area-based Conservation Measures (OECMs). The objectives of these surveys are to document as much biodiversity as possible in the field, identify important habitat for species of conservation concern, and share these results within the communities where they are conducted. CPAWS-NS also endeavors to share relevant information with the academic community. There is an overall gap in available ecological data pertaining to the intertidal biodiversity of Nova Scotia. By physically entering the water and observing community compositions across a spatio-temporal scale, CPAWS-NS aims to fill this gap through observing novel behaviours, species occurrences, and photo documentation.

7.1 Methods

Snorkel surveys were conducted at eight sites (Figure 46, location coordinates in Table A3) in the summer and fall of 2023, with repeated surveys done at the McDiarmid's Cove site in June, August and September. At least three individuals were required to conduct these surveys. For safety, one person would function as shore support; watching for surface hazards and able to quickly notify emergency services should an incident occur. Site selection was based on accessibility from shore or by kayak and informed by knowledge shared by community members and other researchers. Once a site was selected, the snorkellers would don full environmental protection equipment (wetsuits or drysuits depending on the time of year) and enter the water. Snorkellers photographed or video recorded species that could not be identified in the field for later identification, and also for general documentation of species and their behaviours. The cameras used were Olympus TG-6 with PT-059 underwater housing, Sony A6600 mirrorless with 12-16mm lens and Ikelite housing, and GoPro® Hero10.

Each snorkeller was also equipped with a dive slate to write down the observed species, as well as their estimate of abundance. Abundance indices were borrowed and slightly modified from the Reef Environmental Education Foundation (REEF) Volunteer Fish Survey project protocol (REEF, n.d.) and were as follows: S – Single (n = 1), F – Few (n = 2–10), M – Many (n = 11–99), A – Abundant (n = 100+). For algae and colonial animals, % cover estimates and number of colonies was used to equate individuals. The snorkellers would move freely through the site, covering as much area as was safely possible. Current and depth were the main factors influencing the area surveyed. Surveys typically lasted between 40–60 minutes depending on environmental conditions, with the effect of cold temperatures on observers usually dictating survey duration.

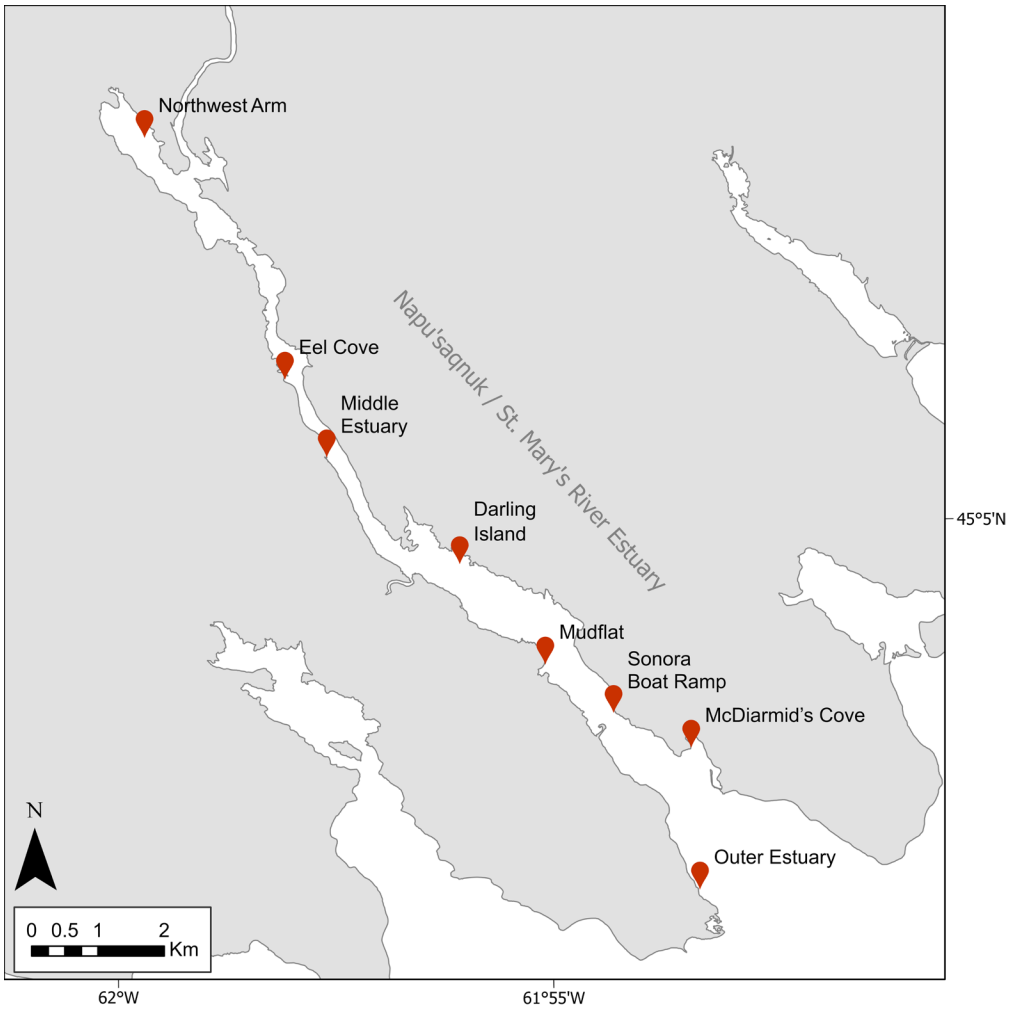

Figure 46. Location of survey sites (marked with red pin) throughout the St. Mary's River Estuary.

7.2 Results and Discussion

In total, 59 flora and fauna species were observed (Table 7, Appendix C) during the 2023 season across ten surveys at eight locations in the estuary (Figure 46, Table A3). The highest number of species documented on a single survey was 27, which occurred at two separate surveys in McDiarmid's Cove (Table 7). Observed species diversity increased towards the outer estuary, which is unsurprising because both marine and freshwater species can occupy this habitat. The outer estuary exhibited high algal diversity; however, many algae are difficult to identify without microscopy and expert practical taxonomic knowledge. Thus, the algal diversity is certainly underestimated from the Outer Estuary site (Table 7).

Several diadromous fish species of regional conservation importance were observed in the estuary, including Rainbow Smelt (*Osmerus mordax*), American Eel (*Anguilla rostrata*), and Gaspereau (*Alosa pseudoharengus*). Young American Eels (elver) were prevalent throughout the upper-middle estuary throughout the field season (Table 7). Salinity is a factor that limits elver distribution in the estuary, but likely sediment also plays a key role (Pratt et al. 2014). Wherever elvers were observed, the sediment consisted of fine sediment or mud where they would quickly burrow into if disturbed by observers. American Eels have complex life histories

that vary within and between populations, with some young eels (approximately 1 year) making trips in and out of estuaries while others remain freshwater residents (Jessop et al. 2002). Juvenile eels are too small to be tracked via radio or acoustic telemetry, and so much of their movement ecology remains unknown.

Other fish species tolerant of brackish water included Northern Pipefish (*Syngnathus fuscus*), Four-spine stickleback (*Apeltes quadracus*), and Three-spine Stickleback (*Gasterosteus aculeatus*). Sticklebacks, in particular Three-spine Stickleback*,* are well-known for exhibiting remarkable plasticity in life history traits such as osmotic tolerance and social behaviour (Baker et al. 2015). Thus, it is not surprising that they were observed throughout the estuary (Table 7). Northern Pipefish are associated with eelgrass (*Zostera marina*) and were typically observed among uprooted eelgrass, which lay in piles across the sediment. A large eelgrass bed nearly spanning the width of the estuary and visible from shore at low tide near the Sonora Boat Ramp and Mudflat sites was observed. The prevailing current from the river cuts a channel into the bed of the estuary, and it was only here that eelgrass was not growing. Sediment piles up on either side, creating excellent growing conditions for eelgrass, which in turn fixes the sediment with its roots.

Davis (1976) performed a similar biodiversity survey of the St. Mary's River estuary in the summer of 1973 and winter 1975 at twelve shore stations that spanned the estuary gradient and covered the diversity of habitats found in the estuary. The survey was conducted over five days (4 days summer of 1973, 1 day in winter 1975) and involved recording visual observations of species and collections of representative plant and animal specimens from each station, either by hand or by sieving the sediments and vegetation in the water (Davis 1976). However, Davis (1976) also surveyed for bottom infauna using a small hand-held dredge. Many of the same aquatic faunal species were observed in 1973/1975 as in 2023, with a few notable differences (Table 8). For instance, the invasive European Green Crab (*Carcinus maenus*) was not found in 1973/1975, but was present in 2023, indicating a potential increase in abundance or spread of the invasive species over that time period. Additionally, some fishes were observed in 1973/1975 but not in 2023, such as the American Shad (*Alosa sapidissima*), Atlantic Silverside (*Menidia menidia*), killifish species (*Fundulus* spp.), and Atlantic Salmon (*Salmo salar*). However, the presence of many of these species has been confirmed in other studies (e.g., Atlantic Salmon, Bowlby et al. 2014; and Killifish, Hernandez-Chavez and Turgeon 2007, Dalziel et al. 2020) and observations likely differ between years due to differences in sampling time as well as tidal stage. Importantly, plankton and bottom meiofauna were not studied in either the 2023 or 1973/1975 surveys.

Overall, the St. Mary's River estuary was found to support a diverse community of fishes, invertebrates, and macrophytes. Various life stages of different species and dynamic communities that shifted across the seasons were observed. This watershed supports habitats that were observed being used by several species of conservation importance, such as American Eel, Rainbow Smelt, and Gaspereau.

Table 7. A list of animal and macrophyte species observed in the St. Mary's estuary at sites: Northwest Arm (upper Estuary), Eel Cove, Middle Estuary, Darling Island, Mudflat, Sonora Boat Ramp, McDiarmid's Cove, and Outer Estuary (see Figure 46 for locations), with survey dates listed below. Abundance indices were estimated following the Reef Environmental Education Foundation (REEF) Volunteer Fish Survey project protocol (REEF, n.d.), where indices include: Single (n = 1), Few (n = 2-10), Many (n = 11-99), Abundant (n = 100+), and — (Not Observed).

Species	Common Name	Northwest Arm 29/09/2023	Eel Cove 01/08/2023	Middle Estuary 26/09/2023	Darling Island 26/09/2023	Mudflat 27/09/2023	Sonora Boat Ramp 13/06/2023	McDiarmid's Cove 13/06/2023	McDiarmid's Cove 01/08/2023	McDiarmid's Cove 25/09/2023	Outer Estuary 28/09/2023
Agarum clathratum	sieve kelp	—	—	—	—	—	—	Few	—	—	—
Alosa pseudoharengus	Gaspereau / Alewife	Many	—	—	—	—	—	—	Many	—	—
***Ammodytes* sp.**	Sand Lance	—	—	—	—	—	Many	Abundant	Abundant	—	—
Anguilla rostrata	American Eel	Few	Many	—	—	Few	—	—	—	—	—
Apeltes quadracus	Four-spine Stickleback	Few	—	Few	—	—	—	—	—	—	—
Ascophyllum nodosum	knotted wrack	—	—	—	Few	—	—	Abundant	Many	Many	Abundant
Asterias rubens	Atlantic Sea Star	—	—	—	—	—	—	—	—	Single	—
Buccinum undatum	Common Whelk	—	—	—	—	—	—	—	Single	—	—
Cancer borealis	Jonah Crab	—	—	—	—	—	—	—	—	—	Few
Cancer irroratus	Rock Crab	—	—	—	—	—	—	Many	—	—	—
Carcinus maenas	European Green Crab	—	Few	Many	Many	Many	Many		Many	Abundant	Many
Chondrus crispus	Irish moss	—	—	—	—	—	—	Many	Many	—	Many
Chorda filum	cordweed	—	—	—	—	—	—	Few	—	—	—
***Cistenides* sp.**	trumpet worm	—	—	—	—	—	—	—	—	—	Few
Codium fragile	oyster-thief	—	—	—	—	—	—	—	—	Single	Few
Corallina officinalis	common coralline	—	—	—	—	—	—	—	Many	Few	Abundant
***Corixidae* sp.**	water boatmen	—	Abundant	—	—	—	—	—	—	—	—
Crangon septemspinosa	Sand Shrimp	—	Many	Abundant	Many	Many	Abundant	—	Abundant	Many	—
Crassostrea virginica	American Oyster	—	—	—	—	Single	—	—	Few	—	—
Crepidula fornicata	Atlantic Slippersnail	—	—	—	—	—	—	Few	Many	Few	Many
***Desmarestia* sp.**	witch's locks	—	—	—	—	—	—	—	Few	—	—
Dyme pumila	sea oak	—	—	—	—	—	—	Many	—	—	—
Ensis leei	Razor Clam	—	—	—	—	—	—	Few	Few	Few	—
Fucus distichus	Rockweed	—	—	—	—	—	—	—	Many	Few	Many
Fucus spiralis	spiral wrack	—	—	—	Few	—	Few	—	Many	Few	Many
Fucus vesiculosus	vesicled wrack	—	—	—	—	—	—	—	—	Few	—
Furcellaria lumbricalis	red forkweed	—	—	—	—	—	—	Few	Few	—	—
Gasterosteus aculeatus	Three-spine Stickleback	—	Single	—	Few	Few	—	—	—	—	—
Halosiphon tomentosum	mermaid's tresses	—	—	—	—	—	—	—	Few	—	—
Lacuna vincta	Northern Lacuna	—	—	—	—	—	—	—	—	—	Many
Laminaria digitata	finger kelp	—	—	—	—	—	—	Few	—	Few	Many

Species	Common Name	Northwest Arm 29/09/2023	Eel Cove 01/08/2023	Middle Estuary 26/09/2023	Darling Island 26/09/2023	Mudflat 27/09/2023	Sonora Boat Ramp 13/06/2023	McDiarmid's Cove 13/06/2023	McDiarmid's Cove 01/08/2023	McDiarmid's Cove 25/09/2023	Outer Estuary 28/09/2023
***Lithothamnion* sp.**	encrusting coralline	—	—	—	—	—	—	Many	Few	—	Abundant
Littorina obtusata	Flat Periwinkle	—	—	—	—	—	—	—	—	—	Few
***Littorina* sp.**	Winkles	—	—	—	Few	Abundant	Many	—	Abundant	Many	Abundant
Metridium senile	Plumose Anemone	—	—	—	—	—	—	—	—	—	—
Microgadus tomcod	Tomcod	—	—	—	—	—	—	—	—	Few	—
Modiolus modiolus	Horse Mussel	—	—	—	—	—	—	—	—	Few	—
Mya areria	Softshell Clam	—	—	Single	Many	Few	—	—	Many	Abundant	—
Myoxocephalus scorpius	Shorthorn Sculpin	—	—	—	—	—	Few	—	—	Few	Few
***Mysis* sp.**	Opossum Shrimp	—	Many	Few	Few	Many	Abundant	Abundant	Abundant	Few	—
Mytilus edulis	Blue Mussel	—	—	—	Few	Few	Few	—	Many	Single	—
Nucella lapillus	Atlantic Dogwhelk	—	—	—	—	—	—	—	—	—	Few
Osmerus mordax	Rainbow Smelt	—	—	—	—	—	—	Many	—	—	—
Pagurus acadianus	Acadian Hermit Crab	—	—	—	—	—	—	—	Many	—	Many
Palmaria palmata	dulse	—	—	—	—	—	—	Few	—	Few	Few
Pholis gunnellus	Rock Gunnel	—	—	—	—	—	—	—	—	—	Single
Praunus flexuosus	Chameleon Shrimp	—	—	—	—	—	—	—	Few	—	—
Pseudopleuronectes americanus	Winter Flounder	—	—	—	—	Single	—	—	Few	Few	Few
Ptilota serrata	serrated red algae	—	—	—	—	—	—	—	—	Few	Many
Sacchari latissima	sugar kelp	—	—	—	—	—	—	Few	—	Few	—
Semibalanus balanoides	Common Rock Barnacle	—	—	—	—	—	Abundant	—	—	Many	Abundant
***Spiorbis* sp.**	coilworm	—	—	—	—	—	—	Abundant	—	—	—
Syngthus fuscus	Northern Pipefish	—	—	Few	Few	—	—	—	—	—	—
Testudilia testudilis	Tortoiseshell Limpet	—	—	—	Few	—	—	—	—	Few	Many
Tiaropsis multicirrata	N/A	—	—	—	—	—	Abundant	Few	—	—	—
Ulva lactuca	sea lettuce	—	—	—	—	—	—	—	Few	Few	—
***Urophycis* sp.**	Hake	—	—	—	—	—	—	—	Few	—	—
Vertebrata lanosa	N/A	—	—	—	—	—	—	—	Many	Abundant	Abundant
Zostera marina	eelgrass	—	—	—	—	Abundant	Abundant	—	—	—	—

Table 8. Cumulative Species List observed in St. Mary's River estuary as part of the 2023 faunal snorkel surveys and documented in Davis (1976) surveys, including infaunal communities surveyed with a hand-held dredge, conducted in the summer of 1973 and January of 1975. See Table 7 for breakdown of site-specific species lists and abundance indices within the St. Mary's estuary based on the 2023 surveys. Dash (—) indicates species not noted.

Species	Common Name	2023 Faunal Surveys	Davis (1976)
Acrosiphonia arcta	Arctic sea moss	—	X
Agarum clathratum	sieve kelp	X	—
Alaria esculenta	winged kelp	—	X
Alosa pseudoharengus	Gaspereau / Alewife	X	X
Alosa sapidissima	American Shad	—	X
Ameritella agilis	Northern Dwarf-tellin	—	X
Ammodytes sp.	Sand Lance	X	—
Amphipoda	N/A	—	X
Anguilla rostrata	American Eel	X	X
Apeltes quadracus	Four-spine Stickleback	X	X
Apohyale prevostii	N/A	—	X
Ascophyllum nodosum	Knotted Wrack	X	X
Asterias rubens	Atlantic Sea Star	X	X
Balanus crenatus	Acorn Barnacle	—	X
Brevoortia tyrannus	Atlantic Menhaden	—	X
Buccinum undatum	Common Whelk	X	X
Cancer borealis	Jonah Crab	X	—
Cancer irroratus	Rock Crab	X	X
Carcinus maenas	Green Crab	X	—
Chiridotea coeca	Sand isopod	—	X
Chondrus crispus	Irish moss	X	X
Chorda filum	cordweed	X	—
Chordaria flagelliformis	black whip weed	—	X
Cistenides sp.	trumpet worm	X	—
Cladophora spp.	N/A	—	X
Codium fragile	oyster-thief	X	—
Corallina officinalis	common coralline	X	X
Corixidae	water boatmen	X	—
Corophium	N/A	—	X
Crangon crangon	Brown Shrimp	—	X
Crangon septemspinosa	Sand Shrimp	X	—
Crassostrea virginica	American Oyster	X	—
Crepidula fornicata	Atlantic Slippersnail	X	—
Desmarestia sp.	witch's locks	X	X
Dictyosiphon foeniculaceus	N/A	—	X
Dynamena pumila	sea oak	X	—
Ecrobia truncata	Minute Hydrobia	—	X
Ectocarpus siliculosus	N/A	—	X
Ectopleura larynx	ringed tubularia	—	X
Ensis leei	Razor Clam	X	—
Euspira heros	Northern Moon Snail		X
Fucus distichus	rockweed	X	—
Fucus spiralis	spiral wrack	X	X
Fucus vesiculosus	vesicled wrack	X	X
Fundulus - hybrid	N/A	—	X
Fundulus diaphanus	Banded Killifish	—	X
Fundulus heteroclitus	Common Killifish / Mummichog	—	X
Furcellaria lumbricalis	Clawed fork weed	X	—
Gammarellus angulosus	N/A	—	X
Gammarus sp.	N/A	—	X
Gammarus mucronatus	N/A	—	X
Gammarus oceanicus	N/A	—	X
Gammarus tigrinus	N/A	—	X
Gasterosteus aculeatus	Three-spine Stickleback	X	—
Haliclona oculata	mermaid's glove		X
Halosiphon tomentosum	mermaid's tresses	X	—
Homarus americanus	American Lobster		X
Hydroidolina	N/A	—	X

Species	Common Name	2023 Faunal Surveys	Davis (1976)
Hyperia	N/A		X
Jaera albifrons	N/A	—	X
Jassa falcata	N/A	—	X
Lacuna vincta	Northern Lacuna	X	X
Laminaria digitata	finger kelp	X	X
Lepidonotus squamatus	scale worm	—	X
Limonium carolinianum	Carolina sea lavender	—	X
Lithothamnion sp.	encrusting coralline	X	—
Littorina littorea	Common Periwinkle	—	X
Littorina obtusata	Flat Periwinkle	X	X
Littorina saxatilis	Rough Periwinkle	—	X
Littorina sp.	Winkles	X	—
Melosira sp.	N/A	—	X
Menidia menidia	Atlantic Silverside	—	X
Metridium senile	Plumose Anemone	X	—
Microgadus tomcod	Tomcod	X	X
Modiolus modiolus	Horse Mussel	X	—
Mya arenaria	Softshell Clam	X	X
Myoxocephalus aenaeus	Grubby Sculpin	—	X
Myoxocephalus scorpius	Shorthorn Sculpin	X	—
Mysis sp.	Opossum Shrimp	X	—
Mytilus edulis	Blue Mussel	X	X
Nemertea	N/A	—	X
Alitta virens	sandworm	—	X
Nucella lapillus	Atlantic Dogwhelk	X	X
Ophiopholis aculeatus	Daisy Brittle Star	—	X
Osmerus mordax	Rainbow Smelt	X	X
Pagurus acadianus	Acadian Hermit Crab	X	—
Palmaria palmata	dulse	X	—
Pelagia noctiluca	Mauve Stinger	—	X
Petalonia fascia	false kelp	—	X
Petromyzon marinus	Sea Lamprey	—	X
Pholis gunnellus	Rock Gunnel	X	X
Pyilaiella littoralis	sea felt	—	X
Plantago maritima var. juncoides	seaside plantain	—	X
Porphyra umbilicalis	laver	—	X
Praunus flexuosus	Chameleon Shrimp	X	—
Pseudopleuronectes americanus	Winter Flounder	X	—
Ptilota serrata	serrated red algae	X	—
Pungitius pungitius	Ninespine Stickleback	—	X
Rhizoclonium riparium	N/A	—	X
Sabellaria	N/A	—	X
Saccharina latissima	sugar kelp	X	X
Salicornia maritima	slender glasswort	—	X
Salmo salar	Atlantic Salmon	—	X
Salvelinus fontinalis	Brook Trout	—	X
Scytosiphon lomentaria	beanweed	—	X
Semibalanus balanoides	Common Rock Barnacle	X	X
Spartina alterniflora	smooth cordgrass	—	X
Spirorbis sp.	coilworm	X	—
Strongylocentrotus droebachiensis	Green Sea Urchin	—	X
Sueda esteroa	estuary seablite	—	X
Syngnathus fuscus	Northern Pipefish	X	—
Testudinalia testudinalis	Tortoiseshell Limpet	X	X
Tiaropsis multicirrata	N/A	X	—
Trichocorixa spp.	N/A	—	X
Ulva lactuca	sea lettuce	X	—
Ulva spp.	N/A	—	X
Urophycis sp.	Hake	X	—
Vertebrata lanosa	N/A	X	—
Zannichellia palustris	horned pondweed	—	X
Zostera marina	eelgrass	X	X

8 Knowledge Gaps

This report provides a preliminary overview of the ecological and physical features of the St. Mary's River estuary. Although time was limited to one field season (summer 2023), the study provided initial insights into the physical oceanography, sediment dynamics, macrophyte distribution and condition, and faunal diversity. Further work across extended timescales would allow additional insights into interannual variability in both oceanographic and biological processes. While some insights into future change can be examined using the oceanographic model, further *in situ* data collection within a long-term monitoring framework would be useful. Additionally, inclusion of Indigenous and local knowledge would also help strengthen our understanding of the St. Mary's River estuary ecosystem. More specific knowledge gaps related to the different aspects examined in this study are also evident and discussed below.

The oceanographic modelling revealed that processes within the river channel were strongly influenced by the ocean. The influences from the ocean, however, are not well understood due to the lack of field observations and model research. In particular, the role of storm events and climate change on physical oceanography processes in the estuary require more attention. Climate change will also influence river discharge levels and frequency, and future research is needed to understand how changes to freshwater delivery may affect biological and physical processes in the estuary (Condie et al. 2012, Kimmerer 2002).

The sediment work provided insights into sediment conditions across the estuary as well as turbidity dynamics and relationships with water currents and significant wave heights. The sediment work was, however, limited to a few months in the summer season. In fact, the anomalous rainfall events during the summer were not fully captured by the instrumentation, although their long-term outcomes were evident. A full understanding of the sediment dynamics in the St. Mary's River estuary would require longer time-series measurements that span the year, capturing seasonal events that likely play a key role in structing sediment dynamics in the estuary, such as the spring river freshet. Moored instruments at different locations along the river estuary would allow understanding of how changing physical conditions (i.e., freshwater discharge, tidal currents) influence processes such as the turbidity maximum and sediment transport.

Using remote sensing techniques (Section 6.2), it was found that seagrass distribution has varied seasonally and in some cases annually over the last 15 years, but total extent has remained relatively constant from 2016 to 2023. It remains unknown why summer seagrass distribution in 2008 was so drastically reduced compared to recent years (2016–2023). Further work could focus on understanding the mechanisms underlying this interannual variability and observed changes. Given that seagrass species composition, distribution, and function are predicted to change in response to climate change (Micheli et al. 2008, Hensel et al. 2023, Daru and Rock 2023), remote sensing of benthic habitat may be a valuable tool for long-term monitoring of their persistence. However, remote sensing may only be useful in the mid to lower estuary, as high CDOM in more freshwaters of the upper estuary significantly limit its ability to detect seagrass. A more thorough investigation of remote sensing applications in these sub-optimal conditions could strengthen the ability to track changes in macrophyte habitat across the entire estuary, and in other areas of the Nova Scotia coast that experience similar conditions. Currently, underwater surveys remain essential to document macrophyte distribution in the upper estuary, and to distinguish different macrophyte species in mixed assemblages.

The drop-camera and in-depth condition surveys of seagrass beds indicated that multiple species of seagrass (eelgrass, widgeongrass, horned pondweed) were present in the estuary. Their location was likely dependent on both temperature and salinity conditions, with widgeongrass being located in warmer less saline waters in the upper estuary. Although some eelgrass co-existed with widgeongrass, it was more prevalent in the cooler and more saline waters in the lower estuary. Climate change is predicted to affect seagrass species assemblages and persistence over time (Short and Neckles 1999, Daru and Rock 2023). Shifts from eelgrass to more widgeongrass-dominated communities have been recently documented and are linked to warming waters (Johnson et al. 2003, Richardson et al. 2018, Hensel et al. 2023). In the St. Mary's River estuary, long-term monitoring is necessary to evaluate seagrass distribution and changes to species composition. In-depth condition surveys that measure multiple indicators of health (i.e., bed structure, morphology, physiology) could provide insights into mechanisms underlying observed changes. Further research could also focus on seagrass genetic diversity, which plays a significant role in their resilience to change.

A high diversity of fishes and invertebrates were documented in this study, with several being species of regional importance in the DFO Maritimes region. While many different fish and invertebrate species were recorded, infaunal species were not easily sampled. Given the importance of infauna for benthic production, nutrient cycling, and coastal food webs, additional work should sample fauna living within the soft sediments. These data could then be compared with those collected by Davis (1976) to document changes since 1975. Additionally, both abiotic and biotic factors associated with climate change can affect faunal species assemblages and persistence. Monitoring of physical and faunal aspects could provide insights into mechanisms underlying changes to faunal communities. Preliminary environmental DNA (eDNA) sampling has been conducted in the estuary (results in prep, DFO Aquatic Invasive Species group, pers. communication) and will provide a complementary method for biodiversity monitoring within the estuary. Using both eDNA and underwater visual surveys can enable greater species detection across taxa and overall species representation, including invasive or species at risk (DFO 2020, Muenzel et al. 2024). Furthermore, use of other species detection methods such as acoustic tracking can also provide additional insights into species of interest relevant for conservation planning and management within the St. Mary's River estuary (Halfyard et al. 2012, 2013).

9 Summary

The Napu'saqnuk / St. Mary's River estuary is a strong ESA candidate, as it meets the ESA criteria of being a highly productive, sensitive, and unique area with a high degree of naturalness (DFO 2023a), as demonstrated in this report. The estuary is highly productive based on its macrophyte communities, soft-sediment habitats, and estuarine oceanographic dynamics that together support a diverse assemblage of fishes and invertebrates. These assemblages include both important fisheries species and species of conservation concern. Eelgrass in particular plays a potentially key role in the estuary, providing various ecosystem services such as carbon storage and provision of food and shelter for fishes. Although eelgrass has some capacity to adapt to changing conditions, it is a sensitive habitat that can be adversely affected by human activities as well as natural events. In particular, eelgrass is highly sensitive to warming waters associated with climate change, light limitation from reduced water clarity associated with agriculture runoff and sediment inputs from coastal development, physical habitat loss from boat damage, dredging, or construction activities, and changes to water delivery and flow (Lefcheck et al. 2017, Murphy et al. 2021, Orth et al. 2006). The presence of

eelgrass along with other species of interest (i.e., wild Atlantic Salmon, American Eel) may provide opportunities to develop conservation and protection objectives should the watershed and estuary become an ESA candidate. Furthermore, true estuarine ecosystems are not prevalent along the Atlantic coast of Nova Scotia, and so the Napu'saqnuk / St. Mary's River estuary represents a regionally unique area, that has limited coastline development and a high degree of naturalness. While there are knowledge gaps outlined in this report, including the absence of multi-year *in situ* data that captures the variation in physical and biological conditions on annual and interannual time scales, this report contributes information that can support the development of conservation and protection actions for this area. In summary, from information collected as part of this ecological overview study, the St. Mary's River estuary is characterized by:

1. highly productive and well-connected biogenic habitats including seagrasses and macroalgae that are widely recognized to provide numerous ecosystem services, including the potential provision of nursery habitat for juvenile fishes such as the Southern Upland Atlantic Salmon, a regional conservation priority;
2. a regionally unique estuarine system with complex oceanographic conditions that create abundant habitats and support diverse faunal communities; and
3. a high degree of naturalness which includes extensive sand flats and macrophyte communities that are sensitive to coastal development, pollution and climate change.

Acknowledgements

We thank Shawn Roach, Katie Thistle, Ed Horne, Jordy Thomson, Chris Corriveau and Benedikte Vercaemer for field and laboratory support. We also thank Kris Hunter with the Atlantic Salmon Federation and DFO staff Jennifer MacDonald, Shannan Murphy, Harri Pettitt-Wade and Ulrike Irlich for providing comments that improved the manuscript. Funding was provided by DFO Fish and Fish Habitat Protection Program.

References

Legal Sources

Fisheries Act, R.S.C. 1985, c. F-14.

Species at Risk Act, S.C. 2002, c. 29.

Literature Cited

Able KW, Fahay MP (2010) Ecology of estuarine fishes: temperate waters of the western North Atlantic. The Johns Hopkins University Press, Baltimore 566 pp. ISBN 978-0-8018-9471-8

Aiken, G.R., McKnight, R.L., Wershaw and MacCarthy, P. (1985) Humic substances in Soil, Sediment and Water: Geochemistry, Isolation and Characterization. J Wiley and Sons, New York, 692 p.

Allard, K., Hanson, A., and Mahoney, M. (2014) Summary: Important Marine Habitat Areas for Migratory Birds in Eastern Canada. Canadian Wildlife Service Technical Report Series 530: iii + 20 p.

Andrews, S. N., Dadswell, M. J., Buhariwalla, C. F., Linnansaari, T., and Curry, R. A. (2019) Looking for Striped Bass in Atlantic Canada: The reconciliation of local, scientific, and historical knowledge. *Northeastern Naturalist*, *26*(1), 1-30. doi: 10.1656/045.026.0105.

ASF (Atlantic Salmon Federation). (2021). Marine Conservation and Atlantic Salmon: A position paper on the proposed Eastern Shore Islands Marine Protected Area.

Baker J. A., Wund M. A., Heins D. C., King R. W., Reyes M. L., and Foster S. A. (2015) Life-history plasticity in female tThreespine Stickleback. *Heredity* 115: 322-334.

Barbier, E. B., Hacker, S. D., Kennedy, C., Koch, E. W., Stier, A. C., and Silliman, B. R. (2011) The value of estuarine and coastal ecosystem services. *Ecological monographs*, 81(2), 169-193. DOI:10.1890/10-1510.1.

Beckman Coulter. (2011) Instruction for Use: LS 13 320 Laser Diffraction Particle Size Analyzer. PN B05577AB. https://www.beckmancoulter.com

Bouchama, K., Rouabhi, R. and Bouchiha, H. (2019) Phytoremediation and Removal of Contaminants by Algae and Seagrasses. In Ecotoxicology of Marine Organisms, pp. 128-157. CRC Press. DOI:10.1201/b22000.

Bowlby, H.D., Horsman, T., Mitchell, S.C., and Gibson, A.J.F. (2014) Recovery Potential Assessment for Southern Upland Atlantic Salmon: Habitat Requirements and Availability, Threats to Populations, and Feasibility of Habitat Restoration. DFO Can. Sci. Advis. Sec. Res. Doc. 2013/006. vi + 155 p.

Breiman L, Cutler A, Liaw A, Wiener R. (2022) *randomForest:* Breiman and Cutler's Random Forests for Classification and Regression. R package version 4.7-1.1.

Bundy, A., Themelis, D., Sperl, J. and den Heyer, N. (2014) Inshore Scotian Shelf Ecosystem Overview Report: Status and Trends. DFO Can. Sci. Advis. Sec. Res. Doc. 2014/065. xii + 213 p.

Chaput, G., Carr, J., Daniels, J., Tinker, S., Jonsen, I. & Whoriskey, F. (2019). Atlantic salmon (Salmo salar) smolt and early post-smolt migration and survival inferred from multi-year and multi-stock acoustic telemetry studies in the Gulf of St. Lawrence, northwest Atlantic. *ICES Journal of Marine Science*, Volume 76, Issue 4, pp. 1107–1121, https://doi.org/10.1093/icesjms/fsy156

Charrad M, Ghazzali N, Boiteau V, Niknafs A. (2022) *NbClust*: Determining the Best Number of Clusters in a Data Set. R package version 3.0.1.

Chen C, Liu H, Beardsley RC. (2003) An unstructured grid, finite-volume, three-dimensional, primitive equations ocean model: Application to coastal ocean and estuaries. *J Atmos Oceanic Technol 20*: 159-186

Chen, R.F., Bissett, P., Coble, P., Conmy, R., Gardner, G.B., Moran, M.A., Wang, X., Wells, M.L., Welan, P., Zepp, R.G. (2004) Chromophoric dissolved organic matter (CDOM) source characterization in the Louisiana Bight. *Mar Chem* 89 (2004) 257–272. doi: 10.1016/j.marchem.2004.03.017

Clark, C.D., Litz, L.P., Grant, S.B. (2008) Salt marshes as a source of chromophoric dissolved organic matter (CDOM) to Southern California coastal waters. *Limnol Oceanogr,* 53(5), 2008, 1923–1933. doi: 10.4319/lo.2008.53.5.1923

Clark, K.J., Clark, D.S., Andrushchenko, I.V. and Swain, D.P. (2015) Recovery Potential Assessment (RPA) for the Southern Designatable Unit (NAFO Divisions 4X5Yb and 5Zjm) of Atlantic Cod (Gadus morhua). DFO Can. Sci. Advis. Sec. Res. Doc. 2015/069. v + 58 p.

Condie, S.A., Hayes, D., Fulton, E.A., Savina, M. (2012) Modelling ecological changes over half a century in a subtropical estuary: impacts of climate change, land-use, urbanization and freshwater extraction. Mar. Ecol. Prog. Ser. 457: 43-66. Doi: 10.3354/meps09718

COSEWIC. (2010). COSEWIC assessment and status report on the Atlantic Salmon *Salmo salar* (Nunavik population, Labrador population, Northeast Newfoundland population, South Newfoundland population, Southwest Newfoundland population, Northwest Newfoundland population, Quebec Eastern North Shore population, Quebec Western North Shore population, Anticosti Island population, Inner St. Lawrence population, Lake Ontario population, Gaspé-Southern Gulf of St. Lawrence population, Eastern Cape Breton population, Nova Scotia Southern Upland population, Inner Bay of Fundy population, Outer Bay of Fundy population) in Canada. Committee on the Status of Endangered Wildlife in Canada. Ottawa. x|vii + 136 pp. (www.sararegistry.gc.ca/status/status_e.cfm).

Cotas, J., Gomes, L., Pacheco, D., Pereira, L. (2023) Ecosystem services provided by seaweeds. Hydrobiologia. *2*(1): 75-96. doi: 10.3390/hydrobiology2010006

Dalziel, A. C., Tirbhowan, S., Drapeau, H. F., Power, C., Jonah, L. S., Gbotsyo, Y. A., and Dion-Côté, A. M. (2020) Using asexual vertebrates to study genome evolution and animal physiology: Banded (*Fundulus diaphanus*) x Common Killifish (*F. heteroclitus*) hybrid lineages as a model system. Evolutionary applications, 13(6), 1214-1239. doi: 10.1111/eva.12975.

Daru, B.H. and Rock, B.M. (2023) Reorganization of seagrass communities in a changing climate. *Nature Plants, 9:* 1034:1043. doi: 10.1038/s41477-023-01445-6

Davies-Colley, R.J. and Smith, D.G. (2001) Turbidity, Suspended Sediment and Water Clarity: A Review. Journal of the American Water Resources Association, 37(5): 1085 - 1101. doi: 10.1111/j.1752-1688.2001.tb03624.x

Davis, D.S. (1976) The Estuary of the St. Mary's River Nova Scotia 1973 (Curatorial Report #34). Nova Scotia Museum. https://ojs.library.dal.ca/NSM/article/view/3952.

DFO (Fisheries and Oceans Canada). (2019) Biophysical and Ecological Overview of the Eastern Shore Islands Area of Interest (AOI). DFO Can. Sci. Advis. Sec. Sci. Advis. Rep. 2019/016.

DFO. (2020) Advice on the Use of Targeted Environmental DNA (eDNA) Analysis for the Management of Aquatic Invasive Species and Species at Risk. DFO Can. Sci. Advis. Sec. Sci. Advis. Rep. 2020/058.

DFO. (2021) Recovery Potential Assessment for Common Lumpfish (Cyclopterus Lumpus) in Canadian Waters. DFO Can. Sci. Advis. Sec. Sci. Advis. Rep. 2021/019

DFO. (2023a) National Framework for Identifying, Establishing and Managing ESAs. Fish and Fish Habitat Protection Program. 24 pp.

DFO. (2023b). Stock Status Update of Atlantic Salmon to 2022 in Salmon Fishing Areas (SFAs) 19-21 and 23. DFO Can. Sci. Advis. Sec. Sci. Resp. 2023/043.

DFO. (2024, April 29) Marine Conservation network sites for the Scotian Shelf-Bay of Fundy Bioregion [Website]. https://www.dfo-mpo.gc.ca/oceans/networks-reseaux/scotian-shelf-plateau-neo-ecossais-bay-baie-fundy/sites-eng.html

Egbert, G.D. and Erofeeva, S.Y. (2002) Efficient inverse modeling of barotropic ocean tides. Journal of Atmospheric and Oceanic Technology, 19(2), pp.183-204.

Enríquez, S., Olivé, I., Cayabyab, N., Hedley, J.D. (2019) Structural complexity governs seagrass acclimatization to depth with relevant consequences for meadow production macrophyte diversity and habitat carbon storage capacity. *Scientific Reports: Nature Research.* 9:14657. doi: 10.1038/s41598-019-51248-z

Falkegård, M., Lennox, R. J., Thorstad, E. B., Einum, S., Fiske, P., Garmo, Ø. A., ... & Forseth, T. (2023). Predation of Atlantic salmon across ontogenetic stages and impacts on populations. *Canadian Journal of Fisheries and Aquatic Sciences*, *80*(10), 1696-1713. doi: 10.1139/cjfas-2023-0029.

Folk, R.L. and Ward, W.C. (1957) *A* Study in the Significance of Grain-Size Parameters. Journal of Sedimentary Petrology, 27, 3-26.

Fonseca, M.S. and Bell, S.S. (1998) Influence of physical setting on seagrass landscapes near Beaufort, North Carolina, USA. Marine Ecology Progress Series 171: 109-121. doi: 10.3354/meps171109

Fonseca, M.S., Whitfield, P. E., Kelly, N. M., and Bell, S. S. (2002) Modelling seagrass landscape pattern and associated ecological attributes. Ecol. App. 12, 218–237. doi: 10.1890/1051-0761(2002)012[0218:mslpaa]2.0.co;2

Fourqurean, J. W., Duarte, C. M., Kennedy, H., Marbà, N., Holmer, M., Mateo, M. A., ... and Serrano, O. (2012) Seagrass ecosystems as a globally significant carbon stock. Nature geoscience, 5(7), 505-509. doi:10.1038/ngeo1477.

French, E. and Moore, K. (2018) Canopy Functions of *R. maritima* and *Z. marina* in the Chesapeake Bay. Front. Mar. Sci., 5:461. Doi: 10.3389/fmars.2018.00461

Gibson, A.J.F., H.D. Bowlby, D.L. Sam, and P.G. Amiro. 2009. Review of DFO Science information for Atlantic Salmon (*Salmo salar*) populations in the Southern Upland region of Nova Scotia. DFO Canadian Science Advisory Secretariat Research Document 2009/081.

Gibson, A.J.F., and Bowlby, H.D. (2013) Recovery Potential Assessment for Southern Upland Atlantic Salmon: Population Dynamics and Viability DFO Can. Sci. Advis. Sec. Res. Doc. 2012/142. iv + 129 p.

Gibson, A. J. F., Halfyard, E. A., Bradford, R. G., Stokesbury, M. J., & Redden, A. M. (2015). Effects of predation on telemetry-based survival estimates: insights from a study on endangered Atlantic salmon smolts. *Canadian Journal of Fisheries and Aquatic Sciences*, *72*(5), 728-741. doi: 10.1139/cjfas-2014-0245.

Goodman, J.L., K.A. Moore, and W.C. Dennison. (1995) Photosynthetic responses of eelgrass (*Zostera-marina* L) to light and sediment sulfide in a shallow barrier-island lagoon. *Aquatic Botany* 50: 37–47. doi: 10.1016/0304-3770(94)00444-Q

Halfyard, E.A., Ruzzante, D.E., Stokesbury, M.J.W., Gibson, A.J.F., and Whoriskey, F.W. (2012) Estuarine migratory behaviour and survival of Atlantic Salmon smolts from the Southern Upland, Nova Scotia, Canada. J. Fish Biol. 81: 1626–1645. doi:10.1111/j.1095-8649.2012.03419.x. PMID:23020565.

Halfyard, E.A., Gibson, A.J.F., Stokesbury, M.J.W., Ruzzante, D.E., and Whoriskey, F.W. (2013) Correlates of estuarine survival of Atlantic Salmon post smolts from the Southern Upland, Nova Scotia, Canada. Canadian Journal of Fisheries and Aquatic Sciences. 70: 452–460 (2013) dx.doi.org/10.1139/cjfas-2012-0287

Helms, JJ, Stubbins A, Ritchie JD, Minor EC, Kieber DJ, Mopper K. (2008) Absorption spectral slopes and slope ratios as indicators of molecular weight, source, and photobleaching of chromophoric dissolved organic matter. *Limnol. Oceanogr*. 53: 955–969, doi:10.4319/lo.2008.53.3.0955

Hensel, E., Patrick, C.J., Wilson, S.J., Song, B., Reay, W.G., Orth, R.J. (2024) Incorporating generalist seagrasses enhances habitat restoration in a changing environment. Journal of Applied Ecology, 00, 1-12. doi: 10.1111/1365-2664.14643

Hensel, M.J.S., Patrick, C.J., Orth, R.J., Lefcheck, J.S. (2023) Rise of *Ruppia* in Chesapeake Bay: Climate change-driven turnover of foundation species creates new threats and management opportunities. PNAS 120(23): e2220678120. doi: 10.1073/pnas.2220678120

Hernández Chávez, C., and Turgeon, J. (2007). Asexual and sexual hybrids between *Fundulus diaphanus* and *F. heteroclitus* in the Canadian Atlantic region. Molecular Ecology, 16(7), 1467-1480. doi: 10.1111/j.1365-294X.2007.03239.x.

Hijmans, R. J, Bivand, R., Pebesma, E., and Sumner, M.D. (2024) *terra:* Spatial Data Analysis version 1.7-71. https://rspatial.github.io/terra/

Jabbari, A., Wu, Y., Wong, M.C., Dowd, M. (2024) Modelling water temperature dynamics for eelgrass (*Zostera marina*) areas in the nearshore Scotian Shelf. Frontiers in Mar Sci, 11: 1374884. doi: 10.3389/fmars.2024.1374884

Jago CF, Jones SE, Sykes P, Rippeth T (2006) Temporal variation of suspended particulate matter and turbulence in a high energy, tide- stirred, coastal sea: relative contributions of resuspension and disaggregation. Cont Shelf Res 26: 2019−2028.

Jean-Michel, L., Eric, G., Romain, B.B., Gilles, G., Angélique, M., Marie, D., Clément, B., Mathieu, H., Olivier, L.G., Charly, R. and Tony, C. (2021) The Copernicus global 1/12 oceanic and sea ice GLORYS12 reanalysis. Frontiers in Earth Science, 9, p.698876.

Jeffery, N.W., Heaslip, S.G., Stevens, L.A., and Stanley, R.R.E. (2020) Biophysical and Ecological Overview of the Eastern Shore Islands Area of Interest (AOI). DFO Can. Sci. Advis. Sec. Res. Doc. 2019/025. xiii + 138 p.

Jessop B. M., Shiao J.-C., Iizuka Y., Tzeng W.-N. (2002) Migratory behaviour and habitat use by American eels *Anguilla rostrata* as revealed by otolith microchemistry. *Marine Ecology Press Series* 233: 217-229.

Johnson, M.R., Williams, S.L, Lieberman, C.H., Solbak, A. (2003) Changes in the abundance of the seagrasses *Zostera marina* L. (eelgrass) and *Ruppia maritima* L. (widgeongrass) in San Diego, California, following an El Nino event. *Estuaries* 26(1): 106-115. doi: 10.1007/BF02691698

Kimmerer, W. J. (2002). Effects of freshwater flow on abundance of estuarine organisms: physical effects or trophic linkages?. Mar. Ecol. Prog. Ser., *243*, 39-55. doi: 10.3354/meps243039

Koch, M.S., Schopmeyer, S., Kyhn-Hansen, C., Madden, C.J. (2007) Synergistic effects of high temperature and sulfide on tropical seagrass. *Journal of Experimental Marine Biology and Ecology* 341(1): 91-101. doi: 10.1016/j.jembe.2006.10.004

Krumhansl, K.A., Dowd, M., Wong, M.C. (2021) Multiple metrics of temperature, light, and water motion drive gradients in eelgrass productivity and resilience. *Frontiers in Marine Science* 8:597707. doi: 10.3389/fmars.2021.597707

Kuhn, M. (2020) *caret:* Classification and regression training. R package version 6.0.86.

Kutser, T., Hedley, J., Giardina, C., Roelfsema, C., Brando, V. (2020) Remote sensing of shallow waters - A 50-year retrospective and future directions. *Remote Sensing of Environment*. 240: 111619. doi: 10.1016/j.rse.2019.111619

Langenkämper, D., M. Zurowietz, T. Schoening, T.W. Nattkemper (2017) Biigle 2.0 – browsing and annotating large marine collections. *Frontiers in Marine Science* 4:83. doi: 10.3389/fmars.2017.00083

Law BA, Hill PS, Maier I, Milligan TG, Page F (2014) Size, settling velocity and density of small suspended particles at an active salmon aquaculture site. Aquacult Environ Interact 6: 29−42.

Lee, K-S., Park S.R., Kim, Y.K. (2007) Effects of irradiance, temperature, and nutrients on growth dynamics of seagrasses: a review. Journal of Experimental Marine Biology and Ecology 350(1-2): 144-175. doi: 10.1016/j.jembe.2007.06.016

Lefcheck, J.S., Wilcox, D.J., Murphy, R.R., Marion, S.R., Orth, R.J. (2017) Multiple stressors threaten the imperiled coastal foundation species eelgrass (*Zostera marina)* in Chesapeake Bay, USA. Glob. Chan. Biol. 23: 3474-3483. doi: 10.1111/gcb.13623

Jean-Michel, L., Eric, G. and Romain, B.B. (2021) The Copernicus global 1/12 oceanic and sea ice GLORYS12 reanalysis. Front Earth Sci 9: 698876.

Loring, D.H, R.TT Rantala, and TG. Milligan (1996) Metallic contaminants in the sediments of coastal embayments of Nova Scotia. Can. Tech. Rep. Fish. Aquat. Sci. 2111: viii + 268 p.

Luczak, C., Janquin, M.-A., Kupka, A. (1997) Simple standard procedure for the routine determination of organic matter in marine sediment. Hydrobiologica 345: 87-94. doi: 10.1023/A:1002902626798

Lyzenga, D.R. (1978) Passive remote sensing techniques for mapping water depth and bottom features. *Appl. Opt.*, *17*, 379, doi:10.1364/ao.17.000379.

Mahar, Brian. (2022) iNaturalist observations: https://www.inaturalist.org/observations/131342285. Accessed on May 5, 2024.

Mannino, A., Russ, M.E., Hooker, S.B. (2008) Algorithm development and validation for satellite-derived distributions of DOC and CDOM in the U.S. Middle Atlantic Bight. *J Geophys Res*, 113:C07051, doi:10.1029/2007JC004493

Mannino, A., M. G. Novak, N. B. Nelson, M. Belz, J.- F. Berthon5, N. V. Blough, E. Boss, A. Bricaud, J. Chaves, C. Del Castillo, R. Del Vecchio, E. J. D'Sa, S. Freeman, A. Matsuoka, R. L. Miller, A. R. Neeley, R. Röttger, M. Tzortziou, and P. J. Werdell (2019) Measurement protocol of absorption by chromophoric dissolved organic matter (CDOM) and other dissolved materials, In Inherent Optical Property Measurements and Protocols: Absorption Coefficient, Mannino, A. and Novak, M. G. (eds.), IOCCG Ocean Optics and Biogeochemistry Protocols for Satellite Ocean Colour Sensor Validation, Volume ###, IOCCG, Dartmouth, NS, Canada.

Marsh, J.A., Dennison, W.C., Alberte, R.S. (1986) Effects of temperature on photosynthesis and respiration in eelgrass (*Zostera marina* L.) J. Exp. Mar. Biol. Ecol., 101: pp. 257-267. doi: 10.1016/0022-0981(86)90267-4

Massicotte, P., Asmala, E., Stedman, C., Markager, S. (2017) Global distribution of dissolved organic matter along the aquatic continuum: Across rivers, lakes and oceans. *Science of the Total Environment.* 609: 180-191. doi: 10.1016/j.scitotenv.2017.07.076

Mayer, F.L. Jr. and Low J.B. (1970) The Effect of Salinity on Widgeongrass. The Journal of Wildlife Management 34(3): 558-661. doi: 10.2307/3798882

Mérette, D., Bourret, A., and Turgeon, J. (2009). Diversity and distribution of gynogenetic hybrids between *Fundulus diaphanus* and *Fundulus heteroclitus* in Porter's Lake (Nova Scotia) in relation to salinity. Journal of Fish Biology, 75(5), 1115-1122. doi: 10.1111/j.1095-8649.2009.02396.x.

Micheli, F., Bishop, M.J., Peterson, C.H., Rivera, J. (2008) Alteration of seagrass species composition and function over two decades. *Ecological Monographs, 78*(2): 224-244. doi: 10.1890/06-1605.1

Mitchell, S. C. (2012). Fish communities of the St. Mary's River watershed: An analysis of community diversity and structure. St. Mary's River Association Technical Report #014. 23 pp. https://www.stmarysriverassociation.com/uploads/6/7/6/5/67652351/fish_communities_2012.pdf.

Moir, H. J., Gibbins, C. N., Soulsby, C., & Webb, J. (2004). Linking channel geomorphic characteristics to spatial patterns of spawning activity and discharge use by Atlantic salmon (Salmo salar L.). *Geomorphology*, *60*(1-2), 21-35. doi: 10.1016/j.geomorph.2003.07.014.

Moore, A.F.P. and Duffy, J. (2016) Foundation species identity and trophic complexity affect experimental seagrass communities. Marine Ecological Progress Series. 556:105-121. doi: 10.3354/meps11785

Moore, K.A., Shields, E.C., Parrish, D.B. (2014) Impacts of varying estuarine temperature and light conditions on *Zostera marina* (eelgrass) and its interactions with *Ruppia maritima* (widgeongrass). Estuaries and Coasts 37 (Suppl 1):20-30. doi: 10.1007/s12237-013-9667- 3.

Muenzel, D., Bani, A., De Brauwer, M., Stewart, E., Djakiman, C., Halwi, P., Purnama, R., Yusuf, S., Santoso, P., Hukom, F. D., Struebig, M. J., Jompa, J., Limmon, G., Dumbrell, A., & Beger, M. (2024) Combining environmental DNA and visual surveys can inform conservation planning for coral reefs. *PNAS 121*(17): e2307214121. doi: 10.1073/pnas.2307214121

Murphy, G.E.P., Dunic, J.C., Adamczyk, E.M., Bittick, S.J., Côté, I.M., Cristiani, J., Geissinger, E.A., Gregory, R.S., Lotze, H.K., O'Connor, M.I., Araújo, C.A.S., Rubidge, E.M., Templeman, N.D., and Wong, M.C. (2021) From coast to coast to coast: ecology and management of seagrass ecosystems across Canada. FACETS. 6: 139–179. doi:10.1139/facets-2020-0020

Nejrup, L.B. and Pedersen, M.F. (2008) Effects of salinity and water temperature on the ecological performance of *Zostera marina.* Aquatic Botany 88(3):239-246. doi: 10.1016/j.aquabot.2007.10.006

Nguyen, H.M., Ralph P.J., Marin Guirao, L., Pernice, M., Procaccini, G. (2021) Seagrasses in an era of ocean warming: a review. Biological Reviews 96(5): 2009-2030. doi: 10.1111/brv.12736

O'Brien, J.M., Wong, M.C., Stanley R.R.E. (2022) Fine-scale ensemble species distribution modeling of eelgrass (*Zostera marina*) to inform nearshore conservation planning and habitat management. Frontiers in Marine Science 9:988858. doi: 10.3389/fmars.2022.988858

Orth, R.J., Carruthers, T.J.B., Dennison, W.C., Duarte, C.M., Fourqurean, J.W., Heck, K.L., Hughes, A.R., Kendrick, G.A., Kenworthy, W.J., Olyarnik, S., Short, F.T., Waycott, M., Williams, S.L. (2006) A Global Crisis for Seagrass Ecosystems. *BioScience*. 56(12): 987–996. doi: 10.1641/0006-3568(2006)56[987:AGCFSE]2.0.CO;2

Pedersen, M.Ø. and Kristensen, E. (2015) Sensitivity of *Ruppia maritima* and *Zostera marina* to sulfide exposure around roots. Journal of Experimental Marine Biology and Ecology 468: 138-145. doi: 10.1016/j.jembe.2015.04.004

Puspendra, I.F. (2019) *irr*: Various coefficients of interrater reliability and agreement. R package version 0.84.1.

Pratt, T.C., Bradford, R.G., Cairns, D.K., Castonguay, M., Chaput, G., Clarke, K.D., and Mathers, A. 2014. Recovery Potential Assessment for the American Eel (Anguilla rostrata) in eastern Canada: functional description of habitat. DFO Can. Sci. Advis. Sec. Res. Doc. 2013/132. v + 49 p.

R Core Team. (2021) R: A language and environment for statistical computing. R Foundation for Statistical Computing, Vienna, Austria. Available from http://www.r-project.org/.

Reef Environmental Education Foundation, REEF (n.d.) Volunteer Fish Survey Project. Retrieved from https://www.reef.org/programs/volunteerfish-survey-project.

Reid, A.J., Eckert, L.E., Lane, J-F., Young, N., Hinch, S.G., Darimont, C.T., Cooke, S.J., Ban, N.C., Marshall, A. (2020) "Two-Eyed Seeing": An Indigenous framework to transform fisheries research and management. *Fish and Fisheries, 22*: 243-261. doi: 10.1111/faf.12516

Richardson, J. P., Lefcheck, J., Orth, R. (2018) Warming temperatures alter the relative abundance and distribution of two co-occurring foundational seagrasses in Chesapeake Bay, USA. Marine Ecological Progress Series 599:65-74. doi: 10.3354/meps12620

Richardson, F. D. (1980) Ecology of *Ruppia maritima* L. in New Hampshire (U.S.A.) tidal marshes. Rhodora 82(831): 403-439. http://www.jstor.org/stable/23311936

Short, F.T. and Neckles, H.A. (1999) The effects of global climate change on seagrasses. Aquat. Bot. 63(304): 169-196. Doi: 10.1016/S0304-3770(98)00117-X

Strazisar, T., Koch, M.S., Frankovich, T.A., Madden, C.J. (2016) The importance of recurrent reproductive events for *Ruppia maritima* seed bank viability in a highly variable estuary. Aquat. Bot. 134: 103-112. doi: 10.1016/j.aquabot.2016.07.005

Ta'n Weji-sqalia'tiek Mi'kmaw Place Names Digital Atlas. (n.d.) Accessed September 9, 2024. https://placenames.mapdev.ca/

Thorstad, E. B., Økland, F., Aarestrup, K., & Heggberget, T. G. (2008). Factors affecting the within-river spawning migration of Atlantic salmon, with emphasis on human impacts. Reviews in Fish Biology and Fisheries, 18, 345-371. doi: 10.1007/s11160-007-9076-4.

Toffolon, M. and Piccolroaz, S., (2015) A hybrid model for river water temperature as a function of air temperature and discharge. Environmental Research Letters, 10(11), p.114011.

Transcriptions of Father Pacifique Guide to Micmac Place Names EHG, 1934, p. 271

Vercaemer, B., O'Brien, J. M., Guijarro-Sabaniel, J. and Wong, M. C. (2022) Distribution and condition of eelgrass (*Zostera marina*) in the historical goldmining region of Goldboro, Nova Scotia. Can. Tech. Rep. Aquat. Sci. 3513: v + 67 p.

Weitkamp, L.A., Goulette, G., Hawkes, J., O'Malley, M., Lipsky, C. (2014) Juvenile salmon in

estuaries: comparisons between North American Atlantic and Pacific salmon populations. *Rev. Fish Biol. Fish,* 24: 713-736, doi: 10.1007/s11160-014-9345-y

Wilson, K.L., Wong, M.C., Devred, E. (2020) Branching algorithm to identify bottom habitat in the optically complex coastal waters of Atlantic Canada using Sentinel-2 satellite imagery. *Front. Environ. Sci*, *8*, 579856, doi:10.3389/fenvs.2020.579856.

Wilson, K.L., Wong, M.C., Devred, E. (2022) Comparing Sentinel-2 and WorldView-3 Imagery for Coastal Bottom Habitat Mapping in Atlantic Canada. *Remote Sens.*, *14*, doi: 10.3390/rs14051254.

Wong, M.C. (2018) Secondary production of microbenthic communities in seagrass (*Zostera marina*, Eelgrass) beds and bare soft sediments across differing environmental conditions in Atlantic Canada. Estuaries and Coasts 41, 536-548. doi: 10.1007/s12237-017-0286-2

Wong, M. C. and Dowd, M. (2021). Sub-seasonal physical dynamics of temperature , light , turbidity , and water motion in eelgrass (Zostera marina) beds on the Atlantic coast of Nova Scotia, Canada. *Can. Tech. Rep. Fish. Aquat. Sci.*, *3447*, v+74.

Wong, M.C. and Dowd, M. (2023) The role of short-term temperature variability and light in shaping the phenology and characteristics of seagrass beds. Ecosphere, 14: e4698. doi: 10.1002/ecs2.4698

Appendix A – Sampling and survey locations

Table A1. List of conductivity-temperature-depth (CTD) castaway station locations measured on July 7, 2023 in the St. Mary's River estuary.

CTD Station	Latitude	Longitude
A	45.13365	-61.9841
B	45.13402	-61.9922
C	45.12437	-61.9777
D	45.11763	-61.9694
E	45.10786	-61.9678
F	45.0963	-61.9593
G	45.08381	-61.9507
H	45.07668	-61.9338
I	45.06985	-61.9165
J	45.05836	-61.9072

Table A2. List of bottom type stations' locations, date surveyed with drop camera and samples collected, depth, and observed sediment type in the St. Mary's River estuary.

STATION	Date surveyed	LATITUDE	LONGITUDE	DEPTH (FT)	SEDIMENT TYPE
1	13-Jun-23	45.13955	-61.99641	3	mud
2	13-Jun-23	45.13471	-61.99675	3.6	mud
3	13-Jun-23	45.13407	-61.99215	4.8	mud
4	13-Jun-23	45.13172	-61.98762	2.2	mud
5	13-Jun-23	45.12965	-61.98627	6.2	mud
6	13-Jun-23	45.12666	-61.98078	1.8	sandy mud
7	13-Jun-23	45.12523	-61.98231	2.2	sandy mud
8	13-Jun-23	45.12397	-61.97806	8.4	sand, mud, broken shell
9	13-Jun-23	45.12015	-61.97115	2.2	mud
10	13-Jun-23	45.11829	-61.97161	3.1	mud
11	13-Jun-23	45.11633	-61.96694	2.5	mud
12	13-Jun-23	45.11441	-61.96861	21.5	sand/mud/shell/boulders
13	13-Jun-23	45.10495	-61.96692	2.8	mud
14	13-Jun-23	45.10656	-61.96315	3.4	soft mud
15	13-Jun-23	45.09941	-61.96297	20.1	mud & shell
16	13-Jun-23	45.09157	-61.95726	3.9	mud
17	13-Jun-23	45.08157	-61.94859	10.2	sandy
18	13-Jun-23	45.07898	-61.93747	3	sandy
19	13-Jun-23	45.0794	-61.93366	3.6	mud
20	13-Jun-23	45.07666	-61.93387	24.3	sand
21	13-Jun-23	45.07335	-61.93275	4.2	sand/mud/algae mat
22	13-Jun-23	45.07369	-61.92748	5.1	sand/mud/algae mat
23	16-Jun-23	45.07323	-61.92245	1.2	sand/mud
24	16-Jun-23	45.06952	-61.92609	1	sand/mud
25	16-Jun-23	45.07231	-61.92235	2.7	sand
26	16-Jun-23	45.07306	-61.92018	1	sand/mud
27	16-Jun-23	45.07063	-61.92096	11	sand
28	16-Jun-23	45.07167	-61.91776	1	sand/mud
29	16-Jun-23	45.06834	-61.91707	1	sand/mud
30	16-Jun-23	45.06875	-61.91455	22.7	sand
31	16-Jun-23	45.06894	-61.91317	1	sand/mud
32	16-Jun-23	45.06523	-61.91589	1	sand/mud
33	16-Jun-23	45.06347	-61.91478	1	sand/mud
34	16-Jun-23	45.06141	-61.91048	20.8	sand
35	16-Jun-23	45.05979	-61.91033	1	sand/mud
36	16-Jun-23	45.06124	-61.90802	1	sand/mud/algae patches
37	16-Jun-23	45.06071	-61.90666	1	bare & algae patches
38	16-Jun-23	45.05834	-61.9072	22	sand
39	24-Oct-23	45.052438	-61.905129	5.2	sand
40	24-Oct-23	45.054151	-61.899363	16.4	sand/broken shell
41	6-Jul-23	45.05142	-61.90002	6.9	sand
42	24-Oct-23	45.052856	-61.898129	4.6	sand and cobble
43	24-Oct-23	45.051019	-61.89786	9.2	sand
44	24-Oct-23	45.051459	-61.896745	4.9	cobble and boulders
45	6-Jul-23	45.04976	-61.89858	11.5	sand
46	6-Jul-23	45.04819	-61.89573	11.2	rock, rubble
47	6-Jul-23	45.048	-61.89256	15.4	sand
48	6-Jul-23	45.05017	-61.88887	6.6	sand
49	6-Jul-23	45.04761	-61.88955	15.4	sand, shell, cobble
50	6-Jul-23	45.04614	-61.89184	11.8	hard (sand, shell, cobble)
51	6-Jul-23	45.04199	-61.89291	17.7	sand, rockweed
53	6-Jul-23	45.03923	-61.88385	32.5	sand
54	6-Jul-23	45.04267	-61.88532	26.9	sand

Table A3. List of faunal community survey sites and dates for the St. Mary's River estuary.

Site Name	Site Coordinates	Survey Date
Sonora Boat Ramp	45.05° N, 61.90° W	13/06/23
McDiarmid's Cove	45.05° N, 61.88° W	13/06/23
McDiarmid's Cove	45.05° N, 61.88° W	01/08/23
Eel Cove	45.10° N, 61.97° W	01/08/23
McDiarmid's Cove	45.05° N, 61.88° W	25/09/23
Darling Island	45.07° N, 61.93° W	26/09/23
Middle Estuary	45.09° N, 61.96° W	26/09/23
Mudflat	45.06° N, 61.88° W	27/09/23
Outer Estuary	45.03° N, 61.88° W	28/09/23
Northwest Arm	45.13° N, 61.99° W	29/09/23

Appendix B – Macrophyte Communities – Supplementary Tables

Table B1. Percent cover mean and ± standard error (SE) by bottom type category and station surveyed by drop camera drifts, with subsequent image extraction and annotation of a 100 point grid. *Other seagrasses include widgeongrass and horned pondweed.

Station	# of Image replicates	Eelgrass Mean	Eelgrass SE	*Other Seagrasses Mean	*Other Seagrasses SE	Kelp & other Macroalgae Mean	Kelp & other Macroalgae SE	Detritus & Epiphytes Mean	Detritus & Epiphytes SE	Turfs Mean	Turfs SE	Bare Sand/ Mud Mean	Bare Sand/ Mud SE	Bare Rock Mean	Bare Rock SE
1	4	0	0	19.2	8.8	0	0	0	0	29.3	12.5	51.5	16.1	0	0
2	3	0	0	17.7	8.2	0	0	75.3	8.8	0	0	7.0	2.1	0	0
3	7	1.6	1.0	1.9	1.0	0	0	0	0	63.9	16.6	32.7	17.5	0	0
4	5	0	0	51.9	5.2	0	0	8.8	2.3	0	0	39.3	6.0	0	0
5	5	0	0	0	0	0	0	5.8	2.7	0	0	94.2	2.7	0	0
6	7	32.2	14.2	0	0	0	0	0.7	0.4	0	0	67.1	14.2	0	0
7	5	10.1	4.3	14.7	2.5	0	0	63.6	7.7	0	0	11.6	5.7	0	0
8	4	0	0	0	0	0	0	14.3	6.2	0	0	85.7	6.2	0	0
9	6	2.7	1.7	2.0	1.4	0	0	6.5	4.3	0.3	0.3	88.4	5.2	0	0
10	7	0	0	0	0	0	0	0	0	0	0	100	0.0	0	0
11	3	0	0	7.5	2.4	0	0	6.9	1.0	0	0	85.6	2.9	0	0
12	5	0	0	0	0	0	0	0	0	0	0	5.1	3.5	94.9	3.5
13	3	0	0	0	0	0	0	0	0	0	0	100.0	0	0	0
14	3	0	0	2.0	1.0	0	0	8	7.5	0	0	90.0	8.0	0	0
15	2	0	0	0	0	0	0	0	0	0	0	50.0	50.0	50.0	50.0
16	3	0	0	0	0	0	0	1.7	1.2	0	0	98.3	1.2	0	0
17	5	0	0	0	0	0	0	62.6	10.1	0	0	37.4	10.1	0	0
18	5	0	0	0	0	0	0	12.0	7.4	20.4	12.6	67.6	9.6	0	0
19	5	0	0	0	0	0	0	57.0	7.6	2.0	2.0	40.9	8.7	0	0
20	9	0	0	0	0	0	0	15.8	2.7	0	0	84.2	2.7	0	0
21	7	0	0	0	0	0.9	0.9	5.1	1.7	80.6	4.8	13.3	2.9	0.1	0.1
22	3	0	0	0	0	6.0	3.3	16.3	13.1	48.5	17.1	29.1	2.4	0	0
23	2	83.6	0.9	0	0	0	0	0.6	0.6	0	0	15.8	0.3	0	0
24	2	39.1	12.9	0	0	0	0	21.8	18.7	4.8	4.8	33.2	11.7	1.2	1.2
25	3	0	0	0	0	0	0	2.2	1.7	7.7	7.7	89.6	6.6	0.5	0.5
26	4	93.8	3.9	0	0	0	0	0	0	0	0	6.3	3.9	0	0
27	4	0	0	0	0	0	0	0.5	0.5	0	0	99.5	0.5	0	0
28	4	72.5	10.9	0	0	0	0	1.3	1.0	0	0	26.2	10.6	0	0
29	3	98	0.6	0	0	0	0	0	0	0.3	0.3	1.7	0.3	0	0
30	5	0	0	0	0	0	0	1.0	0.8	0	0	99.0	0.8	0	0
31	2	0	0	0	0	0	0	0	0	93	6.0	7.0	6.0	0	0
32	4	98.7	0.8	0	0	0	0	0	0	0	0	1.3	0.8	0	0
33	4	94.6	1.2	0	0	0	0	1.8	1.5	0	0	3.6	1.6	0	0
34	6	0	0	0	0	0	0	1.5	1.0	0	0	98.5	1.0	0	0
35	4	33.2	19.2	0	0	0	0	3.3	2.0	31.1	19.6	32.4	9.2	0	0

Station	# of Image replicates	Eelgrass Mean	Eelgrass SE	*Other Seagrasses Mean	*Other Seagrasses SE	Kelp & other Macroalgae Mean	Kelp & other Macroalgae SE	Detritus & Epiphytes Mean	Detritus & Epiphytes SE	Turfs Mean	Turfs SE	Bare Sand/ Mud Mean	Bare Sand/ Mud SE	Bare Rock Mean	Bare Rock SE
36	7	0	0	0	0	0.3	0.3	20.8	9.5	64.5	11.9	14.2	3.6	0.3	0.3
37	4	0.8	0.8	0	0	0	0	37.8	7.1	2.5	2.5	58.9	6.3	0	0
38	6	0	0	0	0	0	0	9.0	4.4	1.7	1.7	89.3	4.4	0	0
39	3	0	0	0	0	0	0	0	0	0	0	100.0	0	0	0
40	2	0	0	0	0	0	0	0	0	0	0	100.0.	0	0	0
41	15	46.5	9.6	0	0	2.0	1.5	5.0	2.6	16.5	5.5	29.4	6.3	0.6	0.6
42	4	0	0	0	0	0	0	15.7	15.7	0	0.0	59.3	24.7	25.0	25.0
43	2	0	0	0	0	0	0	0.5	0.5	17.0	17.0	77.3	22.7	5.2	5.2
44	4	0	0	0	0	0	0	0	0	9.0	9.0	0	0	91.0	9.0
45	5	0	0	0	0	1.0	1.0	0	0	0	0	99.0	1.0	0	0
46	10	0	0	0	0	2.1	0.7	14.1	7.0	75.3	7.9	4.6	0.9	3.9	1.1
47	11	0	0	0	0	0	0	0	0	0	0	100.0	0	0	0.0
48	8	50.0	6.8	0	0	0.7	0.3	5.0	1.6	14.5	3.9	15.1	2.4	14.7	3.1
49	7	0	0	0	0	15.3	2.3	3.0	2.1	31.6	3.9	12.4	4.1	37.7	3.9
50	14	0	0	0	0	71.1	3.8	0.2	0.2	21.8	3.5	0	0	6.9	1.0
51	3	0	0	0	0	24.4	9.5	3.0	1.7	25.8	6.7	43.5	8.5	3.4	2.4
53	4	0	0	0	0	0	0	0	0	0	0	100.0	0	0	0
54	7	0	0	0	0	0	0	1.7	0.7	0	0	98.3	0.7	0	0

Table B2. Sediment particle size percent occurrence and percent organic matter data for all drop camera stations in St. Mary's River estuary. Particle size data shown includes both the dry sieve processed samples and size class samples < 1 mm analyzed using the Beckman Coulter Laser LS13320, combined and pooled to calculate percent occurrences for major size classes Clay (< 3.9 µm), Silt (> 3.9–63 µm), Sand (> 63–2000 µm), and Gravel (> 2000 µm) across all samples.

Station	% Clay	% Silt	% Sand	% Gravel	% Organic Matter
1	2.39	11.35	86.26	0.00	1.05
2	24.03	74.94	0.23	0.79	17.91
3	23.32	75.45	1.23	0.00	15.96
4	9.84	55.50	33.80	0.86	5.34
5	6.44	24.90	58.56	10.10	3.65
6	5.72	24.68	61.55	8.05	2.55
7	17.21	71.51	11.26	0.01	10.12
8	3.26	15.31	81.15	0.28	1.33
9	11.59	66.73	20.88	0.80	6.53
10	13.16	74.65	12.18	0.00	5.77
11	12.33	72.98	14.46	0.23	5.95
13	7.91	51.53	40.55	0.00	2.71
14	16.01	79.03	4.64	0.32	8.58
15	11.92	69.75	18.33	0.00	7.64
16	7.52	52.76	39.35	0.36	2.92
17	5.18	37.72	56.79	0.31	2.08
18	3.64	27.27	69.09	0.00	1.45
19	12.57	82.94	4.50	0.00	5.65
20	2.48	7.84	89.57	0.11	0.68
21	4.73	34.27	59.79	1.20	1.46
22	5.55	35.29	59.16	0.00	2.20
23	6.84	45.19	47.97	0.00	3.85
24	4.75	38.19	56.69	0.36	2.66
25	2.90	17.79	79.31	0.00	1.06
26	9.89	67.62	21.59	0.90	6.43
27	1.59	5.46	92.63	0.32	0.81
28	5.53	51.57	42.89	0.00	3.01
29	5.23	43.28	51.20	0.29	3.13
31	3.90	28.15	67.96	0.00	1.54
32	8.74	61.76	28.57	0.94	5.18
33	9.52	65.40	24.90	0.18	5.48
35	3.48	25.18	71.28	0.06	1.53
36	4.64	34.84	60.31	0.21	2.72
37	5.05	36.68	58.27	0.00	1.82
38	3.93	20.18	75.83	0.07	1.69
39	1.64	4.97	93.40	0.00	0.60
40	5.79	20.23	69.53	4.45	0.99
43	1.58	8.79	89.63	0.00	0.49
45	19.58	52.92	25.36	2.14	5.18
47	1.77	8.18	90.05	0.00	0.80
48	2.94	19.88	77.19	0.00	1.13
51	0.45	2.69	91.34	5.51	0.37
53	2.02	12.33	85.65	0.00	0.57

Appendix C – Photographs from Faunal Communities Surveys

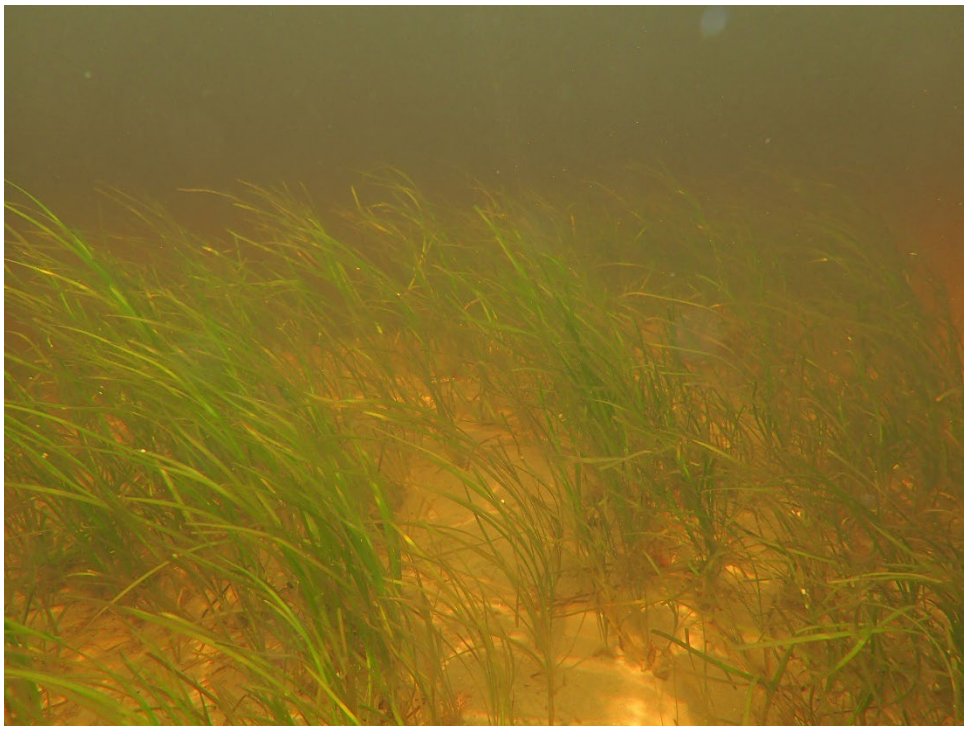

Figure C1. Eelgrass (*Zostera marina*) at Sonora Boat Ramp. Photo credit CPAWS-NS.

Figure C2. Shorthorn sculpin (*Myoxocephalus scorpius*) with *Littorina* sp. Photo credit CPAWS-NS.

Figure C3. A surveyor examines a frond of finger kelp (*Laminaria digitata*). Photo credit CPAWS-NS.

Figure C4. Macroalgae community at McDiarmid's Cove on June 13, 2023. *Chondrus crispus*, *Fucus spiralis*, and *Furcellaria lumbricalis* are present. Photo credit CPAWS-NS.

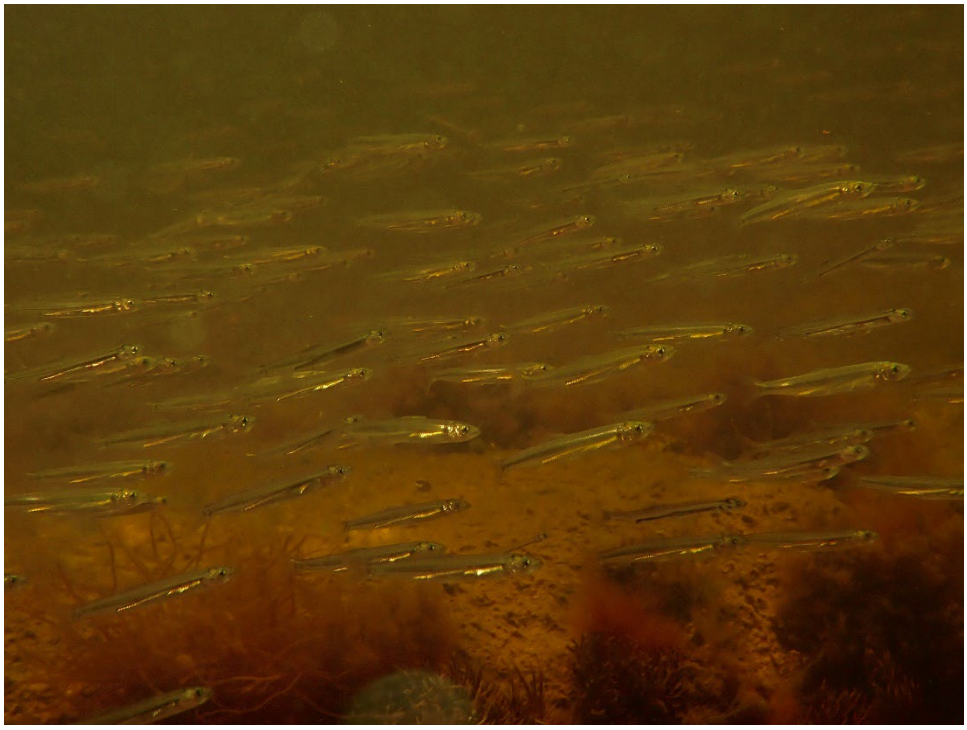

Figure C5. Rainbow Smelt (*Osmerus mordax*) in McDiarmid's Cove on June 13, 2023. Photo credit CPAWS-NS.

Figure C6. Surveyors assess conditions at McDiarmid's Cove. Photo credit CPAWS-NS.

Figure C7. A small hake (*Urophycis* sp.) observed at McDiarmid's Cove on August 1, 2023. Photo credit CPAWS-NS.

Figure C8. American Eel (*Anguilla rostrata*) elver at Eel Cove. Photo credit CPAWS-NS.

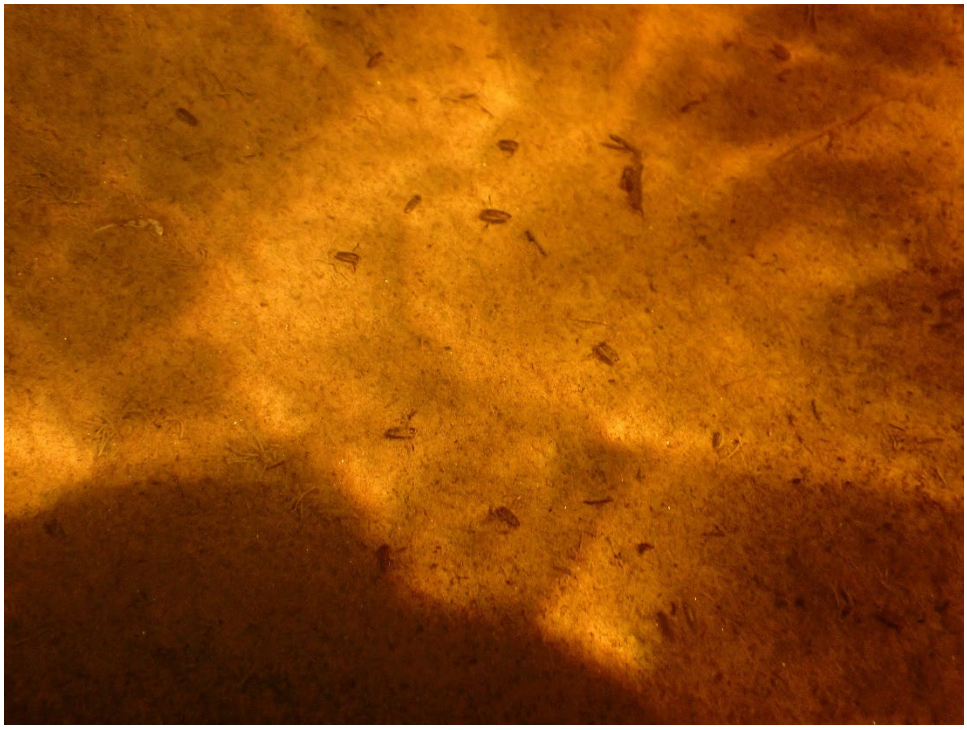

Figure C9. Water boatmen (*Corixidae*) observed at Eel Cove. Photo credit CPAWS-NS.

Figure C10. *Ptilota serrata* and *Mysis* sp. shrimp in the centre, observed at McDiarmid's Cove on September 25, 2023. Photo credit CPAWS-NS.

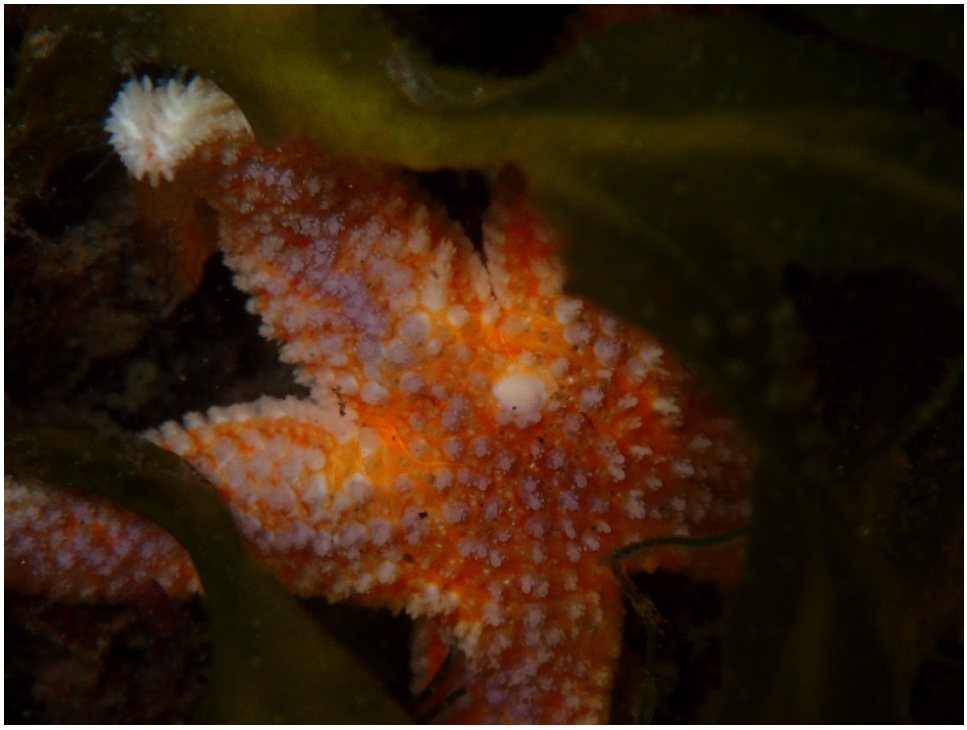

Figure C11. Common sea star (*Asterias rubens*) observed at McDiarmid's Cove on September 25, 2023. Photo credit CPAWS-NS.

Figure C12. Aerial view of Darling Island. Photo credit CPAWS-NS.

Figure C13. Sand shrimp (*Crangon septemspinosa*) observed at Darling Island. Photo credit CPAWS-NS.

Figure C14. Northern pipefish (*Sygnathus fuscus*) observed at Darling Island. Photo credit CPAWS-NS.

Figure C15. Four-spine stickleback (*Apeltes quadracus*) observed at Middle Estuary. Photo credit CPAWS-NS.

Figure C16. Extruded siphons of softshell clam (*Mya arenaria*) observed at Middle Estuary. Photo credit CPAWS-NS.

Figure C17. Aerial view of the Mudflat site, with the extensive eelgrass bed (*Zostera marina*) visible throughout the photo. A channel cut into the sediment by currents is also visible. The surveyors' kayaks are also visible centre-left. Photo credit CPAWS-NS.

Figure C18. Macroalgae diversity in the outer estuary. Photo credit CPAWS-NS.

Figure C19. A snorkeller records various algae species at the Outer Estuary site. Photo credit CPAWS-NS.

Figure C20. Common coralline algae (*Corallina officinalis*) observed at the Outer Estuary. Photo credit CPAWS-NS.

Figure C21. European green crab (*Carcinus maenas*) feeding on a small *Lacuna vincta* snail. Photo credit CPAWS-NS.

Figure C22. Eelgrass (*Zostera marina*) observed at the Outer Estuary. Photo credit CPAWS-NS.

Figure C23. Jonah crab (*Cancer borealis*) observed at the Outer Estuary. Photo credit CPAWS-NS.

Figure C24. Small plumose anemones (*Metridium senile*) observed at the Outer Estuary. Photo credit CPAWS-NS.

Figure C25. Shorthorn sculpin (*Myoxocephalus scorpius*) observed at the Outer Estuary. Photo credit CPAWS-NS.

Figure C26. Gaspereau (*Alosa pseudoharengus*) observed at the Northwest Arm. Photo credit CPAWS-NS.

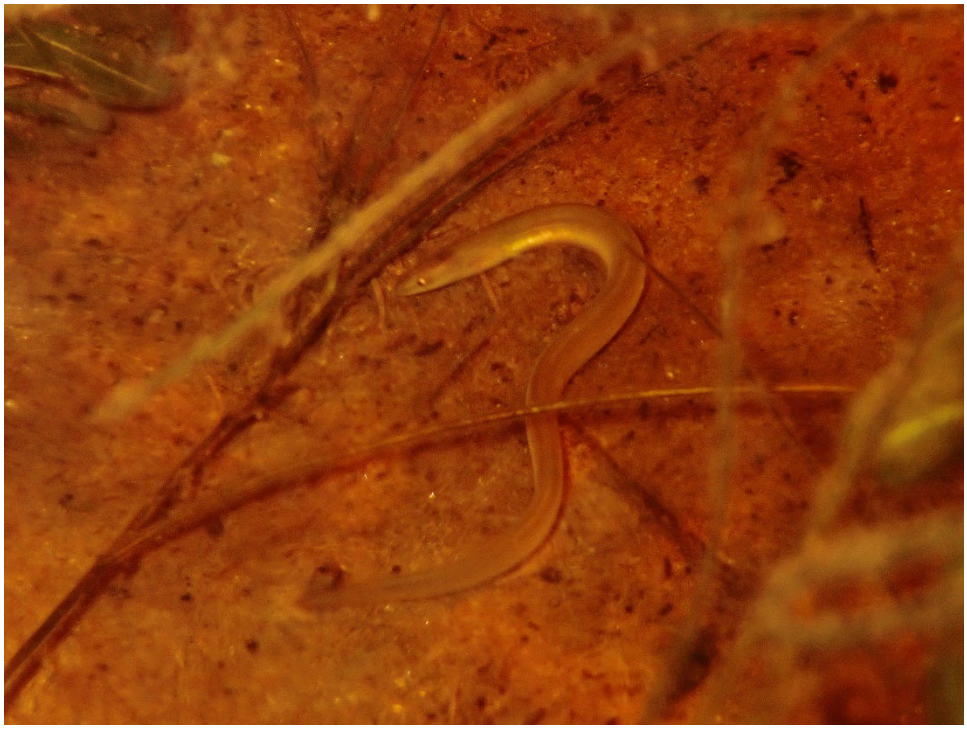

Figure C27. American Eel (*Anguilla rostrata*) elver observed at the Northwest Arm. Photo credit CPAWS-NS.

Figure C28. Four-spine stickleback (*Apeltes quadracus*) observed at the Northwest Arm. Photo credit CPAWS-NS.